# MEASUREMENTS IN MANY-BODY OPEN QUANTUM SYSTEMS

Discrete Time Crystals and Quantum Batteries

GABRIELE CENEDESE


University of Insubria
Department of Science and High Technology
PhD school in Physics and Astrophysics - XXXVIII cycle

October 2025

Gabriele Cenedese: *Measurements in Many-Body Open Quantum Systems,* Discrete Time Crystals and Quantum Batteries, © October 2025

SUPERVISOR:
Prof. Giuliano Benenti

CO-SUPERVISOR:
Dr. Maria Bondani

LOCATION:
Como

TIME FRAME:
October 2025

*To my father, always in my heart.*

# MOTIVATIONS

In 2025, quantum mechanics celebrates its centenary. From the early days of the first quantum revolution in 1925 until well into the second half of the century, few scientists would have ever thought of exploiting the peculiarities of the quantum world for technological applications. Famous is the statement of Erwin Schrödinger, one of the founding fathers of the theory, who in 1952 stated: *"We never experiment with just one electron or atom... any more than we can raise Ichthyosauria in the zoo."*

Since then, starting from the invention of the laser (1960) which, not immediately but shortly after its discovery, would become one of the main protagonists of the second quantum revolution, many things have changed. If I had to choose a symbolic beginning for what we now call the second quantum revolution, I would, as a theoretical physicist, point to the vision of Richard Feynman. In 1981 he famously stated: *"Nature isn't classical, dammit, and if you want to make a simulation of nature, you'd better make it quantum mechanical, and by golly it's a wonderful problem, because it doesn't look so easy."*

From then on, quantum information science grew exponentially with a series of breakthrough results, first theoretical (among them, the BB84 communication protocol in 1984, and Shor's algorithm in 1994) and later experimental (e. g., the demonstration of quantum teleportation in 1997). Today, quantum technologies are at the forefront of scientific research, with virtually every university hosting groups dedicated to topics ranging from quantum cryptography and quantum computing to quantum sensing, metrology, and quantum thermodynamics, both from the theoretical and experimental point of view.

Yet much remains to be done. As Feynman predicted, dealing with quantum systems "is not so easy". Decoherence and interaction with the surrounding environment remain major obstacles that limit the technological exploitation of quantum systems. Handling noise is therefore fundamental.

This is the starting point of this thesis. As a theoretical physicist working in the field of quantum information, my main goal is to identify new phenomena and new applications of this fascinating theory. At the same time, I believe that experiments should never be forgotten: theory and experiment should always go hand in hand.

The way we, as poorly classical beings, interact with nature is through the measurement of observables. The concept of measurement in the quantum realm is itself a subtle and still open problem (on which I will not elaborate any further here), but it plays a central role in the quantum theory and in this work: if engineered carefully, measurements can become a powerful ally for the realistic implementation of quantum technologies and the mitigation of noise.

In this thesis I will illustrate this concept in two contexts: first, discrete time measurements applied to discrete time crystals, which are promising candidates for quantum sensing; and second, continuous measurements applied to the field of quantum batteries, a branch of quantum thermodynamics.

# PUBLICATIONS

## PUBLICATIONS DISCUSSED IN THIS THESIS


[1] Gabriele Cenedese, Samuel T Mister, Mauro Antezza, Giuliano Benenti, and Gabriele De Chiara. "Thermodynamics and protection of discrete time crystals." In: *Physical Review B* 112.5 (2025), p. 054303.

[2] Gabriele Cenedese, Marco G Genoni, Dario Ferraro, and Giuliano Benenti. "Daemonic ergotropy enhancement in correlated quantum battery-charger systems." In: *Preparation* (2025).


## OTHER PUBLICATIONS


[1] Gabriele Cenedese, Giuliano Benenti, and Maria Bondani. "Correcting coherent errors by random operation on actual quantum hardware." In: *Entropy* 25.2 (2023), p. 324.

[2] Gabriele Cenedese, Maria Bondani, Dario Rosa, and Giuliano Benenti. "Generation of pseudo-random quantum states on actual quantum processors." In: *Entropy* 25.4 (2023), p. 607.

[3] Silvia Cassina, Gabriele Cenedese, Alessia Allevi, and Maria Bondani. "Speckled-speckle field as a resource for imaging techniques." In: *Scientific Reports* 14.1 (2024), p. 15161.

[4] Silvia Cassina, Gabriele Cenedese, Marco Lamperti, Maria Bondani, and Alessia Allevi. "On the use of superthermal light for imaging applications." In: *Physics Letters A* 495 (2024), p. 129300.

[5] Luca Razzoli, Gabriele Cenedese, Maria Bondani, and Giuliano Benenti. "Efficient implementation of discrete-time quantum walks on quantum computers." In: *Entropy* 26.4 (2024), p. 313.

[6] Silvia Cassina, Gabriele Cenedese, Maria Bondani, and Alessia Allevi. "Application of superthermal light to imaging and quantum communication protocols." In: *International Journal of Quantum Information* 22.06 (2024), p. 2450025.

[7] Gabriele Cenedese, Maria Bondani, Alexei Andreanov, Matteo Carrega, Giuliano Benenti, and Dario Rosa. "Shallow quantum circuits are robust hunters for quantum many-body scars." In: *The European Physical Journal Plus* 140.6 (2025), p. 517.

# CONTENTS

## LIST OF TABLES

# ACRONYMS

| | |
|---|---|
| CPTP | Completely Positive Trace-Preserving |
| PVM | Projection-Valued Measure |
| POVM | Positive Operator-Valued Measure |
| GKSL | Gorini-Kossakowski-Sudarshan-Lindblad |
| RWA | Rotating Wave Approximation |
| TLS | Two-Level System |
| SME | Stochastic Master Equation |
| PD | Photo-Detection |
| HD | Homodyne Detection |
| SSE | Stochastic Schrödinger Equation |
| DTC | Discrete Time Crystal |
| CTC | Continuous Time Crystal |
| BTC | Boundary Time Crystal |
| MBL | Many-Body Localization |
| QB | Quantum Battery |
| SYK | Sachdev-Ye-Kitaev |
| NMR | Nuclear Magnetic Resonance |

# Part I

# INTRODUCTION

Part I serves as the theoretical backbone of the thesis, developing the formal tools required to analyze open quantum systems influenced by measurement processes.

The discussion begins with the fundamental postulates of quantum mechanics, reformulated in a modern language of quantum information theory, that take into account composite systems, reduced dynamics, and the operational role of measurements. This establishes a working framework in which non-isolated quantum systems can be rigorously studied.

The focus then shifts to the theory of open quantum systems, where dissipation and decoherence arise naturally through interactions with an environment: in realistic scenarios, no quantum system is truly isolated, and understanding how the external world influences its evolution is essential for both fundamental insight and technological advancement. Different approaches to derive dissipative dynamics are presented, with the aim of explaining how irreversible behaviour emerges from unitary evolution and how it is affected by measurements.

Finally, the foundations of quantum thermodynamics are introduced, providing a consistent description of work, heat, and entropy in quantum settings, and addressing the problem of energy extraction in quantum systems.

Altogether, Part I equips the reader with the conceptual framework necessary to interpret the phenomena investigated in the subsequent chapters.

# 1

# POSTULATES OF QUANTUM MECHANICS AND OPEN QUANTUM SYSTEMS

Quantum mechanics is, at its core, a mathematical framework built upon a set of postulates that provide the fundamental assumptions for predicting the physical behaviour of quantum systems. The interpretation of these postulates is a profound and debated issue that lies beyond the scope of this thesis; here, I will adopt the Copenhagen interpretation.

This introductory chapter presents the postulates of quantum mechanics from the modern viewpoint of quantum information theory and establishes the notation used throughout the thesis. In addition to the postulates, we will derive the master equations governing open quantum systems and systems subject to continuous measurement.

The discussion of the postulates will follow the treatment given in [1], while the derivation of the master equations will be based primarily on the works of [2, 3, 4].

## 1.1 CLOSED AND MULTIPARTITE QUANTUM SYSTEMS

This section provides an overview of the mathematical framework of quantum mechanics and introduces a modern reformulation of its basic postulates, tailored to the description of quantum systems interacting with their environment and with measuring or processing devices. Although beginning with the postulates might seem redundant, given their familiarity, it serves several essential purposes: to make explicit the assumptions of the standard formulation, to establish the notation used throughout this thesis, and to give a reformulation in modern terms of quantum information and quantum technologies.

We will employ Dirac's bra-ket notation throughout. For clarity and conciseness, the discussion will focus on finite-dimensional Hilbert spaces and observables with discrete spectra, but of course many of the results here reported can be extended to infinite-dimensional settings and continuous spectra.

For the purposes of this thesis, the postulates provide a set of prescriptions that can be grouped and summarized as follows: they establish how the states of a physical system are described, how measurements on the system are performed and finally, how the system evolves, whether under its intrinsic dynamics or as a result of measurements.

### 1.1.1 *States*

The states of a quantum system are fully and deterministically described by vectors $|\psi\rangle$ of a Hilbert space $\mathbb{H}$ over a complex field $\mathbb{C}$. States must be normalized, i.e., $\langle\psi|\psi\rangle = 1$, where $\langle\bullet|\bullet\rangle$ is the inner product associated to the Hilbert space.

Quantum systems involving multiple degrees of freedom, or consisting of several copies of the same system, are referred to as *composite systems*. Their mathematical description is given by the tensor product of the Hilbert spaces corresponding to the individual degrees of freedom: $\mathbb{H}_{\text{tot}} = \mathbb{H}_1 \otimes \mathbb{H}_2 \otimes \dots$. In general, however, the state of the composite system cannot always be expressed as a tensor product of states of the individual subsystems. In this case, we speak of non-separable states or, equivalently, of *quantum entanglement*. If the state is described as we have just

introduced, we speak of *pure states*. For a closed quantum system and, in the case of composite systems, when considered globally, a description in terms of pure states is sufficient. However, in most practical situations we deal with systems that interact, or have interacted, with the rest of the universe, either during their dynamical evolution or as a consequence of measurement. At this point, and throughout the remaining of this section, it is therefore convenient to adopt also a more general formulation in terms of density operators.

An operator is a linear map $\hat{A} : \mathbb{H} \to \mathbb{H}$, and we denote $\mathcal{L}(\mathbb{H})$ the vector space of linear operators on $\mathbb{H}$. The trace of an operator is a linear functional $\mathrm{Tr} : \mathcal{L}(\mathbb{H}) \to \mathbb{C}$ defined as $\mathrm{Tr}[\hat{A}] \equiv \sum_j \langle e_j | \hat{A} | e_j \rangle$ where $\{|e_j\rangle\}$ is an orthonormal basis of the Hilbert space $\mathbb{H}$.
Accordingly, the first postulate can be restated as: the state of a quantum system is represented by an operator acting on the Hilbert space $\mathbb{H}$ known as the density operator $\rho$ which must satisfy the following conditions:

- **Semi-definite positivity**: meaning that all its eigenvalues are non-negative;
- **Normalization**: $\mathrm{Tr}[\rho] = 1$;
- **Purity**: $\mathrm{Tr}[\rho^2] \leqslant 1$.

If $\mathrm{Tr}[\rho^2] = 1$, $\rho$ reduces to a rank-1 projector (an operator with all zero eigenvalues except one). The quantity $\mathrm{Tr}[\rho^2]$, known as the *purity* of the state, provides a convenient way to distinguish between pure states ($\mathrm{Tr}[\rho^2] = 1$) and mixed states ($\mathrm{Tr}[\rho^2] < 1$). The purity is also lower bounded as $\mathrm{Tr}[\rho^2] \geqslant \frac{1}{d}$, where $d$ denotes the dimension of the Hilbert space. The lower bound corresponds to the maximally mixed state $\rho = \frac{1}{d}\mathbb{I}_d$, where $\mathbb{I}_d$ is the identity operator. In practice, purity is a particularly useful quantity when dealing with open quantum systems, as it provides a simple measure of how much coherence the system has lost due to interactions with its environment. It can also serve as a measure of quantum entanglement when the composite system is not in a pure state (see, e.g., [3]).

Let's consider a statistical mixture of pure quantum states $\{p_k, |\psi_k\rangle\}$, representing uncertainty in the preparation of the

system, where $p_k$ denotes the probability of preparing the state $|\psi_k\rangle$ and $\sum_k p_k = 1$. The corresponding density operator is then defined as

$$\rho = \sum_k p_k |\psi_k\rangle \langle\psi_k| . \tag{1.1}$$

This formulation offers a straightforward physical interpretation of density operators, linking them directly to ensembles of quantum states. Finally, like any operator, the density operator can be represented in terms of its matrix elements in a chosen basis: $\rho = \sum_{i,j} \rho_{ij} |e_i\rangle \langle e_j|$ where $\rho_{ij} = \langle e_i| \rho |e_j\rangle$ is commonly called the *density matrix* of the system. The matrix is diagonal if the basis is formed by eigenvectors of $\rho$; otherwise, it will include off-diagonal elements. These requirements and definition also hold for composite systems, although with some differences with the respect to pure states regarding the separability criterion (see again [3] for more details). Special attention is needed, however, when applying the trace operation to the degrees of freedom of subsystems.

Suppose we have a bipartite quantum system $\mathbb{H}_{AB} = \mathbb{H}_A \otimes \mathbb{H}_B$. The global state $\rho_{AB}$ belongs to this composite space, while the reduced state of subsystem A is obtained by performing the partial trace over subsystem B: $\rho_A = \mathrm{Tr}_B[\rho_{AB}] = \sum_i \langle e_i|\rho_{AB}|e_i\rangle$, where $\{|e_i\rangle\}$ is a basis of $\mathbb{H}_B$. Similarly, the reduced state of subsystem B is given by $\rho_B = \mathrm{Tr}_A[\rho_{AB}]$. The partial traces $\rho_A$ and $\rho_B$ of a density operator $\rho_{AB}$ of a bipartite system are themselves valid density operators for the reduced subsystems. This result holds true even for multipartite systems.

### 1.1.2 *Evolution*

The second postulate of quantum mechanics describes how states evolve, particularly in the case of closed systems. In the most general formulation, the state of a closed quantum system evolves through unitary operators acting on the Hilbert space of the system:

$$|\psi'\rangle = \hat{U} |\psi\rangle , \tag{1.2}$$

or, equivalently, in terms of density operators,

$$\rho' = \hat{U}\rho\hat{U}^\dagger. \tag{1.3}$$

For $\hat{U}$ to be unitary, it must satisfy the condition $\hat{U}^\dagger\hat{U} = \mathcal{I}$, where $\hat{U}^\dagger$ denotes the adjoint of $\hat{U}$ and $\mathcal{I}$ denotes the identity operaror.[1] An important property of unitary evolution is that any unitary operator can be expressed as the exponential of an Hermitian operator (hence an *observable*, as we shall specify later). In the specific case of dynamical evolution, this Hermitian operator is precisely the Hamiltonian $\hat{\mathcal{H}}$ of the system:

$$\hat{U}(t) = e^{-i\hat{\mathcal{H}}t/\hbar}, \tag{1.4}$$

where, for simplicity, we have considered a time-independent Hamiltonian. This directly leads to the time-dependent Schrödinger equation, which governs the evolution of closed quantum systems. Starting from the latter relation, one can derive the fundamental dynamical law of quantum mechanics. By considering the infinitesimal time evolution of a state,

$$|\psi(t+\delta t)\rangle = \hat{U}(\delta t)\,|\psi(t)\rangle \simeq \left(\mathcal{I} - \frac{i}{\hbar}\hat{\mathcal{H}}\,\delta t\right)|\psi(t)\rangle\,, \tag{1.5}$$

and taking the limit $\delta t \to 0$, we obtain the *time-dependent Schrödinger equation*:

$$i\hbar\frac{d}{dt}\,|\psi(t)\rangle = \hat{\mathcal{H}}\,|\psi(t)\rangle\,. \tag{1.6}$$

Equivalently, in the density operator formalism, the evolution of a closed system is described by the *von Neumann equation*:

$$i\hbar\frac{d}{dt}\rho(t) = \left[\hat{\mathcal{H}}, \rho(t)\right], \tag{1.7}$$

which can be regarded as the generalization of the Schrödinger

$[\hat{\mathcal{A}}, \hat{\mathcal{B}}]$ *is the commutator between the operator* $\hat{\mathcal{A}}$ *and* $\hat{\mathcal{B}}$*, defined as* $[\hat{\mathcal{A}}, \hat{\mathcal{B}}] = \hat{\mathcal{A}}\hat{\mathcal{B}} - \hat{\mathcal{B}}\hat{\mathcal{A}}$.

1 More generally, given an operator $\hat{\mathcal{A}}$, its adjoint $\hat{\mathcal{A}}^\dagger$ is defined as the unique operator satisfying

$$\langle\psi|\hat{\mathcal{A}}\phi\rangle = \langle\hat{\mathcal{A}}^\dagger\psi|\phi\rangle, \quad \text{for all } |\psi\rangle, |\phi\rangle \in \mathbb{H}.$$

equation to mixed states. Both the Schrödinger and von Neumann equations remain valid also for time-dependent Hamiltonians $\hat{\mathcal{H}}(t)$, although in this case the unitary evolution must be generalized as

$$\hat{\mathcal{U}}(t) = \mathcal{T} \exp\left[-\frac{i}{\hbar}\int_0^t \hat{\mathcal{H}}(t')\,dt'\right], \tag{1.8}$$

where $\mathcal{T}$ is the time-ordering operator, which ensures that operators are ordered according to time, with earlier times appearing to the right.

Physically, the Hamiltonian represents (in most of the cases) the total energy of the system and serves as the generator of time translations. The unitarity of the time-evolution operator ensures that probabilities are preserved and coherence is maintained throughout the dynamics, as we shall see from the probabilistic interpretation introduced in the next postulate: while the second postulate describes the deterministic, continuous evolution of closed quantum systems under unitary dynamics, the third postulate addresses the fundamentally probabilistic nature of quantum measurements.

However, in some situations, such as the evolution of reduced systems, unitary evolution is no longer sufficient. Instead, the dynamics of interacting systems are described by Completely Positive Trace-Preserving (CPTP) maps. A CPTP map $\mathcal{E}$ must satisfy the following conditions:

- **Linearity**: $\mathcal{E}\left[\sum_i p_k \rho_k\right] = \sum_k p_k \mathcal{E}[\rho_k]$;
- **Complete positivity**: any extended map $\mathcal{E} \otimes \mathcal{I}_B$ is positive on any extended space $\mathbb{H} \otimes \mathbb{H}_B$;
- **Trace preservation**: $\mathrm{Tr}[\mathcal{E}[\rho]] = \mathrm{Tr}[\rho]$.

CPTP maps can also be expressed in the *Kraus representation*:

$$\mathcal{E}[\rho] = \sum_k \hat{\mathcal{K}}_k\, \rho\, \hat{\mathcal{K}}_k^\dagger, \tag{1.9}$$

where the set of operators $\{\hat{\mathcal{K}}_k\}$ satisfies the completeness relation

$$\sum_k \hat{\mathcal{K}}_k^\dagger \hat{\mathcal{K}}_k = \mathcal{I}. \tag{1.10}$$

These properties are essential to preserve the statistical interpretation of the density operator. In particular, complete positivity ensures that the map remains physically valid even when the system is part of a larger Hilbert space, allowing a consistent description of reduced states in composite systems.

### 1.1.3 *Measurements*

In practice, no measurement can extract complete information about a quantum system without disturbing it. The third postulate formalizes how measurement outcomes are related to the system state and how the state itself is updated as a result of observation. In other words, whereas unitary evolution governs reversible dynamics, the measurement postulate captures the discrete, stochastic changes induced by the act of measurement, which are essential to the quantum description of nature.

Measurements are mathematically associated with a set of operators $\{\hat{\mathcal{M}}_n\}$, where the index $n$ labels the possible measurement outcomes. The most common type of measurement in closed systems is the Projection-Valued Measure (PVM). In a PVM, the measurement operators are projection operators $\hat{\mathcal{M}}_n = \hat{P}_n$, which satisfy:

- $\hat{P}_n \hat{P}_m = \delta_{nm} \hat{P}_n$, ensuring idempotence and orthogonality;
- $\sum_n \hat{P}_n = \mathcal{I}$, guaranteeing that the projectors span the Hilbert space and allowing a consistent statistical interpretation.

Each PVM is associated with an Hermitian operator $\hat{\mathcal{O}}$, called *observable*, which admits a spectral decomposition $\hat{\mathcal{O}} = \sum_i o_i \hat{P}_i$. The eigenvalues $o_i$ correspond to the possible measurement outcomes and they are real due to the Hermiticity of $\hat{\mathcal{O}}$. When measuring an observable $\hat{O}$ on a pure state $|\psi\rangle$, the probability (*Born rule*) of obtaining outcome $o_i$ is

$$p_i = \langle\psi|\hat{P}_i|\psi\rangle, \tag{1.11}$$

and the post-measurement state is

$$|\psi_i\rangle = \frac{\hat{P}_i\,|\psi\rangle}{\sqrt{p_i}}. \tag{1.12}$$

For mixed states described by a density operator $\rho$, these relations generalize to

$$p_i = \mathrm{Tr}[\rho \hat{P}_i], \quad \rho_i = \frac{\hat{P}_i \rho \hat{P}_i}{p_i}. \tag{1.13}$$

For composite systems, the formalism extends naturally. Measurements on one or more subsystems can be described using the Positive Operator-Valued Measures (POVMs) formalism, which generalize PVMs. A POVM is a collection of positive operators $\{\hat{\Pi}_n\} \geqslant 0$ satisfying

$$\sum_n \hat{\Pi}_n = \mathcal{I}, \tag{1.14}$$

but without the stronger requirement of being projectors. To describe the post-measurement state, it is necessary to introduce a set of operators known as *detection operators*, $\{\hat{\mathcal{M}}_n\}$, satisfying

$$\hat{\Pi}_n = \hat{\mathcal{M}}_n^\dagger \hat{\mathcal{M}}_n. \tag{1.15}$$

This set is not unique, and different realizations of the same POVM can lead to different post-measurement states even for the same outcome.[2] The probabilities of outcomes and the resulting states are then given by

$$p_i = \mathrm{Tr}[\rho \hat{\Pi}_i], \quad \rho_i = \frac{\hat{\mathcal{M}}_i \rho \hat{\mathcal{M}}_i^\dagger}{p_i}. \tag{1.16}$$

Notice that the post-measurement state depends not only on the outcome but also on the specific realization of the measurement.

A natural question arises when introducing generalized measurements: are POVMs physically justified, and how? The answer is provided by the *Naimark theorem*, which establishes a connection between generalized and standard measurements. Any generalized measurement described by a POVM can be realized as a standard projective measurement on an enlarged Hilbert space. Conversely, any standard measurement on a composite systems can be viewed as a generalized measurement on a subsystem.

2 There is a residual freedom in designing the post-measurement state. In fact, since $\hat{\Pi}_n$ is a positive operator $\hat{\mathcal{M}}_n = \sqrt{\hat{\Pi}_n}$ exists and satisfies the constraint, as well as any operator of the form $\hat{\mathcal{M}}_n = \hat{u}_n \sqrt{\hat{\Pi}_n}$ with $\hat{u}_n$ unitary.

Physically, this means that when measuring an observable, one often deals with a larger system including the measurement apparatus or ancillas. While the observable can be represented as a standard operator on this extended space, tracing out the apparatus degrees of freedom typically yields a POVM on the subsystem. Conversely, any POVM can always be implemented as a projective measurement on a suitably enlarged Hilbert space. This shows that generalized measurements are fully compatible with standard quantum mechanics and are physically meaningful. In this way, CPTP maps and POVMs together provide the mathematical tools to describe the reduced non-unitary dynamics of composite quantum systems, preserving both the statistical interpretation of the density operator and the physical consistency of composite systems.

### 1.1.4 *Representations*

All the postulates discussed in the previous sections have been presented in the *Schrödinger picture*, in which operators are considered constant (except for any explicit time dependence) and the time evolution is carried by the states or density operators.

However, in some cases it is useful to adopt different representations of quantum dynamics. In the *Heisenberg picture*, for instance, the states are considered time independent while the operators evolve in time according to

$$\hat{\mathcal{O}}_H(t) = \hat{\mathcal{U}}^\dagger(t)\,\hat{\mathcal{O}}_S\,\hat{\mathcal{U}}(t), \tag{1.17}$$

where $\hat{\mathcal{U}}(t)$ is the usual unitary evolution operator and the subscripts $H$ and $S$ indicate the considered representation. This representation is particularly convenient when focusing on the evolution of observables rather than states. The dynamics is governed by the Heisenberg equation:

$$\frac{d}{dt}\hat{\mathcal{O}}_H(t) = \frac{i}{\hbar}\left[\hat{\mathcal{H}}_H(t), \hat{\mathcal{O}}_H(t)\right] + \left(\frac{\partial \hat{\mathcal{O}}_S}{\partial t}\right)_H. \tag{1.18}$$

A third useful representation is the *interaction picture*, particularly convenient when the Hamiltonian can be split into a time-independent part $\hat{\mathcal{H}}_0$ and an interaction term $\hat{\mathcal{H}}_1(t)$. In this

picture, both states and operators evolve: the operators evolve according to $\hat{\mathcal{H}}_0$, as in the Heisenberg picture, while the states evolve under the effect of the interaction Hamiltonian. The resulting dynamical equation takes the form

$$i\hbar \frac{d}{dt}\rho_I(t) = \left[\hat{\mathcal{H}}_{1,I}(t), \rho_I(t)\right], \tag{1.19}$$

where $\hat{\mathcal{H}}_{1,I}(t)$ denotes the interaction Hamiltonian in the interaction picture.

Overall, these different pictures are mathematically equivalent and physically consistent, but choosing the appropriate one can simplify calculations and clarify the interpretation of the dynamics.

## 1.2 OPEN QUANTUM SYSTEMS

In this section, we review the theoretical framework of open quantum systems [2, 5]. By an open system we mean a quantum system whose dynamics is not isolated but instead influenced by the interaction with external degrees of freedom, usually referred to as the environment (also known as a *bath* or *reservoir*).

A central feature of open systems is that their reduced dynamics is, in general, no longer unitary. Instead, it must be described by CPTP maps, which ensure the consistency of the probabilistic interpretation of quantum mechanics. In the first part of this section, we will therefore introduce this formalism and show how it naturally leads to a description of quantum dynamics beyond unitary evolution.

We will then move to a microscopic derivation of master equations [2], where the reduced dynamics of a system is obtained starting from a unitary description of the global system-environment evolution and tracing out the environment degrees of freedom. This approach provides a clear physical picture of the approximations involved in deriving effective dynamical equations for the system alone, and leads to the celebrated Gorini-Kossakowski-Sudarshan-Lindblad (GKSL) master equation, also known as the Lindblad master equation, which provides the most general form of Markovian quantum dynamics [6, 7].

Finally, we will discuss a collision model approach [8], where the environment is represented as a collection of ancillary systems sequentially interacting with the system of interest. This perspective is not only conceptually insightful but also particularly useful for the study of continuous quantum measurements [4], which will play a role in the later parts of this thesis.

### 1.2.1 *CPTP Derivation*

In the quantum operation formalism, the system's state at two infinitesimally separated times, $\rho(t)$ and $\rho(t+dt)$, are related through a superoperator[3] $\mathcal{S}(t+dt,t)$ acting on $\rho(t)$. Using the Kraus representation, this relation can be written as

$$\rho(t+dt) = \mathcal{S}(t+dt,t)[\rho(t)] = \sum_{k=0}^{M-1} \hat{\mathcal{K}}_k \, \rho(t) \, \hat{\mathcal{K}}_k^\dagger, \tag{1.20}$$

where the $\hat{\mathcal{K}}_k$ are the Kraus operators, and their number $M$ is at most $N^2$, with $N$ the dimension of the system Hilbert space. Differently from the usual case where Kraus operators describe finite transformations, here they are associated with an infinitesimal step of the evolution. To guarantee that $\mathcal{S}(t,t) = \mathcal{I}$, Kraus operators have to be written in the following way:

$$\hat{\mathcal{K}}_0 = \mathcal{I} + \frac{1}{\hbar}(-i\hat{\mathcal{H}} + \hat{\Gamma})\, dt, \qquad \hat{\mathcal{K}}_k = \hat{\mathcal{L}}_k \sqrt{dt}, \quad (k = 1, \dots, M-1), \tag{1.21}$$

where $\hat{\mathcal{H}}$ and $\hat{\Gamma}$ are Hermitian operators, and the operators $\hat{\mathcal{L}}_k$ are known as *Lindblad operators*. The normalization condition $\sum_k \hat{\mathcal{K}}_k^\dagger \hat{\mathcal{K}}_k = \mathcal{I}$ then implies

$$\frac{2}{\hbar}\hat{\Gamma} dt + \sum_{k=1}^{M-1} \hat{\mathcal{L}}_k^\dagger \hat{\mathcal{L}}_k dt + O(dt^2) = 0, \tag{1.22}$$

that is

$$\hat{\Gamma} = -\frac{\hbar}{2} \sum_{k=1}^{M-1} \hat{\mathcal{L}}_k^\dagger \hat{\mathcal{L}}_k. \tag{1.23}$$

3 A superoperator is a linear map $\mathcal{S} : \mathcal{B}(\mathbb{H}) \to \mathcal{B}(\mathbb{H})$ acting on the vector space of bounded operators $\mathcal{B}(\mathbb{H})$ on a Hilbert space $\mathbb{H}$.

By substituting these expressions into the Kraus expansion, one finds

$$\begin{aligned}\rho(t+dt) &= \rho(t) - \frac{i}{\hbar}\left[\hat{\mathcal{H}}, \rho(t)\right] dt + \\ &+ \sum_{k=1}^{M-1} \left(\hat{\mathcal{L}}_k \rho(t) \hat{\mathcal{L}}_k^\dagger - \tfrac{1}{2}\hat{\mathcal{L}}_k^\dagger \hat{\mathcal{L}}_k \rho(t) - \tfrac{1}{2}\rho(t)\hat{\mathcal{L}}_k^\dagger \hat{\mathcal{L}}_k\right) dt + \\ &+ O(dt^2). \end{aligned} \tag{1.24}$$

Assuming an expansion of the form $\rho(t+dt) = \rho(t) + \dot{\rho}(t)dt + O(dt^2)$, we obtain the celebrated GKSL master equation (see [6] and [7]):

$$\begin{aligned}\dot{\rho}(t) &= -\frac{i}{\hbar}\left[\hat{\mathcal{H}}, \rho(t)\right] + \sum_{k=1}^{M-1} \left(\hat{\mathcal{L}}_k \rho(t) \hat{\mathcal{L}}_k^\dagger - \tfrac{1}{2}\left\{\hat{\mathcal{L}}_k^\dagger \hat{\mathcal{L}}_k, \rho(t)\right\}\right) \equiv \\ &\equiv -\frac{i}{\hbar}\left[\hat{\mathcal{H}}, \rho(t)\right] + \sum_k \mathcal{D}[\hat{\mathcal{L}}_k]\rho(t), \end{aligned} \tag{1.25}$$

*$\{\hat{\mathcal{A}}, \hat{\mathcal{B}}\}$ is the anticommutator between the operator $\hat{\mathcal{A}}$ and $\hat{\mathcal{B}}$, defined as $\{\hat{\mathcal{A}}, \hat{\mathcal{B}}\} = \hat{\mathcal{A}}\hat{\mathcal{B}} + \hat{\mathcal{B}}\hat{\mathcal{A}}$.*

where we defined the superoperator $\mathcal{D}[\hat{\mathcal{A}}]\bullet = \hat{\mathcal{A}} \bullet \hat{\mathcal{A}}^\dagger - \frac{1}{2}\{\hat{\mathcal{A}}^\dagger \hat{\mathcal{A}}, \bullet\}$. It is worth emphasizing that this derivation relies on the Markovian approximation, which allows us to expand the infinitesimal map in this way, assuming the absence of long memory times: the future evolution depends only on the state at time t and not on its history.

### 1.2.2 *Microscopic Derivation*

Here we present a second derivation of the Markovian master equation, this time based on a microscopic model, which provides clear physical understanding of the approximations involved. To investigate the influence of an external environment on a quantum system S, we follow the standard formulation of open quantum systems weakly coupled to their environment (see, for instance, Ref. [2]). In this setting, the total Hamiltonian of the combined system-environment can be written as

$$\hat{\mathcal{H}} = \hat{\mathcal{H}}_S + \hat{\mathcal{H}}_B + \hat{\mathcal{H}}_I, \tag{1.26}$$

where $\hat{\mathcal{H}}_S$ represents the system Hamiltonian, $\hat{\mathcal{H}}_B$ denotes the bath Hamiltonian, and $\hat{\mathcal{H}}_I$ the interaction term between the two.

Starting from the interaction picture von Neumann equation, and assuming without loss of generality[4] $\mathrm{Tr}_B\left[\hat{\mathcal{H}}_I(t), \rho(0)\right] = 0$, the quantum master equation for the system density matrix reads:

$$\frac{d}{dt}\rho_S(t) = -\int_0^t ds\, \mathrm{Tr}_B\left[\hat{\mathcal{H}}_I(t), \left[\hat{\mathcal{H}}_I(s), \rho(s)\right]\right], \tag{1.27}$$

where $\rho$ represents the joint system-bath density matrix, and $\rho_S$ denotes the system density matrix obtained by tracing out the reservoir degrees of freedom, by employing the partial trace $\mathrm{Tr}_B$, and finally $\hat{\mathcal{H}}_I(t)$ is the time-dependent interaction picture version of $\hat{\mathcal{H}}_I$ (from now on, we will refer to operators without explicit time dependence as operators in the Schrödinger picture, and those with explicit time dependence as operators in the interaction picture). Here, for simplicity, we have assumed units in which $\hbar = 1$. We assume that the coupling between the system and the reservoir is weak, allowing us to apply the *Born approximation*. In this case, the system-bath density matrix can be approximated as separable: $\rho(s) \simeq \rho_S(s) \otimes \rho_B$, where $\rho_B$ is the initial state of the reservoir assumed constant. To further simplify, we perform the *Markov approximation* by replacing the integrand $\rho_S(s)$ with $\rho_S(t)$ in Eq. (1.27). This ensures that the evolution of the system density matrix depends only on the state $\rho_S(t)$ at time $t$. As a result, we obtain the so-called *Redfield equation*, which is local in time but not yet fully Markovian. To derive the Markovian master equation, we replace $s$ with $t - s$ in the integrand and extend the upper limit of the integral to infinity. This change of variables highlights that, for a stationary bath, the correlation functions depend only on the time difference. This approximation is valid when the timescale $\tau_R$ over which the open system's state varies is much larger than the reservoir's characteristic correlation time $\tau_B$. At this point the master equation reads:

$$\frac{d}{dt}\rho_S(t) = -\int_0^\infty ds\, \mathrm{Tr}_B\left[\hat{\mathcal{H}}_I(t), \left[\hat{\mathcal{H}}_I(t-s), \rho_S(t) \otimes \rho_B\right]\right]. \tag{1.28}$$

4 The assumption simply removes the first order contribution of the interaction Hamiltonian, which would otherwise correspond to a mean-field shift of the system energies. This can always be achieved by redefining the system Hamiltonian to absorb the average bath effect, so that the interaction term describes only bath fluctuations.

At this stage, we can perform the Rotating Wave Approximation (RWA) by averaging over the rapidly oscillating terms. To achieve this, we have to explicitly introduce the interaction Hamiltonian, which, without loss of generality, can be written, in the Schrödinger's picture, as:

$$\hat{\mathcal{H}}_I = \sum_\alpha \hat{\mathcal{A}}_\alpha \otimes \hat{\mathcal{B}}_\alpha, \tag{1.29}$$

where $\hat{\mathcal{A}}_\alpha$ and $\hat{\mathcal{B}}_\alpha$ are two sets of Hermitian operators of the system and the bath, respectively. Let us define the eigenstates of the system's Hamiltonian: $\hat{\mathcal{H}}_S |\epsilon\rangle = \epsilon |\epsilon\rangle$, with energy eigenvalues $\epsilon$. The RWA is easily performed by decomposing the interaction Hamiltonian $\hat{\mathcal{H}}_I$ into the energy eigenbasis $\{|\epsilon\rangle\}$:

$$\hat{\mathcal{A}}_\alpha(\omega) \equiv \sum_{\epsilon'-\epsilon=\omega} |\epsilon\rangle \langle\epsilon|\hat{\mathcal{A}}_\alpha|\epsilon'\rangle \langle\epsilon'|, \tag{1.30}$$

where the sum is restricted to all energies $\epsilon$ and $\epsilon'$ with a fixed difference $\omega$. We notice that $\sum_\omega \hat{\mathcal{A}}_\alpha(\omega) = \hat{\mathcal{A}}_\alpha$ by using the completeness relation and that these operators are no longer Hermitian: $\hat{\mathcal{A}}_\alpha^\dagger(\omega) = \hat{\mathcal{A}}_\alpha(-\omega)$. It is easy to see that the interaction picture version of $\hat{\mathcal{A}}_\alpha(\omega)$ can be written as

$$\hat{\mathcal{A}}_{\alpha,\omega}(t) = e^{i\hat{\mathcal{H}}_S t}\hat{\mathcal{A}}_\alpha(\omega)e^{-i\hat{\mathcal{H}}_S t} = e^{-i\omega t}\hat{\mathcal{A}}_\alpha(\omega), \tag{1.31}$$

which allows us to rewrite the interaction Hamiltonian, in the interaction picture, as

$$\begin{aligned}\hat{\mathcal{H}}_I(t) &= \sum_{\alpha,\omega} e^{-i\omega t}\hat{\mathcal{A}}_\alpha(\omega) \otimes \hat{\mathcal{B}}_\alpha(t) \\ &= \sum_{\alpha,\omega} e^{i\omega t}\hat{\mathcal{A}}_\alpha^\dagger(\omega) \otimes \hat{\mathcal{B}}_\alpha^\dagger(t),\end{aligned} \tag{1.32}$$

where $\hat{\mathcal{B}}_\alpha(t) = e^{i\hat{\mathcal{H}}_B t}\hat{\mathcal{B}}_\alpha e^{-i\hat{\mathcal{H}}_B t}$ is the bath interaction term in the interaction picture. By inserting $\hat{\mathcal{H}}_I(t)$ into the master equation we obtain after some algebra:

$$\begin{aligned}\frac{d}{dt}\rho_S(t) &= \sum_{\omega\omega'}\sum_{\alpha\beta} e^{i(\omega'-\omega)t}\Gamma_{\alpha\beta}(\omega) \\ &\times \left[\hat{\mathcal{A}}_\beta(\omega)\rho_S(t)\hat{\mathcal{A}}_\alpha^\dagger(\omega') - \hat{\mathcal{A}}_\alpha^\dagger(\omega')\hat{\mathcal{A}}_\beta(\omega)\rho_S(t)\right] \\ &+ \text{h.c.},\end{aligned} \tag{1.33}$$

where h.c. stands for the Hermitian conjugated, and

$$\Gamma_{\alpha\beta}(\omega) \equiv \int_0^\infty ds e^{i\omega s} \langle \hat{\mathcal{B}}_\alpha^\dagger(t) \hat{\mathcal{B}}_\beta(t-s) \rangle$$

is the Fourier transform of the reservoir correlation functions:

$$\begin{aligned} \langle \hat{\mathcal{B}}_\alpha^\dagger(t) \hat{\mathcal{B}}_\beta(t-s) \rangle &= \langle \hat{\mathcal{B}}_\alpha^\dagger(s) \hat{\mathcal{B}}_\beta(0) \rangle \\ &\equiv \mathrm{Tr}\left[ \hat{\mathcal{B}}_\alpha^\dagger(s) \hat{\mathcal{B}}_\beta(0) \rho_B \right], \end{aligned} \tag{1.34}$$

where the first equality holds assuming $\rho_B$ as a stationary state of the reservoir. The RWA consists in neglecting rapidly oscillating terms for which $\omega \neq \omega'$. The typical timescale $\tau_S$ of the system's intrinsic evolution is given by the characteristic value of $|\omega - \omega'|^{-1}$. If $\tau_S$ is small compared to the relaxation time $\tau_R$, the terms $e^{i(\omega'-\omega)t}$ oscillates rapidly compared to the timescale over which the system changes appreciably. Therefore, these terms can be neglected, resulting in the following master equation:

$$\begin{aligned} \frac{d}{dt}\rho_S(t) &= \sum_\omega \sum_{\alpha\beta} \Gamma_{\alpha\beta}(\omega) \\ &\times \left[ \hat{\mathcal{A}}_\beta(\omega) \rho_S(t) \hat{\mathcal{A}}_\alpha^\dagger(\omega) - \hat{\mathcal{A}}_\alpha^\dagger(\omega) \hat{\mathcal{A}}_\beta(\omega) \rho_S(t) \right] \\ &+ \text{h.c.}. \end{aligned} \tag{1.35}$$

In general we can write $\Gamma_{\alpha\beta}(\omega) = \frac{1}{2}\gamma_{\alpha\beta}(\omega) + iS_{\alpha\beta}(\omega)$, where, for fixed $\omega$, $\gamma_{\alpha\beta}(\omega) = \int_{-\infty}^\infty ds e^{i\omega s} \langle \hat{\mathcal{B}}_\alpha^\dagger(s) \hat{\mathcal{B}}_\beta(0) \rangle$ is a positive matrix and $S_{\alpha\beta}(\omega)$ is a Hermitian matrix. With these definitions the master equation becomes:

$$\begin{aligned} \frac{d}{dt}\rho_S(t) &= -i\left[ \hat{\mathcal{H}}_{LS}, \rho_S(t) \right] \\ &+ \sum_\omega \sum_{\alpha\beta} \gamma_{\alpha\beta}(\omega) \Big( \hat{\mathcal{A}}_\beta(\omega) \rho_S(t) \hat{\mathcal{A}}_\alpha^\dagger(\omega) \\ &- \frac{1}{2} \left\{ \hat{\mathcal{A}}_\alpha^\dagger(\omega) \hat{\mathcal{A}}_\beta(\omega), \rho_S(t) \right\} \Big), \end{aligned} \tag{1.36}$$

where the first term gives a Hamiltonian contribution to the dynamics and contains the so-called Lamb shift Hamiltonian $\hat{\mathcal{H}}_{LS} = \sum_\omega \sum_{\alpha\beta} S_{\alpha\beta}(\omega) \hat{\mathcal{A}}_\alpha^\dagger(\omega) \hat{\mathcal{A}}_\beta(\omega)$, the second term describes the dissipation and it is usually known as the dissipator. The Schrödinger

picture master equation is simply obtained by adding the system Hamiltonian to the unitary part of Eq. 1.36. In this way $\hat{\mathcal{H}}_{LS}$, since it commutes with $\hat{\mathcal{H}}_S$, effectively acts as a renormalization of the energy levels of $\hat{\mathcal{H}}_S$ due to the coupling between the system and the reservoir. However, in many cases, the contribution of $\hat{\mathcal{H}}_{LS}$ is negligible, for this reason, from this point forward, we will neglect $\hat{\mathcal{H}}_{LS}$ for the sake of simplicity.

Eq. 1.36 can be brought to the Lindblad form by diagonalizing $\gamma_{\alpha\beta}(\omega)$:

$$\begin{aligned}\frac{d}{dt}\rho_S(t) &= -i\left[\hat{\mathcal{H}}_S, \rho_S(t)\right] \\ &+ \sum_{\omega}\sum_{\alpha}\tilde{\gamma}_{\alpha}(\omega)\Big(\hat{\mathcal{C}}_{\alpha}(\omega)\rho_S(t)\hat{\mathcal{C}}^{\dagger}_{\alpha}(\omega) \\ &- \frac{1}{2}\left\{\hat{\mathcal{C}}^{\dagger}_{\alpha}(\omega)\hat{\mathcal{C}}_{\alpha}(\omega), \rho_S(t)\right\}\Big),\end{aligned} \tag{1.37}$$

where $\hat{\mathcal{C}}_{\alpha}(\omega)$ are related to $\hat{\mathcal{A}}_{\alpha}(\omega)$ by the diagonalization matrix. Up to this point the derivation of the master equation is general; now we explicitly model the bath to get an expression for $\gamma_{\alpha\beta}(\omega)$. We consider a generic ensemble of Two-Level Systems (TLSs) coupled to a bath of harmonic oscillators:

$$\hat{\mathcal{H}}_B = \sum_{k=1}^{\infty}\omega_k \hat{b}^{\dagger}_k \hat{b}_k, \tag{1.38}$$

where the operators $\hat{b}_k$ ($\hat{b}^{\dagger}_k$) represent the annihilation (creation) operators of oscillator $k$, $\omega_k$ being the charateristic frequency of the $k$-th mode. The bath initial state is the Gibbs thermal state at inverse temperature $\beta$: $\rho_B = \exp(-\beta\hat{\mathcal{H}}_B)/\mathcal{Z}$, where $\mathcal{Z} = \mathrm{Tr}[\exp(-\beta\hat{\mathcal{H}}_B)]$ is the partition function and we assumed $k_B = 1$. As an interaction Hamiltonian we consider the following, which is fairly standard in the spin-bosons model case (see [2, 9, 10]), where we assume that the oscillators couple to each TLS in the same way:

$$\hat{\mathcal{H}}_I = \sum_{i=1}^{N}\hat{\sigma}^{\alpha}_i \otimes \sum_{k=1}^{\infty} g_k(\hat{b}^{\dagger}_k + \hat{b}_k) \equiv \hat{\mathcal{V}} \otimes \hat{\mathcal{B}}, \tag{1.39}$$

where $g_k$ is the bath coupling strength between the $k$-th mode and the system. Here, we have not yet specified which spin

direction is coupled to the bath and the index $\alpha$ is left generic for this reason. Under these assumptions it is straightforward to show (see Appendix H of [10] for the explicit calculation) that the reservoir correlation function takes the following form:

$$\begin{aligned}\langle\hat{\mathcal{B}}(t)\hat{\mathcal{B}}(0)\rangle &= \sum_{k=0}^{\infty}\frac{g_k^2}{1-e^{-\beta\omega_k}}\left(e^{-i\omega_k t}+e^{i\omega_k t-\beta\omega_k}\right)\\ &= \int_0^{\infty}d\tilde{\omega}\,\frac{J(\tilde{\omega})}{1-e^{-\beta\tilde{\omega}}}\\ &\times \left(e^{-i\tilde{\omega}t}+e^{i\tilde{\omega}t-\beta\tilde{\omega}}\right), \end{aligned} \tag{1.40}$$

where, after the second equality, we have replaced the sum over $k$ with an integral over $\tilde{\omega}$ by defining the bath spectral function $J(\tilde{\omega}) \equiv \sum_k g_k^2\,\delta(\tilde{\omega}-\omega_k)$, which characterizes how different frequencies of the bath modes couple to the system. We want to stress that in this expression $\tilde{\omega}$ refers to the frequencies of the environment modes, and thus $\tilde{\omega}\in[0,+\infty)$. At this point, we only need to calculate the Fourier transform of this expression to derive the rates $\gamma(\omega)$:

$$\begin{aligned}\gamma(\omega) &= \int_{-\infty}^{\infty}dt\,e^{i\omega t}\int_0^{\infty}d\tilde{\omega}\,\frac{J(\tilde{\omega})}{1-e^{-\beta\tilde{\omega}}}\left(e^{-i\tilde{\omega}t}+e^{i\tilde{\omega}t-\beta\tilde{\omega}}\right)\\ &= \int_0^{\infty}d\tilde{\omega}\,2\pi J(\tilde{\omega})\Big[[n(\tilde{\omega})+1]\,\delta(\omega-\tilde{\omega})\\ &+ n(\tilde{\omega})\delta(\omega+\tilde{\omega})\Big], \end{aligned} \tag{1.41}$$

where, from the first to the second line, we calculated the Fourier transform using the properties of the Dirac's delta function and we defined $n(\tilde{\omega}) = (e^{\beta\tilde{\omega}}-1)^{-1}$, that is the thermal occupation number of a bosonic mode with energy $\tilde{\omega}$. This last equation offers an interesting physical interpretation: one finds two terms, both proportional to the spectral density, the first term describes emission of energy into the environment while the second describes the probability of absorption of energy from the environment, which is only possible if a mode of energy $\omega$ is occupied

(absorption occurs when $\omega < 0$). Furthermore, this final integral can be computed exactly, yielding:

$$\begin{aligned}\gamma(\omega) &= 2\pi\Big[J(\omega)\,[n(\omega)+1]\,\Theta(\omega) + J(-\omega)n(-\omega)\Theta(-\omega)\Big] \\ &= 2\pi J(|\omega|)\Big[[n(|\omega|)+1]\,\Theta(\omega) + n(|\omega|)\Theta(-\omega)\Big] \\ &= \frac{2\pi J(|\omega|)}{1-e^{-\beta|\omega|}}(\Theta(\omega) + e^{-\beta|\omega|}\Theta(-\omega)), \end{aligned} \tag{1.42}$$

where $\Theta(\omega)$ is the Heaviside function.

In summary, the master equation can be written as follows:

$$\begin{aligned}\frac{d}{dt}\rho_S(t) &= -i\left[\hat{\mathcal{H}}_S, \rho_S(t)\right] \\ &+ \sum_\omega \left(\hat{\mathcal{L}}_\omega \rho_S(t) \hat{\mathcal{L}}_\omega^\dagger - \frac{1}{2}\left\{\hat{\mathcal{L}}_\omega^\dagger \hat{\mathcal{L}}_\omega, \rho_S(t)\right\}\right), \end{aligned} \tag{1.43}$$

with the jump operators $\hat{\mathcal{L}}_\omega$ defined as:

$$\begin{aligned}\hat{\mathcal{L}}_\omega &= \sqrt{\gamma(\omega)} \sum_{\epsilon'-\epsilon=\omega} |\epsilon\rangle\langle\epsilon|\hat{\mathcal{V}}|\epsilon'\rangle\langle\epsilon'| \\ &= \sqrt{\gamma(\omega)} \sum_{\epsilon'-\epsilon=\omega} |\mathcal{V}_{\epsilon\epsilon'}||\epsilon\rangle\langle\epsilon'|, \end{aligned} \tag{1.44}$$

with $\omega = \epsilon' - \epsilon$, $|\epsilon\rangle$ ($|\epsilon'\rangle$) being an eigenstate of $\hat{\mathcal{H}}_S$ with energy $\epsilon$ ($\epsilon'$) and finally $\mathcal{V}_{\epsilon\epsilon'} = \langle\epsilon|\hat{\mathcal{V}}|\epsilon'\rangle$.

The resulting master equation is precisely the GKSL form, consistent with the derivation presented in the previous section. In addition, the microscopic approach provides a recipe to identify the Lindblad operators, which will be essential later on to recover a consistent thermodynamic description of open quantum systems. We now turn to an alternative approach, based on collision models, which will prove particularly useful in the context of continuous measurements.

### 1.2.3 *Collision Model Derivation*

In order to make the derivation of the stochastic master equation for continuously monitored quantum systems more transparent, let us consider the following pedagogical derivation of the

Lindblad master equation within the framework of input-output theory [4]. This approach clearly illustrates how the collision model emerges from a microscopic description and provides the ideal setting for deriving the stochastic master equation. Let us consider a generic quantum system S interacting with an environment of bosonic modes B. The total Hamiltonian of the system can be generically written as

$$\hat{\mathcal{H}} = \hat{\mathcal{H}}_S + \hat{\mathcal{H}}_B + \hat{\mathcal{H}}_I, \tag{1.45}$$

where $\hat{\mathcal{H}}_S$ is a generic Hamiltonian acting on the system degrees of freedom, while

$$\hat{\mathcal{H}}_B = \int_0^\infty d\omega\, \omega \hat{b}_\omega^\dagger \hat{b}_\omega, \tag{1.46}$$

where the operators $\hat{b}_\omega$ satisfy the bosonic commutation relations $[\hat{b}_\omega, \hat{b}_{\omega'}^\dagger] = \delta(\omega - \omega')$. A further assumption is that the interaction Hamiltonian is linear in $\hat{b}_\omega$, meaning:

$$\hat{\mathcal{H}}_I = i \int_0^\infty d\omega \sqrt{\frac{\kappa(\omega)}{2\pi}} (\hat{c}\hat{b}_\omega^\dagger - \hat{c}^\dagger \hat{b}_\omega), \tag{1.47}$$

with $\hat{c}$ being a generic system operator. $\kappa(\omega)$ determines the strength of the interaction between the system and the bosonic mode $\omega$. Let us now move to the interaction picture with respect to the free Hamiltonian $\hat{\mathcal{H}}_0 = \hat{\mathcal{H}}_S + \hat{\mathcal{H}}_B$, first we assume that the interaction strength is constant ($\kappa(\omega) = \kappa$) within a large frequency bandwidth ($\mathcal{W} = [\omega_0 - \xi, \omega_0 + \xi]$) and zero outside this region. The large frequency bandwidth is crucial for the validity of the Markovian approximation in the system's dynamics. Second, we assume that the interaction picture system operators acquires a phase $\hat{c}(t) = \hat{c}e^{-i\omega_0(t-t_0)}$, where $t_0$ is the initial time when the Schrodinger and the interaction pictures coincide. It is easy to prove that the interaction picture interaction Hamiltonian can be written as

$$\hat{\mathcal{H}}_{int}(t) = e^{i\hat{\mathcal{H}}_0(t-t_0)} \hat{\mathcal{H}}_{int} e^{-i\hat{\mathcal{H}}_0(t-t_0)} = i\sqrt{k}(\hat{c}\hat{b}_t^\dagger - \hat{c}^\dagger \hat{b}_t), \tag{1.48}$$

where we have defined the so-called input modes as

$$\hat{b}_t = \frac{1}{\sqrt{2\pi}} \int_{\mathcal{W}} d\omega\, \hat{b}_\omega e^{-i(\omega-\omega_0)(t-t_0)}. \tag{1.49}$$

This system can be effectively interpreted as a continuous collision model, where the input modes act as auxiliary subsystems that sequentially interact with the main system, while the output modes correspond to the input modes after the interaction. Indeed, by evaluating the commutation relations of the input modes, we find that:

$$\left[\hat{b}_t, \hat{b}^\dagger_{t'}\right] = \frac{1}{2\pi}\int_{-\theta}^{\theta} d\omega\, e^{-i\omega(t-t')} \simeq \delta(t-t'), \tag{1.50}$$

where the last equality holds when the frequency bandwidth is much larger than all the other frequencies entering the dynamics (i.e. $\theta \gg \kappa$). Thus, the input modes can be effectively regarded as white-noise operators, delta-correlated in time. The resulting dynamics can then be interpreted as an infinite collection of uncorrelated quantum systems that interact with the main system one at a time, effectively realizing the continuum limit of a collision model, as previously discussed. However, the input operators $\hat{b}_t$ cannot be interpreted as proper annihilation operators, as their equal-time commutation relation is not well defined. For this reason, we define:

$$\delta\hat{b}_t = \int_t^{t+\delta t} dt'\, \hat{b}_{t'}, \tag{1.51}$$

leading to the commutator:

$$\left[\delta\hat{b}_t, \delta\hat{b}^\dagger_t\right] = \mathcal{I}\,\delta t. \tag{1.52}$$

In the infinitesimal limit $\delta t \to dt$ by definition, we have $\delta\hat{b}_t \to d\hat{b}_t = \hat{b}_t\, dt$, leading to:

$$\left[d\hat{b}_t, d\hat{b}^\dagger_t\right] = \left[\hat{b}_t, \hat{b}^\dagger_t\right] dt^2 = \mathcal{I}\, dt. \tag{1.53}$$

Finally, by defining $\hat{B}_t = \frac{1}{\sqrt{dt}}\hat{b}_t$ we obtain a new set of bosonic operators that act as proper creation and annihilation operators and satisfy the canonical commutation relations at each time, i.e.

$$\left[\hat{B}_t, \hat{B}^\dagger_t\right] = \mathcal{I}. \tag{1.54}$$

In this way, we can formally interpret the global Hilbert space as a tensor product between the system $\mathbb{H}_S$ and an infinite-dimensional Hilbert space $\mathbb{H}_{B_t}$ composed of independent input modes, each corresponding to a quantum harmonic oscillator:

$$\mathbb{H} = \mathbb{H}_S \bigotimes_{t\in\mathbb{R}} \mathbb{H}_{B_t}. \tag{1.55}$$

In order to derive a master equation in the Lindblad formalism, we need to make some (rather standard) assumptions. First, we assume that the global state of the system and the environment remains factorized, with the bath remaining in a fixed reduced state $\forall t$:

$$\rho_{tot}(t) = \rho(t) \otimes \rho_t, \tag{1.56}$$

with $\rho_t = |0\rangle_t \langle 0|_t$ being the vacuum state of $\mathbb{H}_{B_t}$ satisfying $\hat{B}_t |0\rangle_t = 0$ and $\hat{B}_t^\dagger |0\rangle_t = |1\rangle_t$ at each $t$. This choice corresponds to considering the environment as a bosonic bath in thermal equilibrium at zero temperature at all times. This is sufficient for our purposes; however, the more general case of a thermal environment at non-zero temperature can be derived with similar arguments. The environment in the vacuum state at each time, together with the delta-correlated white-noise nature of the input operators, ensures Markovianity in the dynamics, i.e., the environment's correlation time is much shorter than the characteristic timescale of the system's evolution (see [4] for details). This corresponds to the standard Born-Markov approximation used before in the derivation of the Lindblad master equation. The evolved state for an infinitesimal time interval $dt$ can be written, in the interaction picture, as

$$\begin{aligned} \rho_{tot}(t+dt) &= \hat{\mathcal{U}}(t, t+dt)\rho_{tot}(t)\hat{\mathcal{U}}(t, t+dt)^\dagger = \\ &= e^{-i\hat{\mathcal{H}}_I(t)dt}\rho_{tot}(t)e^{i\hat{\mathcal{H}}_I(t)dt}, \end{aligned} \tag{1.57}$$

from this, the state of the system is obtained by tracing out the environmental degrees of freedom $\rho(t+dt) = \mathrm{Tr}_B\left[\rho_{tot}(t+dt)\right]$. We now expand to the second order the evolution operator:

$$\begin{aligned} \hat{\mathcal{U}}(t, t+dt) &= e^{-i\hat{\mathcal{H}}_I(t)dt} = \exp\left[\sqrt{\kappa}dt\left(\hat{c}\hat{b}_t^\dagger - \hat{c}^\dagger\hat{b}_t\right)\right] \\ &= \exp\left[\sqrt{\kappa dt}\left(\hat{c}\hat{B}_t^\dagger - \hat{c}^\dagger\hat{B}_t\right)\right] \\ &\approx \mathcal{I} + \sqrt{\kappa dt}\left(\hat{c}\hat{B}_t^\dagger - \hat{c}^\dagger\hat{B}_t\right) + \\ &+ \frac{1}{2}\kappa dt\left(\hat{c}^2\hat{B}_t^{\dagger 2} + \hat{c}^{\dagger 2}\hat{B}_t^2 - \hat{c}\hat{c}^\dagger\hat{B}_t^\dagger\hat{B}_t - \hat{c}^\dagger\hat{c}\hat{B}_t\hat{B}_t^\dagger\right) \end{aligned} \tag{1.58}$$

which, for $\rho_{tot}(t) = \rho(t) \otimes |0\rangle_t \langle 0|_t$, yields up to the first order in $dt$:

$$\begin{aligned} \rho_{tot}(t+dt) &\approx \rho(t) \otimes |0\rangle_t \langle 0|_t + \\ &+ \sqrt{\kappa}\big(\hat{c}\rho(t) \otimes |1\rangle_t \langle 0|_t + \rho(t)\hat{c}^\dagger \otimes |0\rangle_t \langle 1|_t\big)\sqrt{dt} + \\ &+ \kappa\big(\hat{c}\rho(t)\hat{c}^\dagger \otimes |1\rangle_t \langle 1|_t\big)dt + \\ &+ \frac{\kappa}{2}\big(\sqrt{2}\hat{c}^2\rho(t) \otimes |2\rangle_t \langle 0|_t - \hat{c}^\dagger\hat{c}\rho(t) \otimes |0\rangle_t \langle 0|_t + \text{h.c.}\big)dt. \end{aligned} \tag{1.59}$$

Finally, the partial trace over the environment gives

$$\rho(t+dt) = \rho(t) + \kappa\hat{c}\rho(t)\hat{c}^\dagger dt - \frac{\kappa}{2}\big\{\hat{c}^\dagger\hat{c}, \rho(t)\big\}dt, \tag{1.60}$$

which can be written as a differential equation as

$$\frac{d\rho(t)}{dt} = \kappa\hat{c}\rho(t)\hat{c}^\dagger - \frac{1}{2}k\big\{\hat{c}^\dagger\hat{c}, \rho(t)\big\} = \kappa\mathcal{D}[\hat{c}]\rho(t), \tag{1.61}$$

The latter equation can, of course, be generalized by adding a Hamiltonian term acting on the system (with the caveat that the Hamiltonian evolution must be slow enough to preserve Markovianity). Moreover, the operator $\hat{c}$ can be replaced by a collection of jump operators $\{\hat{c}_i\}$, which yields the usual general form of a Markovian Lindblad master equation:

$$\frac{d\rho(t)}{dt} = -i\big[\hat{\mathcal{H}}, \rho(t)\big] + \sum_i \kappa_i \mathcal{D}[\hat{c}_i]\rho(t) \equiv \mathcal{L}\rho(t) \tag{1.62}$$

## 1.3 CONTINUOUSLY MONITORED QUANTUM SYSTEMS

In the previous section, we derived the Markovian master equation describing open quantum systems in three different fashions, the last of which modeled the environment as a continuous stream of harmonic oscillators $\hat{B}_t$, with the environmental degrees of freedom traced out after their interaction with the system. We now move to the case where the environment is continuously monitored: after each infinitesimal interaction, the environment state associated with the operator $\hat{B}_t$ is measured. This framework, known as a collision model [8], provides a clear description of the interplay between system and environment and offers a systematic route to connect unconditional Lindblad dynamics

with conditional stochastic evolutions under continuous measurements.

The markovian dynamics of an open quantum systems is characterized by a continuous leakage of information into the environment. By performing measurements on it, is possible to retrieve part of this lost information and thereby gain insight into the system. Such monitoring, however, is indirect and intrinsically inefficient, since only a fraction of the information can be recovered. As a result, the measurement back-action exerts only a weak influence on the system state. When these weak measurements are performed continuously, the system follows a stochastic evolution that manifests as random trajectories of its quantum state, usually referred to as quantum trajectories. These stochastic evolutions have been observed experimentally in several physical platforms, including superconducting qubits [11, 12, 13], optomechanical devices [14, 15], and hybrid systems [16], and have been employed in a variety of contexts such as feedback protocols and cooling strategies.

The theoretical description of such dynamics is provided by the framework of Stochastic Master Equations (SMEs) [17]. In this picture, the deterministic evolution of open quantum systems is supplemented with stochastic contributions that capture the randomness introduced by continuous measurements. The form of the SME depends on the measurement protocol: for example, PD gives rise to quantum jump trajectories, while Homodyne Detection (HD) leads to diffusive stochastic dynamics [18, 19]. Both cases will be analyzed in the following.

### 1.3.1 *Photo-detection*

The POVM associated with a photo-detector is given by the Fock basis $\{|n\rangle_t \langle n|_t\}$ (from now on we will omit the subscript $t$ for simplicity). Since we consider the environment initially in the ground state, the only possible measurement outcomes are either photon detection $|1\rangle\langle 1|$ or no detection $|0\rangle\langle 0|$. In the former case, the conditional (unnormalized) state after the measurement can be easily found from 1.59 as

$$\tilde{\rho}_0^c(t+dt) = \langle 0|\rho_{tot}(t+dt)|0\rangle = \rho^c(t) - \frac{\kappa}{2}\{\rho^c(t), \hat{c}^\dagger\hat{c}\}dt, \quad (1.63)$$

with probability

$$p_0(t+dt) = \mathrm{Tr}\left[\tilde{\rho}_0^c(t+dt)\right] = 1 - \kappa\langle\hat{c}^\dagger\hat{c}\rangle_t\, dt, \tag{1.64}$$

which gives the normalized state:

$$\begin{aligned}
\rho_0^c(t+dt) &= \frac{\tilde{\rho}_0^c(t+dt)}{p_0(t+dt)} \approx \\
&\approx \left(\rho^c(t) - \frac{\kappa}{2}\left\{\rho^c(t), \hat{c}^\dagger\hat{c}\right\}dt\right)\left(1 + \kappa\langle\hat{c}^\dagger\hat{c}\rangle_t\, dt\right) \approx \\
&\approx \rho^c(t) + \rho^c(t)\langle\hat{c}^\dagger\hat{c}\rangle_t\kappa\, dt - \frac{\kappa}{2}\left\{\rho^c(t), \hat{c}^\dagger\hat{c}\right\}dt \equiv \\
&\equiv \rho^c(t) - \frac{\kappa}{2}\mathcal{H}[\hat{c}^\dagger\hat{c}]\rho^c(t)dt,
\end{aligned} \tag{1.65}$$

where we defined the superoperator $\mathcal{H}[\hat{A}]\bullet = \hat{A}\bullet + \bullet\hat{A}^\dagger - \langle\hat{A} + \hat{A}^\dagger\rangle\bullet$. When no photons are detected, the conditional state reads

$$\tilde{\rho}_1^c(t+dt) = \langle 1|\,\rho_{tot}(t+dt)\,|1\rangle = \kappa\hat{c}\rho^c(t)\hat{c}^\dagger dt, \tag{1.66}$$

with probability

$$p_1(t+dt) = \mathrm{Tr}\left[\tilde{\rho}_1^c(t+dt)\right] = \kappa\langle\hat{c}^\dagger\hat{c}\rangle_t\, dt, \tag{1.67}$$

and thus the normalized state:

$$\rho_1^c(t+dt) = \frac{\tilde{\rho}_1^c(t+dt)}{p_1(t+dt)} = \frac{\hat{c}\rho^c(t)\hat{c}^\dagger}{\langle\hat{c}^\dagger\hat{c}\rangle_t}. \tag{1.68}$$

The conditional evolution of the density matrix associated with the two possible measurement outcomes can be unified by introducing a stochastic increment $dN_t$, corresponding to a Poisson process. This type of process is commonly used to describe the random occurrence of discrete events over time and is characterized by a time-dependent rate $\lambda(t)$, indicating the expected number of events per unit time. During an infinitesimal time interval $dt$, the probability of observing more than one event becomes negligible, and the probability of detecting a single event scales linearly with $\lambda(t)dt$. Accordingly, the increment $dN_t$ is a binary random variable taking values in $\{0, 1\}$, where the probabilities depend on the instantaneous event rate. In our context, the mean number of detection events within the interval $[t, t+dt]$ is given by the expectation $\mathbb{E}[dN_t] = \kappa\langle\hat{c}^\dagger\hat{c}\rangle_t dt$, which

determines the probability of a quantum jump occurring due to photon detection. In this way the equation for the conditional density operator can be conveniently written as

$$\begin{aligned} d\rho^c(t) &= \rho^c(t+dt) - \rho^c(t) = dN_t(\rho_1^c(t+dt) - \rho^c(t)) + \\ &+ (1 - dN_t)(\rho_0^c(t+dt) - \rho^c(t)), \end{aligned} \tag{1.69}$$

which up to the first order in $dt$ becomes

$$d\rho^c(t) = -\frac{\kappa}{2}\mathcal{H}[\hat{c}^\dagger\hat{c}]\rho^c(t)dt + \left(\frac{\hat{c}\rho^c(t)\hat{c}^\dagger}{\langle\hat{c}^\dagger\hat{c}\rangle_t} - \rho^c(t)\right)dN_t. \tag{1.70}$$

By averaging over all possible outcomes of the measurement, one recovers the evolution of the system's density matrix in the absence of any conditioning, that is, a Lindblad-type master equation:

$$\mathbb{E}[d\rho_c(t)] = \kappa\mathcal{D}[\hat{c}]\rho(t)\,dt. \tag{1.71}$$

In other words, ignoring (or tracing over) the measurement results corresponds to summing over all possible stochastic trajectories. This procedure yields the same master equation as if no measurement had occurred. Individual realizations generated by the monitoring process are referred to as a quantum trajectory ensemble, and together they provide an unraveling of the master equation for the unconditional state $\rho(t) = \mathbb{E}[\rho_c(t)]$.

An important remark is that when the detection is perfectly efficient (which is not always the case, as we shall see), the SME preserves the purity of pure quantum states. In such cases, if the initial state is pure $|\psi_0\rangle$, the evolution can be described directly by a Stochastic Schrödinger Equation (SSE) for the state vector $|\psi^c(t)\rangle$. This evolution reads:

$$d|\psi^c(t)\rangle = \left[\frac{\kappa}{2}\left(\langle\hat{c}^\dagger\hat{c}\rangle_t - \hat{c}^\dagger\hat{c}\right)dt + \left(\frac{\hat{c}}{\sqrt{\langle\hat{c}^\dagger\hat{c}\rangle_t}} - 1\right)dN_t\right]|\psi^c(t)\rangle\,, \tag{1.72}$$

where we decomposed the infinitesimal increment of the conditional density matrix in terms of a pure state: $d\rho^c = \left(d|\psi^c\rangle\right)\langle\psi^c| + |\psi^c\rangle\left(d\langle\psi^c|\right) + \left(d|\psi^c\rangle\right)\left(d\langle\psi^c|\right)$. Since the SSE describes the evolution of pure state vectors instead of density matrices, it effectively

reduces the dimensionality of the problem. This makes it a powerful and efficient tool for numerically simulating open quantum systems, especially when averaging over many trajectories is computationally feasible. In realistic situations, measurements are not always perfectly efficient. For this reason, it is common to introduce a detection efficiency parameter $\eta \in [0, 1]$, which represents the probability that a given photon event is actually observed. As a result, only a fraction $\eta$ of the emission events contribute to the measurement back-action, while the remaining $1-\eta$ are effectively ignored and contribute to the average (unmonitored) dynamics. Starting from the Lindblad master equation, this inefficiency can be incorporated by decomposing the dissipator as follows:

$$\frac{d\rho(t)}{dt} = \eta\kappa\mathcal{D}[\hat{c}]\rho(t) + (1-\eta)\kappa\mathcal{D}[\hat{c}]\rho(t), \tag{1.73}$$

where only the term proportional to $\eta$ is associated with the measurement-induced stochastic evolution. Applying the same methodology as for the fully efficient case, it is easy to deduce the stochastic master equation for imperfect photo-detection:

$$\begin{aligned} d\rho(t) &= -\frac{\eta\kappa}{2}\mathcal{H}[\hat{c}^\dagger\hat{c}]\rho(t)\,dt + \left(\frac{\hat{c}\rho(t)\hat{c}^\dagger}{\langle\hat{c}^\dagger\hat{c}\rangle_t} - \rho(t)\right) dN_t + \\ &+ (1-\eta)\kappa\mathcal{D}[\hat{c}]\rho(t)\,dt. \end{aligned} \tag{1.74}$$

### 1.3.2 *Homodyne Detection*

In the case of HD, the operators associated with measurement outcomes are $\{|x_\theta\rangle\langle x_\theta|\}$, the eigenstates of the quadrature operator $\hat{\mathfrak{X}}_\theta = (e^{i\theta}\hat{B}_t + e^{-i\theta}\hat{B}_t^\dagger)/\sqrt{2}$. The (unnormalized) conditional state is then

$$\begin{aligned} &\tilde{\rho}^c(t+dt) = \\ &= \mathrm{Tr}\big[\hat{\mathcal{U}}(t, t+dt)(\rho(t)\otimes|0\rangle\langle 0|)\hat{\mathcal{U}}(t, t+dt)^\dagger(\mathcal{I}\otimes|x_\theta\rangle\langle x_\theta|)\big] = \\ &= \langle x_\theta|\,\hat{\mathcal{U}}(t, t+dt)(\rho(t)\otimes|0\rangle\langle 0|)\hat{\mathcal{U}}(t, t+dt)^\dagger\,|x_\theta\rangle, \end{aligned} \tag{1.75}$$

with probability

$$p_{x_\theta}(t+dt) = \mathrm{Tr}\big[\tilde{\rho}^c(t+dt)\big]. \tag{1.76}$$

The conditional state can be expanded at lowest order as

$$\begin{aligned}\tilde{\rho}^c(t+dt) &\approx |\langle x_\theta||0\rangle|^2\rho^c(t) + \\ &+ \big(\hat{c}\rho^c(t)\langle x_\theta||1\rangle\langle 0||x_\theta\rangle + \\ &+ \rho^c(t)\hat{c}^\dagger\langle x_\theta||0\rangle\langle 1||x_\theta\rangle\big)\sqrt{\kappa dt} + o(\sqrt{\kappa dt}) = \\ &= \frac{1}{\sqrt{\pi}}e^{-x_\theta^2}\big[\rho^c(t) + \big(\hat{c}\rho^c(t)e^{i\theta} + \\ &+ \rho^c(t)\hat{c}^\dagger e^{-i\theta}\big)x_\theta\sqrt{2\kappa dt}\big] + o(\sqrt{\kappa dt}), \qquad (1.77)\end{aligned}$$

where we have used $|\langle x_\theta|0\rangle|^2 = \frac{1}{\sqrt{\pi}}e^{-x_\theta^2}$ and the identity $\langle x_\theta|1\rangle = \sqrt{2}e^{i\theta}\langle x_\theta|0\rangle$. This result leads to the expression for the probability up to order $dt$:

$$\begin{aligned}p_{x_\theta}(t+dt) &= p_{x_\theta}(t)\big(1+\sqrt{2\kappa dt}x_\theta\langle\hat{c}e^{i\theta} + \hat{c}\,\dagger\, e^{-i\theta}\rangle_t\big) + o(\sqrt{\kappa dt}) = \\ &\approx \frac{1}{\sqrt{\pi}}\exp\left[-\left(x_\theta - \sqrt{\frac{\kappa dt}{2}}\langle\hat{c}e^{i\theta} + \hat{c}^\dagger e^{-i\theta}\rangle_t\right)^2\right]. \qquad (1.78)\end{aligned}$$

To derive the conditional state and interpret it in terms of a stochastic process, we introduce the stochastic increment $dy_t$ and define the photocurrent $I(t)$, which takes into account the result of the measurement at time $t$. Specifically, we write:

$$dy_t = I(t)\,dt = \sqrt{2}\,dt\,x_\theta = \sqrt{\kappa}\langle\hat{c}e^{i\theta} + \hat{c}^\dagger e^{-i\theta}\rangle_t\,dt + dw_t, \quad (1.79)$$

where $dw_t$ is a stochastic (Gaussian) noise term known as a Wiener increment. This term has zero mean, $\mathbb{E}[dw_t] = 0$, and its square is a deterministic variable $dw_t^2 = dt$. These properties follow from Itô calculus [20] and are fundamental for working with continuous-time stochastic processes. The photocurrent can then be written as:

$$I(t) = \sqrt{\kappa}\langle\hat{c}e^{i\theta} + \hat{c}^\dagger e^{-i\theta}\rangle_t + \xi(t), \qquad (1.80)$$

where the term $\xi(t) = \frac{dw_t}{dt}$ represents a white noise delta-correlated contribution. In essence, the measured current is the expectation value of the selected quadrature (determined by the local oscillator phase $\theta$) plus a random Gaussian fluctuation. This decomposition is useful because it allows us to model the measurement outcome as a noisy signal centered around the expected value of the quadrature. Noise arises naturally from

the probabilistic nature of quantum measurements. We can now express $d\rho_c(t)$ (conditioned on the measurement outcome) as:

$$d\rho^c(t) = \sqrt{\kappa}\,\mathcal{H}[\hat{c}e^{i\theta}]\rho^c(t)\,dw_t + o(\sqrt{\kappa dt}). \tag{1.81}$$

To derive the full stochastic master equation for homodyne detection, we note that averaging over all possible realizations of the Wiener process must recover the Lindblad-type dissipative evolution of the unconditional state. Since the Wiener increment has zero mean, the missing term of order $dt$ can be easily computed. This leads to the following SME:

$$d\rho^c(t) = \kappa\mathcal{D}[\hat{c}]\rho^c(t)\,dt + \sqrt{\kappa}\,\mathcal{H}[\hat{c}e^{i\theta}]\rho^c(t)\,dw_t, \tag{1.82}$$

Once again, when the initial state is pure, the SME reduces to a SSE, providing a more efficient way to simulate quantum trajectories due to the reduced dimensionality of pure states:

$$\begin{aligned} d|\psi^c(t)\rangle &= \left[-\frac{\kappa}{2}\left(\hat{c}^\dagger\hat{c} - \hat{c}\langle\hat{c}+\hat{c}^\dagger\rangle_t + \frac{\langle\hat{c}+\hat{c}^\dagger\rangle_t^2}{4}\right)dt + \right. \\ &+ \left.\sqrt{\kappa}\left(\hat{c} - \frac{\langle\hat{c}+\hat{c}^\dagger\rangle_t}{2}\right)dw_t\right]|\psi^c(t)\rangle\,, \end{aligned} \tag{1.83}$$

here we set for simplicity $\theta = 0$. In the case of inefficient detection with efficiency $\eta$:

$$d\rho^c(t) = \kappa\mathcal{D}[\hat{c}]\rho^c(t)\,dt + \sqrt{\kappa\eta}\,\mathcal{H}[\hat{c}e^{i\theta}]\rho^c(t)\,dw_t. \tag{1.84}$$

## 1.4 SUMMARY

This chapter introduced the mathematical framework and a modern formulation of the postulates of quantum mechanics, tailored to systems interacting with an external environment and measurement devices. Restating the postulates served to clarify the assumptions of the standard formulation, fix the notation, and highlight their reinterpretation within quantum information theory. They prescribe how states are represented, how measurements are performed, and how systems evolve under dynamics or measurements.

We then reviewed the theory of open quantum systems, whose reduced dynamics is described by CPTP maps. Different derivations of the Markovian master equation were presented: via the

quantum operation formalism, from a microscopic Hamiltonian model, and through a collision model. All approaches converge to the GKSL equation, the most general description of Markovian quantum dynamics.

Finally, we considered the case of continuously monitored quantum systems. Weak measurements retrieve only partial information about the system, leading to stochastic evolutions known as quantum trajectories. These are described theoretically by SMEs. Depending on the measurement protocol, SMEs take different forms, for instance, quantum jumps under photodetection or diffusive dynamics under homodyne detection.

# 2

# INTRODUCTION TO QUANTUM THERMODYNAMICS

## 2.1 WORK, HEAT AND ENTROPY IN THE QUANTUM WORLD

Having established the general framework of closed and open quantum systems, we now move to the thermodynamic description of quantum processes. Classical thermodynamics provides a phenomenological account of energy conservation and entropy increase, while statistical mechanics connects these notions to equilibrium ensembles and fluctuation theorems. In quantum theory, laws of thermodynamics remain valid but require a careful reformulation, since energy exchanges can be mediated both by coherent control of the Hamiltonian and by incoherent interactions with the environment, while the concept of entropy must be formulated in terms of quantum states. This section is based on the book [21] and the seminal paper by Alicki [22].

### 2.1.1 *The First Principle*

In close analogy with the classical formulation, let us first consider *quasistatic processes*, during which a quantum system remains in equilibrium with a thermal environment while an external control parameter $\lambda$ slowly changes the system Hamiltonian $\hat{\mathcal{H}}_\lambda$. In this setting, the change in internal energy naturally separates into two contributions: variations of the state induced by interaction with the bath correspond to heat exchange, while variations due to changes in the Hamiltonian correspond to work performed on or by the system.

For weak coupling to a heat bath at inverse temperature $\beta$, the equilibrium state is given by the Gibbs thermal state,

$$\rho_{\mathrm{eq},\lambda} = \frac{e^{-\beta \hat{\mathcal{H}}_\lambda}}{\mathcal{Z}_\lambda}, \qquad \mathcal{Z}_\lambda = \mathrm{Tr}[e^{-\beta \hat{\mathcal{H}}_\lambda}], \tag{2.1}$$

and all thermodynamic potentials retain their familiar definitions: the internal energy $E = \mathrm{Tr}\big[\rho_{eq}\hat{\mathcal{H}}\big]$, and the Helmholtz free energy $F = -\beta^{-1}\ln\mathcal{Z}$ (omitting the $\lambda$ subscript for simplicity). With these, the thermodynamic entropy takes the standard Gibbs-von Neumann form:

$$S = \beta(E - F) = -\mathrm{Tr}\big[\rho_{eq}\ln\rho_{eq}\big]. \tag{2.2}$$

For isothermal and quasistatic processes, the entropy variation can then be written as

$$dS = \beta\big(\mathrm{Tr}[d\rho_{eq}\hat{\mathcal{H}}] + \mathrm{Tr}[\rho_{eq}d\hat{\mathcal{H}}] - dF\big) = \beta\,\mathrm{Tr}[d\rho_{eq}\hat{\mathcal{H}}] = \beta\,\delta Q, \tag{2.3}$$

where the second to last equality follows from a straightforward evaluation of $dF$. It is thus possible to distinguish two contributions to the change in internal energy: the part associated with state variations, identified as heat $\delta Q$, and the part associated with changes in the Hamiltonian, identified as work $\delta W = dF$. This directly leads to the first law of thermodynamics:

$$dE = \delta Q + \delta W \equiv \mathrm{Tr}[d\rho_{eq}\hat{\mathcal{H}}] + \mathrm{Tr}[\rho_{eq}d\hat{\mathcal{H}}], \tag{2.4}$$

highlighting the role of free energy as the portion of internal energy that can be converted into useful work, with the remaining contribution associated with the entropic cost of the process.

The same operational definitions of heat and work can be extended beyond equilibrium, to the time-dependent dynamics of open quantum systems. In the weak-coupling, Markovian regime, as we have seen in the previous chapter, the reduced dynamics of a system interacting with a thermal environment is described by a completely positive dynamical semigroup, generated by a Lindblad-type master equation. Within this framework, the instantaneous internal energy,

$$E(t) = \mathrm{Tr}\big[\rho_S(t)\,\hat{\mathcal{H}}_S(t)\big], \tag{2.5}$$

naturally satisfies

$$\dot{E} = \mathrm{Tr}\big[\dot{\rho}_S\hat{\mathcal{H}}_S\big] + \mathrm{Tr}\big[\rho_S\dot{\hat{\mathcal{H}}}_S\big], \tag{2.6}$$

which can be identified with the rate of heat and work exchange following Alicki's formulation:

$$\dot{Q}(t) = \mathrm{Tr}\big[\dot{\rho}_S\hat{\mathcal{H}}_S\big], \qquad \dot{W}(t) = \mathrm{Tr}\big[\rho_S\dot{\hat{\mathcal{H}}}_S\big]. \tag{2.7}$$

Heat corresponds to changes in the system energy due to variations of the state $\rho_S(t)$, i.e. incoherent exchanges with the environment, and it is directly associated with the dissipative part of the dynamics governed by the Lindblad operators $\hat{c}_i$:

$$Q(t) = \sum_i \kappa_i \int_0^t d\tau \, \mathrm{Tr}\left[\mathcal{D}[\hat{c}_i]\rho_S(\tau)\, \hat{\mathcal{H}}_S(\tau)\right], \tag{2.8}$$

while work corresponds to changes induced by external driving:

$$W(t) = \int_0^t d\tau \, \mathrm{Tr}\left[\rho_S(\tau)\, \frac{d\hat{\mathcal{H}}_S(\tau)}{d\tau}\right]. \tag{2.9}$$

This connection provides a natural bridge between equilibrium thermodynamics and the time-dependent dynamics of open quantum systems: in the weak-coupling, Markovian regime, the same definitions of heat and work retain their validity. Outside this regime, however, strong coupling and non-Markovian effects introduce system-bath correlations and memory, invalidating the simple separation between heat and work, as the system no longer remains close to an instantaneous equilibrium state.

### 2.1.2 *The Second Principle*

After establishing the framework for quantum work and heat, we now focus on the analysis of entropy production in quantum systems. To this end, we consider a system initially prepared in a steady-state $\rho_{ss}$ which, however, is not necessarily the Gibbs state of the system corresponding to the temperature of the environment. For a variation of the external parameter $\lambda$, the change in internal energy and von Neumann entropy can be written as

$$\Delta E = W + Q, \qquad \Delta S = \beta Q + \Sigma, \tag{2.10}$$

where $Q$ is the heat exchanged with the environment at inverse temperature $\beta$, and $\Sigma \geqslant 0$ is the irreversible entropy production. Notice that in the quasistatic, reversible limit $\Sigma = 0$, and thus recovering the standard thermodynamic identity $\Delta S = \beta Q$. Exploiting the first principle, the nonequilibrium entropy production can be written as

$$\Sigma = \Delta S - \beta \Delta E + \beta W, \tag{2.11}$$

and expressing the internal energy in terms of the system Gibbs state yields

$$\begin{aligned}\beta E &= \beta \,\mathrm{Tr}\big[\rho_{ss}\hat{\mathcal{H}}\big] = \beta \mathrm{Tr}\big[\rho_{ss}[-\frac{1}{\beta}(\ln \rho_{eq} + \ln \mathcal{Z})]\big] = \\ &= -\mathrm{Tr}\big[\rho_{ss} \ln \rho_{eq}\big] - \ln \mathcal{Z}. \end{aligned} \tag{2.12}$$

For a driving from $\lambda_0$ to $\lambda_1$, it can be shown (see [21]) that the total entropy production reads

$$\begin{aligned}\Sigma &= S(\rho_{ss}(\lambda_0)\|\rho_{eq}(\lambda_0)) - S(\rho_{ss}(\lambda_1)\|\rho_{eq}(\lambda_1)) + \\ &- \int_{\lambda_0}^{\lambda_1} d\lambda \,\mathrm{Tr}\big[\rho_{ss}(\lambda)\, \partial_\lambda \ln \rho_{eq}(\lambda)\big], \end{aligned} \tag{2.13}$$

where $S(\rho\|\sigma) = \mathrm{Tr}[\rho(\ln\rho - \ln\sigma)]$ denotes the quantum relative entropy. This expression provides an exact microscopic formula for the mean nonequilibrium entropy production of a driven open quantum system weakly coupled to a single thermal reservoir, and remains valid even for intermediate states far from equilibrium.

In the Limbladian dynamical setting, we can equivalently write

$$\Sigma = \Delta S - \beta Q = S(\rho(0)\|\rho_\beta) - S(\rho(t)\|\rho_\beta), \tag{2.14}$$

where $\rho_\beta$ is the Gibbs state at inverse temperature $\beta$. The instantaneous entropy production rate,

$$\sigma(t) = -\frac{d}{dt} S(\rho(t)\|\rho_\beta), \tag{2.15}$$

is non-negative ($\sigma(t) \geqslant 0$) in agreement with the second principle of thermodynamics. More generally, if the system relaxes to a non-equilibrium steady state $\bar{\rho}$, we can define

$$\bar{\Sigma} = S(\rho(0)\|\bar{\rho}) - S(\rho(t)\|\bar{\rho}), \qquad \bar{\sigma}(t) = \mathrm{Tr}\{\mathcal{L}[\rho(t)](\ln\bar{\rho} - \ln\rho(t))\}, \tag{2.16}$$

where $\mathcal{L}$ is the Lindblad generator of the dynamics and again $\bar{\sigma}(t) \geqslant 0$, that is known as Spohn's inequality [23].

## 2.2 THE PROBLEM OF WORK EXTRACTION

In the previous section, we gave a general introduction on the thermodynamics of open quantum systems and the fundamental concepts of heat, work, and entropy production. We now turn our attention to a different but closely related question: how to extract work from quantum systems. In particular, we focus on the concept of ergotropy [24, 25]. This quantity offers a fundamental measure of the maximum extractable work from a closed quantum system and will play a central role later on, when discussing the performance of quantum batteries.

In the second part of this chapter, we will extend the discussion to open quantum systems under continuous measurement, taking inspiration from the classical thought experiments of Maxwell's demon and Szilard's engine [26]. These examples illustrate the deep connection between information and thermodynamics, showing how knowledge about a system can be harnessed to extract additional work. To formalize this concept in the quantum scenario, we will introduce the notion of *daemonic ergotropy* [27, 28], which quantifies the extra work made accessible by exploiting the information gained through measurement, going beyond what is possible in the absence of monitoring.

### 2.2.1 *Ergotropy: extracting work from a closed quantum system*

A fundamental aspect in the study of work extraction from closed quantum systems is that these systems evolve under unitary operations, which are inherently non-dissipative. In this framework, the first law of thermodynamics

$$dE = \delta W + \delta Q \tag{2.17}$$

simplifies, as $\delta Q = 0$, and the work performed by the system is considered to be positive. For a finite size quantum system with Hamiltonian $\hat{\mathcal{H}}$ and initial state $\rho_0$, the work extracted through a unitary operarion $\hat{\mathcal{U}}$ is

$$\mathcal{W}_{\hat{\mathcal{U}}} = \mathrm{Tr}\big[\hat{\mathcal{H}}\rho_0\big] - \mathrm{Tr}\big[\hat{\mathcal{H}}(\hat{\mathcal{U}}\rho_0\hat{\mathcal{U}}^\dagger)\big]. \tag{2.18}$$

The maximum extractable work from $\rho_0$, known as *ergotropy*, is formally obtained by optimizing over all possible unitary operations:

$$\mathcal{E}(\rho_0) = \max_{\hat{U}} \mathcal{W}_{\hat{U}}. \tag{2.19}$$

We can further assume that the Hamiltonian of a (d)-dimensional system is written in its energy eigenbasis as

$$\hat{\mathcal{H}} = \sum_{i=0}^{d-1} \epsilon_i |\epsilon_i\rangle \langle\epsilon_i|, \quad \epsilon_i < \epsilon_{i+1}, \tag{2.20}$$

where, for simplicity, the spectrum is assumed to be non-degenerate.

*Passive states* are a central concept for the characterization of ergotropy, these are states from which no work can be extracted through any unitary operation, and they are formally defined as

$$\rho_p : \mathrm{Tr}[\hat{\mathcal{H}}\rho_p] \leqslant \mathrm{Tr}[\hat{\mathcal{H}}(\hat{U}\rho_p\hat{U}^\dagger)], \quad \forall \hat{U}, \tag{2.21}$$

and they can be represented in the Hamiltonian energy eigenbasis as

$$\rho_p = \sum_{i=0}^{d-1} r_i |\epsilon_i\rangle \langle\epsilon_i|, \quad r_i > r_{i+1}. \tag{2.22}$$

It is important to note that the notion of passivity is defined with respect to a specific Hamiltonian. Changing the Hamiltonian, or considering a reduced subsystem, does not guarantee that the state remains passive, as the ordering of populations depends on the particular energy spectrum under consideration. If we express the spectral decomposition of any initial state $\rho_0$ as

$$\rho_0 = \sum_{i=0}^{d-1} r_i |r_i\rangle \langle r_i|, \quad r_i > r_{i+1}, \tag{2.23}$$

then the state $\rho_p$ is said to be the passive state of $\rho_0$. In contrast, *active states* are those from which work can be extracted. The ergotropy of a generic active state can be decomposed into two distinct contributions: a coherent part, associated with the presence of coherences in the energy eigenbasis, and an incoherent part,

related to the populations of the energy levels. While the coherent contribution is extracted by consuming these coherences, the incoherent part arises from rearranging populations to minimize the energy. Since unitary operations preserve the eigenvalues of the density operator, this minimization can only be achieved by reordering the populations such that the largest eigenvalue corresponds to the lowest-energy eigenstate, the second-largest to the next-lowest, and so on. From this characterization, the definition of a passive state as diagonal in the energy eigenbasis, with its eigenvalues arranged in decreasing order with respect to the corresponding energies, becomes clear. Consequently, the unitary transformation that maximizes the extractable work is the one that maps the initial state $\rho_0$ to its associated passive state $\rho_p$, effectively converting all available resources into useful work.

An interesting remark is that thermal Gibbs states constitute a special subset known as *completely passive states*: they remain passive even when multiple copies of the system are considered. In contrast, generic passive states do not necessarily retain their passivity when replicated, as collective unitary operations acting on several copies can extract work that would be inaccessible from each system individually. This phenomenon has no classical analogue and represents one of the first examples of genuinely collective effects in this framework.

Turning back to our work extracion problem, the passive state $\rho_p$ can be obtained from $\rho_0$ by the unitary operation:

$$\hat{U} = \sum_{i=0}^{d-1} |\epsilon_i\rangle \langle r_i| . \tag{2.24}$$

Then the ergotropy can be conveniently espressed as:

$$\mathcal{E}(\rho_0) = \sum_{j,k} \left( |\langle r_j|\epsilon_k\rangle|^2 - \delta_{j,k} \right). \tag{2.25}$$

To conclude, it can be shown that the ergotropy satisfies the following properties:

- Non-negative and bounded: $0 \leqslant \mathcal{E}(\rho) \leqslant E(\rho)$;
- Zero if and only if $\rho$ is passive;

- For pure states: $\mathcal{E}(|\psi\rangle) = E(|\psi\rangle)$;
- Convexity: $\mathcal{E}\left(\sum_i p_i \rho_i\right) \leqslant \sum_i p_i \mathcal{E}(\rho_i)$.

Here we set the ground-state energy $E_{GS}$ to zero. Otherwise, the bounds still hold, but one should subtract this energy from $E(\rho)$.

### 2.2.2 *Daemonic Ergotropy*

The foundations of informational thermodynamics can be traced back to Maxwell's demon, a famous thought experiment introduced by James Clerk Maxwell, which illustrated how information acquisition and control could seemingly violate the classical laws of thermodynamics. In Maxwell's mind, a hypothetical being, the so-called demon [1], is able to monitor the positions and velocities of gas particles within a container divided into two compartments, and can selectively control a gate between them to influence the flow of particles. By allowing only fast particles to pass in one direction and slow ones in the other, the demon would create a temperature gradient without performing mechanical work, apparently violating the second law of thermodynamics.

Building upon this idea, Leo Szilard proposed in 1929 a simplified, quantitative version of Maxwell's thought experiment, now known as the Szilard engine (see Figure 2.1) [26]. It consists of a single particle gas at temperature $T$ confined in a box that can be divided into two equal parts by inserting a partition. The demon then measures the particle's position, determining whether it is in the left or right compartment. After connecting a pulley to the partition containing the particle, the gas is allowed to expand isothermally, extracting an average work of $k_B T \ln 2$, and seemingly violating the second law of thermodynamics in its Kelvin-Planck formulation. This protocol provides a clear illustration of how information about a system can be converted into useful work, highlighting the thermodynamic value of information.

Modern interpretations recast both the demon and the engine operations as measurement and feedback processes: the observer

1 The term demon was originally introduced by Lord Kelvin in his work [29], well before its later popularization by Maxwell.

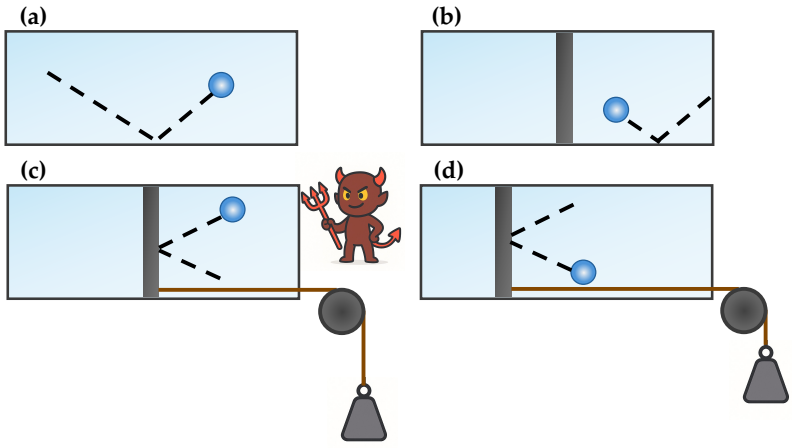


Figure 2.1: The sequence of operations in the Szilard engine: (a) a single-particle gas at temperature T is confined in a box; (b) a partition is inserted, dividing the box into two regions; (c) the demon measures the particle position, and the engine is coupled to the partition containing the particle; (d) the gas is allowed to expand isothermally to extract an average work of $W = k_B T \ln 2$.

performs a measurement on the system, gathers information, and uses it to condition subsequent actions [30, 31, 32, 33]. The apparent paradox was resolved by Landauer and the advent of information theory: Landauer's principle established that the erasure of information in any irreversible process necessarily produces heat, thereby linking informational and thermodynamic irreversibility and grounding information as a physical quantity [34].

In this section, we discuss how measurement-based protocols can be used to enhance the amount of work that can be extracted from a quantum system, inspired by the ideas behind Maxwell's demon and the Szilard engine. Since the ergotropy is convex functional, for a mixed state expressed as a convex combination

$$\rho = \sum_k p_k \rho_k, \tag{2.26}$$

the following inequalitiy holds:

$$\mathcal{E}(\rho) \leqslant \sum_k p_k \mathcal{E}(\rho_k). \tag{2.27}$$

This means that, on average, more work can be extracted by optimizing the protocol for each individual component $\rho_k$ rather than by applying a single protocol optimized for the mixture $\rho$.

This scenario naturally arises in the context of continuously monitored quantum systems: consider a bipartite system composed of a main system S with Hamiltonian $\hat{\mathcal{H}}_S$ and an auxiliary system A, initially prepared in a joint state $\rho_{SA}$, where the auxiliary system typically represents the environment or the bath. The maximum work that can be extracted from S is then given by the ergotropy of its reduced state,

$$\rho_S = \mathrm{Tr}_A\left[\rho_{SA}\right], \quad \mathcal{E}(\rho_S) = \mathrm{Tr}_S\left[\hat{\mathcal{H}}_S\rho_S\right] - \mathrm{Tr}_S\left[\hat{\mathcal{H}}_S(\hat{\mathcal{U}}_{\mathrm{ext}}\rho_S\hat{\mathcal{U}}_{\mathrm{ext}}^\dagger)\right], \tag{2.28}$$

where $\hat{\mathcal{U}}_{\mathrm{ext}}$ is the optimal extracion unitary. If measurements are performed on the auxiliary system via a POVM $\{\hat{\Pi}_A^a\}$, the state of S becomes conditioned on the measurement outcome $a$:

$$\rho_{S|a} = \frac{\mathrm{Tr}_A\left[\rho_{SA}(\mathcal{I}_S \otimes \hat{\Pi}_A^a)\right]}{p_a}, \quad p_a = \mathrm{Tr}_{SA}\left[\rho_{SA}(\mathcal{I}_S \otimes \hat{\Pi}_A^a)\right]. \tag{2.29}$$

The ergotropy of each conditional state is then extracted by the optimal unitary $\hat{\mathcal{U}}_a$ specific to outcome $a$:

$$\mathcal{E}(\rho_{S|a}) = \mathrm{Tr}_S\left[\hat{\mathcal{H}}_S\rho_{S|a}\right] - \mathrm{Tr}_S\left[\hat{\mathcal{H}}_S\hat{\mathcal{U}}_a\rho_{S|a}\hat{\mathcal{U}}_a^\dagger\right]. \tag{2.30}$$

The *daemonic ergotropy* is the average over all possible outcomes of the conditional states ergotropy:

$$\overline{\mathcal{E}}_{\{\hat{\Pi}_A^a\}} = \sum_a p_a\mathcal{E}(\rho_{S|a}) = \mathcal{E}(\rho_S) - \sum_a p_a\mathrm{Tr}_S\left[\hat{\mathcal{H}}_S\hat{\mathcal{U}}_a\rho_{S|a}\hat{\mathcal{U}}_a^\dagger\right], \tag{2.31}$$

where we used $\sum_a p_a\mathrm{Tr}_S\left[\hat{\mathcal{H}}_S\rho_{S|a}\right] = \mathrm{Tr}_S\left[\hat{\mathcal{H}}_S\rho_S\right] = \mathcal{E}(\rho_S)$ since the linearity of the trace. Convexity ensures that the daemonic ergotropy is bounded below by the unconditional ergotropy of the system, and upper bounded by the energy:

$$\mathcal{E}(\rho_S) \leqslant \overline{\mathcal{E}}_{\{\hat{\Pi}_A^a\}} \leqslant \mathcal{E}(\rho_S). \tag{2.32}$$

We can also define the *daemonic gain* as

$$\Delta\mathcal{E}_{\hat{\Pi}_A^a} = \overline{\mathcal{E}}_{\{\hat{\Pi}_A^a\}} - \mathcal{E}(\rho_S) \geqslant 0, \tag{2.33}$$

that quantifies the enhancement in work extraction due to the measurements and feedback. The gain is strictly positive unless the initial state factorizes, $\rho_{SA} = \rho_S \otimes \rho_A$ [27]. Crucially, even if measurements are performed, if the extraction is not optimized for each outcome $\hat{\mathcal{U}}_A \to \hat{\mathcal{U}}_{\text{ext}}$, the average extracted work remains equal to $\mathcal{E}(\rho_S)$, yielding no effective enhancement.

Finally, the physical origin of the daemonic gain lies in the correlations between $S$ and $A$. Measurements allow these correlations to be exploited, effectively converting them into additional extractable work. The enhancement of work extraction due to measurements can thus be understood in terms of one of the fundamental resources of quantum information theory: quantum correlations in the form of quantum discord [35]. In fact, it can be shown [27] that non-zero discord is a sufficient condition for daemonic gain for any possible POVM. In particular, correlations enable the acquisition of information that can be used to perform feedback operations through indirect measurements. However, the role of correlations as a resource for work extraction remains an open question, with ongoing debate about the relative contributions of classical versus quantum correlations [33, 36, 37, 38, 39, 40, 41, 42, 43, 44].

This perspective underscores the deep connection between information, correlations, and the operational meaning of Maxwell's demon in quantum thermodynamics.

## 2.3 SUMMARY

This chapter introduced the basic principles of quantum thermodynamics and their connection to the information theory description of quantum systems. Starting from the notions of work, heat, and entropy in both equilibrium and time-dependent dynamics of open systems governed by CPTP maps, we established the quantum formulation of the first and second laws.

We then addressed the problem of work extraction from closed quantum systems. The concept of *ergotropy* was introduced as the maximum work extractable through unitary operations, determined by difference between the energy of a given state and the energy of its corresponding passive state.

In the final part, we explored how measurement-based protocols can enhance work extraction, inspired by the paradigms of Maxwell's demon and the Szilard engine. By conditioning operations on measurement outcomes, information can be converted into additional work, leading to the definition of *daemonic ergotropy*. The difference between unconditional and daemonic ergotropy, the daemonic gain, was shown to originate from system-environment correlations. This perspective shows how measurement and information can be harnessed as genuine thermodynamic resources, highlighting the fundamental link between information and work extraction in the quantum regime.

# Part II

# ORIGINAL WORK

Part II contains the original contributions of this thesis, developed across two contexts in which measurements play a central role.

The third chapter, based on our work Ref. [45], is devoted to discrete time crystals, a class of driven quantum many-body systems that exhibit robust subharmonic oscillations with potential applications in sensing. The open-system master equation is employed to investigate how environmental coupling affects the temporal properties of the time crystal phase, including its stability and thermodynamic characterization. We show that discrete-time measurements of the system can, in some regimes, contribute to the stabilization of the oscillatory behaviour and serve as a useful tool for identifying and characterizing temporal order.

The fourth chapter, based on our forthcoming work Ref. [46], turns to quantum batteries, devices designed to store and release energy at the microscopic scale. Here, continuous monitoring of the environment is shown to influence the energy extraction process in correlated systems, potentially leading to performance improvements compared to the unmonitored case.

Despite their apparent differences, both studies highlight measurements as active resources. Rather than serving merely as diagnostic tools, they emerge as mechanisms capable of steering, stabilizing, and optimizing the behavior of open quantum systems.

# 3

# DISCRETE TIME CRYSTALS

The study of out-of-equilibrium systems has received a lot of attention in recent years thanks to the advancements in the control and manipulation of experimental quantum platforms for the simulation of many-body systems [47, 48, 49, 50]. In this context, quantum time crystals [51], exhibiting time translation symmetry breaking, are at the centre of many recent works, thanks to their fascinating role in the statistical mechanics of non equilibrium phenomena as well as their applications as time sensors [52, 53, 54, 55]. Time crystals are usually classified as continuous or discrete time crystals, depending on the breaking, continuous or discrete, of the time translation symmetry. discrete time crystals [56, 57, 58, 59, 60], which will be the main subject of this chapter, are periodically driven systems, usually involving disordered localized many-body systems, which respond with an order parameter with periodicity which is an integer multiple of the driving periodicity. Continuous time crystals are typically found in open quantum systems that exhibit emergent oscillations, breaking a continuous time translation symmetry. discrete time crystals have been recently realised experimentally in systems of NV centres in diamond [61, 62], trapped ions [63], optical systems [64] and superconducting systems [65]. Their continuous versions has been realised in cold and ultracold systems [66, 67, 68]. The material presented in the second part of this chapter is largely inspired by our work [45].

## 3.1 INTRODUCTION TO TIME CRYSTALS

The concept of time crystals arises from the extension of spontaneous symmetry breaking, a central paradigm of condensed-matter physics, from the spatial domain to the temporal domain.

In equilibrium systems, spatial crystals emerge when continuous translational (or rotational) symmetry in space is spontaneously broken [56]: the Hamiltonian describing $N$ interacting particles confined in a volume with periodic boundary conditions,

$$\hat{\mathcal{H}} = \sum_{i=1}^{N} \frac{\hat{\mathbf{p}}_i^2}{2m_i} + \frac{1}{2}\sum_{i\neq j}^{N} U(\hat{\mathbf{r}}_i - \hat{\mathbf{r}}_j), \tag{3.1}$$

is invariant under arbitrary spatial translations $\mathbf{r}_i \to \mathbf{r}_i + \mathbf{R}$. Although this symmetry forbids any spatial periodicity in any non-degenerate eigenstate, the two-point correlation function $\rho_2(\mathbf{r}_1, \mathbf{r}_2)$, which gives the probability density of finding a second particle at $\mathbf{r}_2$ given that one has been detected at $\mathbf{r}_1$, can still exhibit a periodic modulation,

$$\rho_2(\mathbf{r}_1, \mathbf{r}_2) = \rho_2(\mathbf{r}_1, \mathbf{r}_2 + \mathbf{a}), \tag{3.2}$$

where $\mathbf{a}$ is a characteristic lattice vector that defines the spatial periodicity of the system. This modulation selects one particular configuration from an infinite family of symmetric ones. When such selection occurs, we say that the system has spontaneously broken a *continuous translational symmetry*, as is typically the case in spatial crystals.

In 2012, Wilczek and Shapere proposed a temporal analog of this phenomenon both in the quantum [51] and the classical realm [69], a *time crystal*, asking whether a time-independent many-body system could spontaneously organize in time and display persistent motion even in its lowest-energy state.

The classical model involved a particle described by a non-canonical Lagrangian,

$$\mathcal{L}(q, \dot{q}) = -\frac{\kappa}{2}\dot{q}^2 + \frac{\lambda}{4}\dot{q}^4, \tag{3.3}$$

leading to the energy

$$E(\dot{q}) = -\frac{\kappa}{2}\dot{q}^2 + \frac{3\lambda}{4}\dot{q}^4. \tag{3.4}$$

The minimum of E satisfies

$$\frac{\partial E}{\partial \dot{q}} = -\kappa \dot{q} + 3\lambda \dot{q}^3 = 0, \tag{3.5}$$

yielding the nontrivial solutions $\dot{q} = \pm\sqrt{\frac{\kappa}{3\lambda}}$. In this simple model, the lowest energy state corresponds to uniform velocity, implying that the system "ground state" evolves periodically in time. This apparent contradiction can be resolved realizing that this Lagrangian cannot be converted into an Hamiltonian smoothly. That is, the Hamiltonian is a multi-valued function of the momentum with cusps corresponding precisely to energy minima at $\dot{q} = \pm\sqrt{\frac{\kappa}{3\lambda}}$, where the Hamilton equations are not well defined.

Wilczek extended this reasoning to quantum many-body systems, proposing a model of N bosons on an Aharonov-Bohm ring [70, 71],

$$\hat{\mathcal{H}} = \sum_{i=1}^{N} \frac{(\hat{p}_i - \alpha)^2}{2} + \frac{g_0}{2} \sum_{i \neq j} \delta(\hat{x}_i - \hat{x}_j), \tag{3.6}$$

where $g_0 < 0$ denotes the strength of attractive contact interactions and $\alpha$ is a magnetic flux. The system exhibits continuous translational symmetry in both time and space. As a result, the probability density of any eigenstate remains invariant under arbitrary time translations and any translation of all particles along the ring. In the mean field limit, when $\alpha = 0$, the system localizes and forms a Bose-Einstein condensate that breaks spatial translational symmetry. Wilczek conjectured that, under the influence of $\alpha$, and in the thermodynamic limit, when $N \to \infty$ and $g_0 \to 0$ but $g_0 N = \text{const}$, the Bose-Einstein condensate could form a soliton moving uniformly around the ring, giving rise to a time-periodic density in their ground state.

However, it was later proven (see [72] and [73]) that such continuous time translation symmetry breaking cannot occur in thermal equilibrium or for systems in the ground state, and the quantum time crystal proposed by Wilczek was actually wrong.

Yet, the notion of time crystals survives in non-equilibrium settings. Depending on the type of time translation symmetry that is broken, one can distinguish between different classes of time crystals. When the symmetry is broken in a continuous manner, the system is said to be a Continuous Time Crystal (CTC). For these

systems, the research is mainly focused on non-equilibrium open quantum systems, where the interplay between coherent and dissipative processes allows for persistent oscillations of macroscopic observables. A paradigmatic example is the Boundary Time Crystal (BTC) [74, 75]. It consists of a system composed by a bulk (with $N_B$ degrees of freedom) interacting with a boundary (typically a spin ensemble, with $N_b$ degrees of freedom). The thermodynamic limit is taken as $N_b, N_B \to \infty$ with $N_b/N_B \to 0$, meaning that the boundary remains infinitesimal compared to the bulk, yet still macroscopic. The interaction induces a dissipative Lindbladian dynamics on the boundary, beyond a critical point, the boundary enters a regime of persistent oscillations, signaling the spontaneous breaking of continuous time translation symmetry. From a spectral perspective, this time crystalline behaviour is encoded in the properties of the Liouvillian operator generating the dissipative dynamics and in the emergence of a large decoherence-free subspace that prevents the system from fully relaxing. In the BTC phase, the real part of the Liouvillian gap [76] closes, leading to a degenerate non-equilibrium steady-state subspace with coherences that persist indefinitely, while the imaginary parts of some Liouvillian eigenvalues within this subspace remain finite, giving rise to nontrivial oscillations in the long time dynamics.

The vast majority of time crystalline phenomena, however, belong to the discrete symmetry-breaking scenario. A Discrete Time Crystal (DTC), or Floquet time crystal [56, 57, 58, 59, 60], arises in periodically driven systems with Hamiltonians $\hat{\mathcal{H}}(t+T) = \hat{\mathcal{H}}(t)$, which are invariant under discrete time translations $t \to t+T$. A DTC corresponds to a non-equilibrium phase in which this discrete symmetry is spontaneously broken to a longer period $nT$. Formally, for an observable $\hat{O}$,

$$\langle \hat{O}(t+T) \rangle \neq \langle \hat{O}(t) \rangle, \qquad \langle \hat{O}(t+nT) \rangle = \langle \hat{O}(t) \rangle. \tag{3.7}$$

This subharmonic response reflects collective synchronization at a frequency $\omega/n$, distinct from the drive frequency $\omega = 2\pi/T$.

However, to claim that a system is in a DTC phase, the symmetry breaking must be stable, in the thermodynamic limit, against weak perturbations of the system parameters [57]. The reason is that even completely isolated quantum systems generally ther-

malize. In such systems, different subsystems effectively act as heat baths for one another, so that the long-time expectation values of local observables under a static Hamiltonian become indistinguishable from those of a thermal state described by the corresponding canonical ensemble. This process is referred to as *thermalization*. In periodically driven systems, however, energy is not conserved, since the drive can continuously inject energy into the system through *Floquet heating*. Thermalization in this context corresponds to the system heating up until it reaches a state that is locally equivalent to an infinite-temperature ensemble [77, 78, 79]. Although certain integrable or non-interacting models can avoid thermalization, they do so only under fine-tuned conditions and typically thermalize once weak perturbations are introduced, effectively breaking any DTC phase. For this reason, the appearance of DTC behaviour requires mechanisms that suppress Floquet heating, such as Many-Body Localization (MBL) or Floquet prethermalization.

In the former case, when disorder is sufficiently strong, an isolated one-dimensional quantum system can enter the MBL phase [80, 81, 82]. In this regime, the system has an extensive number of emergent quasi-local conserved quantities, which prevent it from thermalizing and allow it to retain memory of its initial conditions indefinitely during unitary evolution. Importantly, MBL can also occur in periodically driven systems, where it plays a crucial role in suppressing Floquet heating and thus stabilizing non-equilibrium phases.

However, disorder is not always necessary. Nontrivial Floquet phases can appear even in the absence of MBL, provided we slightly relax the strict requirement for the DTC phase to allow for states that are exponentially, but not infinitely, long lived. When the drive frequency is much larger than the local energy scales of the system, energy absorption from the drive requires distributing it over many excitations. As a result, heating is very slow, and the system can be for an extended time in a quasi-steady state, known as a prethermal state [84, 85, 86, 87], where nontrivial phases, including prethermal DTCs [88], can emerge.

To summarize, a DTC can be understood as a many-body system non-equilibrium steady state that evolves into a stroboscopically periodic configuration, exhibiting long-range temporal

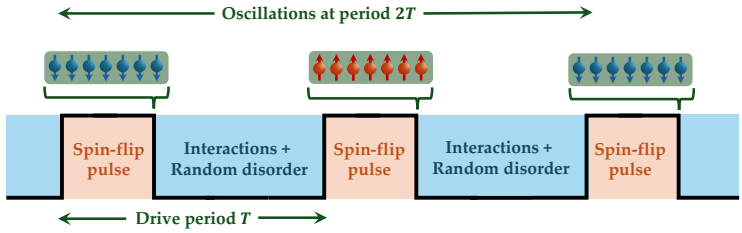


Figure 3.1: The recipe to obtain a DTC: a chain of quantum spins is driven by imperfect spin-flip pulses and subsequently allowed to interact in the presence of random disorder. Although the driving sequence repeats every period T, the system exhibits emergent oscillations with period 2T, the defining signature of a DTC. Adapted from [83].

correlations and robust order against small perturbations: even if the drive parameters are slightly changed the period of the time crystal remains locked. A typical realization [89] involves a 1D chain of quantum spins subjected to imperfect spin-flip pulses followed by interactions among the spins in the presence of disorder, as pictorially shown in Figure 3.1.

To conclude, continuous and discrete time crystals both embody spontaneous breaking of temporal symmetry, but they differ fundamentally in their microscopic origin and physical context:

**CTC:** $\hat{\mathcal{H}}(t) = \hat{\mathcal{H}}, \quad \langle \hat{O}(t+\tau) \rangle = \langle \hat{O}(t) \rangle$ with $\tau$ arbitrary, only out of equilibrium and in open quantum systems;

**DTC:** $\hat{\mathcal{H}}(t+T) = \hat{\mathcal{H}}(t), \quad \langle \hat{O}(t+nT) \rangle = \langle \hat{O}(t) \rangle$ with $n$ integer, robust subharmonic response in disorder Floquet or prethermal systems.

## 3.2 THERMODYNAMICS AND PROTECTION OF DISCRETE TIME CRYSTALS

Despite the huge interest that time crystals have generated, the analysis of their thermodynamics, for instance how much work is necessary to maintain them, their heat exchange and entropy production, has been mostly overlooked. In Ref.[75], the thermodynamics of the so called boundary time crystals, a class of continuous dissipative time crystals [74], has been thoroughly studied by introducing a microscopic model and a consistent framework for the thermodynamic assessment of their dynamics. In Ref.[90], the analysis was extended to two coupled boundary time crystals and it was shown how the system can be used for energy storage.

In this section, we present an extensive thermodynamic analysis of a DTC. We introduce the two-stroke spin-1/2 spin chain Hamiltonian and a thermodynamically consistent Lindblad master equation for the description of its dissipative evolution. Using this framework, in the first part of the section, we evaluate the work and heat exchanged during each period of the time evolution as well as the entropy production. In the second part, we introduce a periodic measurement scheme with the objective of preserving as much as possible the time crystal signature that would otherwise disappear in the presence of an external environment. We show that it is possible to significantly mitigate the damaging effects of the environment on the time crystal, thus preserving the subharmonic oscillations characteristic of the DTC. Although the benefits of the measurement scheme are limited on average, we observe a stabilisation of parameters associated to the staggered magnetisation at the level of individual trajectories.

The section is organized as follows: In subsection 3.2.1 we present the DTC model that is the subject of our studies. In subsections 3.2.2 and 3.2.2.1 we show our results concerning the subharmonic response of the DTC in the presence of a thermal bath and its thermodynamic properties, in particular we show that the signature of the DTC will perish after a certain time regardless of temperature and coupling. In subsection 3.2.2.2 we describe the measurement scheme and show our results. Finally, in subsection 3.2.3 we draw our conclusions.

### 3.2.1 *Model*

In this section we study a driven one-dimensional spin-1/2 chain described by the time-dependent Hamiltonian [59, 91, 92, 89]:

$$\hat{\mathcal{H}}_S(t) = \begin{cases} \hat{\mathcal{H}}_z & \text{if } 0 \leqslant t < T_z, \\ \hat{\mathcal{H}}_x & \text{if } T_z \leqslant t < T = T_x + T_z. \end{cases} \tag{3.8}$$

This Hamiltonian is a periodic function with period $T = T_z + T_x$, where $\hat{\mathcal{H}}_z$ and $\hat{\mathcal{H}}_x$ are defined as follows:

$$\hat{\mathcal{H}}_z = \frac{1}{2}\sum_{i=1}^{N} h_i \hat{\sigma}_i^z, \tag{3.9}$$

$$\hat{\mathcal{H}}_x = \sum_{i=1}^{N-1} J_i \hat{\sigma}_i^x \hat{\sigma}_{i+1}^x, \tag{3.10}$$

where $(\hat{\sigma}_i^x, \hat{\sigma}_i^y, \hat{\sigma}_i^z)$ represent the Pauli operators for spin $i$. The values of the magnetic fields $h_i$ and couplings $J_i$ are randomly drawn from uniform distributions with mean values $\bar{J}$ and $\bar{h}$:

$$J_i = \bar{J} + \delta J \xi_i, \tag{3.11}$$

$$h_i = \bar{h} + \delta h \tilde{\xi}_i, \tag{3.12}$$

where $\xi_i$ and $\tilde{\xi}_i$ are independent uniformly distributed random variables between -1 and 1, $\delta h$ and $\delta J$ are the widths of the distributions. From now on we will refer to the part of the evolution defined by $\hat{\mathcal{H}}_x$ ($\hat{\mathcal{H}}_z$) as the $x$-stroke ($z$-stroke). To observe the DTC effects we need to consider this model in the $\pi$-SG phase [91] (SG=spin glass). Additionally the initial state of the system must break the $\mathbb{Z}_2$ symmetry of the Hamiltonian. We have numerically implemented this model for an N-spin system. Henceforth, we will fix the mean value of $h_i$ as $\bar{h} = \pi$ and of $J_i$ as $\bar{J} = \pi/4$, the width of the distribution is fixed as 0.5 for both the set of parameters. The inital state is fixed as $\rho(0) = |+\rangle\langle+|$, where $|+\rangle$ being the state of all the spins pointing upwards along the $x$ direction: $|+\rangle = |\uparrow_x \ldots \uparrow_x\rangle$. By choosing these parameters and initial state and by setting $T_z = T_x = 1$, the dynamics of the time crystal becomes readily comprehensible: the $z$-stroke simply rotates each spin by $\theta_i = h_i T_z$ around the $z$-axis, then the system

evolves under $\hat{\mathcal{H}}_x$. Here, disorder is needed to keep the system in a many-body localized phase; otherwise, the system would thermalize, destroying the time crystal ordering. The subsequent $z$-stroke approximately returns the spins to their initial positions. Finally, the $x$-stroke localizes the spins again. The emergence of the time crystal can be explored by measuring either the magnetization of a single spin $\langle \hat{\sigma}_i^x(t) \rangle$ or the total magnetization $\langle S_x(t) \rangle = \frac{1}{N} \sum_i \langle \hat{\sigma}_i^x(t) \rangle$, both quantities exhibiting periodicity at half the frequency of the driving. This specific choice of the initial state provides a nice way to visualise these dynamics but we must note that this periodic behaviour is observed for many initial states, however, the amplitude of the signal will depend on the initial value of the chosen signature.

With this setup in mind, we can investigate the role of an external environment on the time crystal behaviour using the Lindblad master equation formalism [2, 9, 10]. Let $\rho_S$ be the system density matrix, obtained by tracing out the environment degrees of freedom, in the weak coupling and Born-Markov approximation the system master equation reads:

$$\begin{aligned} \frac{d}{dt}\rho_S(t) &= -i\left[\hat{\mathcal{H}}_S, \rho_S(t)\right] \\ &+ \sum_\omega \left( \hat{\mathcal{L}}_\omega \rho_S(t) \hat{\mathcal{L}}_\omega^\dagger - \frac{1}{2}\left\{ \hat{\mathcal{L}}_\omega^\dagger \hat{\mathcal{L}}_\omega, \rho_S(t) \right\} \right), \end{aligned} \tag{3.13}$$

with the jump operators $\hat{\mathcal{L}}_\omega$ defined as:

$$\begin{aligned} \hat{\mathcal{L}}_\omega &= \sqrt{\gamma(\omega)} \sum_{\epsilon' - \epsilon = \omega} |\epsilon\rangle \langle \epsilon| \hat{\mathcal{V}} |\epsilon'\rangle \langle \epsilon'| \\ &= \sqrt{\gamma(\omega)} \sum_{\epsilon' - \epsilon = \omega} |\mathcal{V}_{\epsilon\epsilon'}| |\epsilon\rangle \langle \epsilon'|, \end{aligned} \tag{3.14}$$

with $\omega = \epsilon' - \epsilon$, $|\epsilon\rangle$ ($|\epsilon'\rangle$) being an eigenstate of $\hat{\mathcal{H}}_S$ (which can be either $\hat{\mathcal{H}}_z$ or $\hat{\mathcal{H}}_x$) with energy $\epsilon$ ($\epsilon'$) and finally $\mathcal{V}_{\epsilon\epsilon'} = \langle \epsilon| \hat{\mathcal{V}} |\epsilon'\rangle$, with $\hat{\mathcal{V}}$ being the interaction operator between the system and the environment degrees of freedom. The rates $\gamma(\omega)$ are defined as

$$\gamma(\omega) = \frac{\Gamma^2 |\omega| e^{-|\omega|}}{1 - e^{-\beta|\omega|}} (\Theta(\omega) + e^{-\beta|\omega|}\Theta(-\omega)), \tag{3.15}$$

where $\Gamma$ is the system-bath coupling strength and $\beta$ is the inverse temperature of the bath.

Since it will be useful later, let us rewrite the master equation for a single stroke as $\dot{\rho}_S = \mathfrak{L}_{x(z)}\rho_S$, where $\mathfrak{L}_{x(z)}$ is the Lindblad super-operator of the system in the $\hat{\mathcal{H}}_x(\hat{\mathcal{H}}_z)$ stroke. In this framework, the evolution of the system's density matrix is given by the exponential of $\mathfrak{L}_{x(z)}$, introducing the evolution super-operator for each strokes as $\Lambda_{x(z)}(t) \equiv e^{t\mathfrak{L}_{x(z)}}$. For simplicity, we define the evolution super-operator for a single period $T$ as:

$$\Lambda(t) \equiv \begin{cases} \Lambda_z(t) \quad \text{if} \quad 0 \leqslant t < T_z, \\ \Lambda_x(t - T_z)\Lambda_z(T_z) \quad \text{if} \quad T_z \leqslant t \leqslant T, \end{cases} \tag{3.16}$$

where $0 \leqslant t \leqslant T$.

### 3.2.2 *Results*

With the master equation at hand, we can now simulate our time crystal and compute its characteristic signature $\langle S_x(t)\rangle$ as a function of time, using the methods described in the previous section:

$$\langle S_x(t)\rangle = \mathrm{Tr}\left[\rho_S(t)\hat{S}_x\right]. \tag{3.17}$$

Before we begin, we would like to emphasize that the jump operators we derived differ significantly from those proposed in Ref. [92]: $\hat{\mathcal{L}}_{\epsilon\epsilon'} = g(\epsilon')|\mathcal{V}_{\epsilon\epsilon'}|\,|\epsilon\rangle\langle\epsilon'|$, where $g(\epsilon') \propto \exp(-\beta\epsilon')$. Indeed, this approach led to an unexpected dependence of the time crystal signature on temperature: surprisingly, the oscillations became less damped as the bath temperature increased. As we shall see, our model instead reproduces the expected behaviour. This anomalous temperature dependence can be traced back to the specific form of the transition rates $g(\epsilon')$ used in their model, which do not satisfy the detailed balance condition. In contrast, the rates in our master equation do fulfill detailed balance, thus ensuring thermodynamically consistent dynamics. This distinction provides a plausible explanation for the discrepancy and supports the validity of our approach.

First of all we must choose the interaction operator $\hat{\mathcal{V}}$. The choice of interaction operator $\hat{\mathcal{V}}$ with the thermal bath is crucial for the interpretation of the subsequent results. We will consider

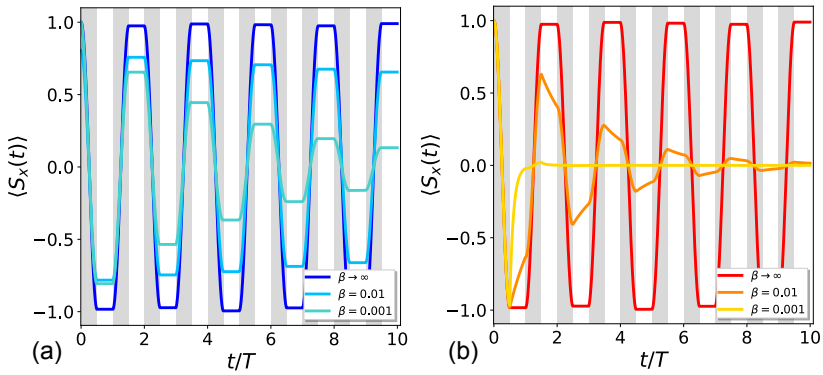


Figure 3.2: The time crystal signature $\langle S_x(t)\rangle$ as a function of time for different inverse temperatures of the bath $\beta$. Grey and white stripes correspond to the $z$- and $x$-strokes, respectively. (a) Shows the results in the $z$-interaction while (b) the ones for $x$-interaction. Here the model parameters are set to $N = 6$ and $\Gamma = 0.01$.

two choices in this paper: $\hat{V} = \sum_i \hat{\sigma}_i^z$ and $\hat{V} = \sum_i \hat{\sigma}_i^x$, which are both relevant to model experimental platforms for the realisation of DTC. Selecting one over the other leads to different and non-trivial outcomes since both do not commute with at least one of the Hamiltonian strokes. If the system is viewed as a collection of two-level systems in the $\hat{\sigma}_z$ basis, the former choice ($z$-interaction) is effectively a dephasing channel. As we will see in the following sections, this results in dephasing during the $z$-stroke and dissipation during the $x$-stroke. The latter choice ($x$-interaction) can be seen as a dissipation channel. However, it is important to note that this channel will cause dissipation during the $\hat{\sigma}_z$ stroke but only dephasing during the $\hat{\sigma}_x$ stroke of the Hamiltonian since it commutes with it. From here on, we will treat these two noise channels separately, highlighting the qualitatively different outcomes that each produces.

We simulate the time crystal made by up to $N = 6$ sites for both interactions at different inverse temperatures $\beta$ and for $\Gamma = 0.01$, obtaining the results shown in Fig. 3.2 for $N = 6$. Our microscopic bath model leads the temperature dependence depicted in the figure, showing that the system decays faster with increasing temperature, as expected but in contrast with Ref. [92]. Additionally, it seems to reveal that the oscillations remain unaffected

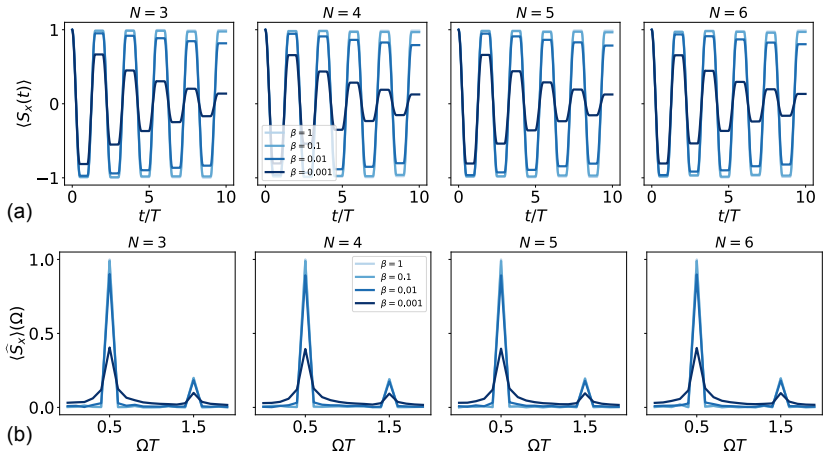


Figure 3.3: Scaling of the DTC signature in the case of $z$-interaction (a) and its Fourier transform (b), all the result are obtained with $\Gamma = 0.01$.

by the thermal bath in the zero-temperature limit. However, the oscillations still decay over long timescales (for finite size crystals) or in the case of large $\Gamma$, indicating that the system is not entirely immune to dissipation. Another notable observation from Fig. 3.2 is that, at the same temperature, the time crystal decays much faster when $\hat{V}$ is an $x$-interaction compared to the case in which it is an $z$-interaction. In the latter, the effect of dephasing in the $\hat{\sigma}_z$ stroke essentially leads to an imperfect spin flip. It is important to emphasize that these fluctuations are incoherent and due to noise, thus they tend to destroy localization and suppress the DTC signature, in contrast to the imperfect but coherent spin flips induced by Hamiltonian disorder. More interesting is what happens in the case of $x$-interaction, which acts as dephasing in the $x$ basis, effectively breaking the many-body localization [93], which is the reason for the much faster decay observed.

In order to investigate the role of system size on the DTC signature, we computed it for different system sizes under both $z$-interaction (Fig. 3.3) and $x$-interaction (Fig. 3.4). To better highlight the subharmonic response, we also calculated the Fourier transform $\langle \widehat{S}_x(t) \rangle$ of the DTC signature. As shown in the plots, in the case of $z$-interaction the DTC signature decays in the same way regardless of the system size for fixed temperature. The situation

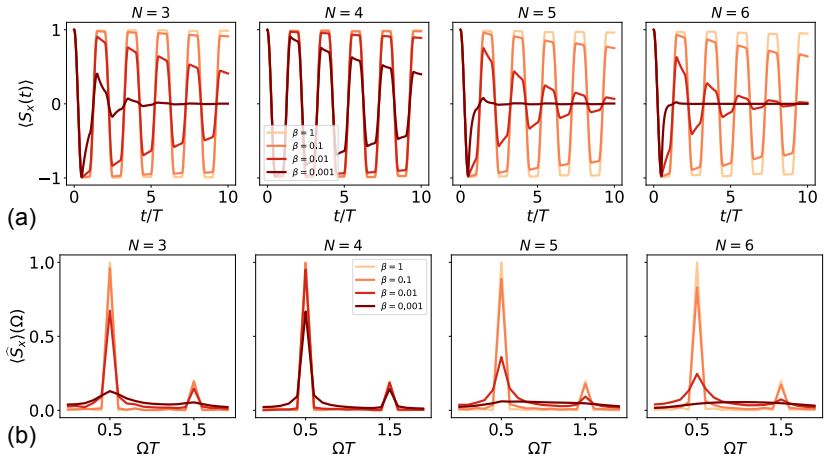


Figure 3.4: Scaling of the DTC signature in the case of x-interaction (a) and its Fourier transform (b), all the result are obtained with $\Gamma = 0.01$.

is markedly different for the x-interaction, where, apart from the special case of $N = 4$, the DTC signature at a fixed temperature. becomes more fragile as the system size increases.

### 3.2.2.1 *Thermodynamics*

Building upon our model of a system that exhibits a discrete time crystal phase coupled to a thermal bath, we now turn our attention to its thermodynamic properties. With this foundation, we can explore the rates of change of key thermodynamic quantities: entropy ($\dot{S}(t)$), heat ($\dot{Q}(t)$), and work ($\dot{W}(t)$). These rates in the weak coupling limit are formally defined as follows [22]:

$$\dot{S}(t) = -\mathrm{Tr}\left[\dot{\rho}\ln\rho\right], \tag{3.18}$$

$$\dot{Q}(t) = \mathrm{Tr}\left[\hat{\mathcal{H}}\dot{\rho}\right], \tag{3.19}$$

$$\dot{W}(t) = \mathrm{Tr}\left[\dot{\hat{\mathcal{H}}}\rho\right]. \tag{3.20}$$

By these conventions, the change in the system's energy defined as $\dot{U}(t) = \frac{d}{dt}\mathrm{Tr}\left[\hat{\mathcal{H}}\rho\right]$ fulfils the first law of thermodynamics:

$$\dot{U}(t) = \dot{W}(t) + \dot{Q}(t). \tag{3.21}$$

This formulation indicates that a positive $\dot{Q}$ corresponds to heat flowing into the system. Our analysis demonstrates that these

thermodynamic properties follow the general trends depicted in Fig. 3.5, for both $z$- and $x$-interactions. Analyzing Fig. 3.5, we can observe several expected behaviours. Whenever the Hamiltonian switches, work is performed on the system, resulting in the injection of heat, which is then gradually dissipated as the system cools until the subsequent switch. The entropy of the system increases monotonically, though at a decreasing rate, which can be attributed to the continuous coupling with the external environment. This increasing entropy is indicative of the system's progression towards thermal equilibrium, driven by the interaction with the thermal bath. As observed in the case of $z$-interaction, during the $z$-stroke evolution (grey stripes in Fig. 3.5 (a)), which corresponds to pure decoherence, we find that $\dot{Q} + \dot{W} = \dot{U} = 0$. This result is consistent with previous thermodynamic studies on pure decoherence [94]. A similar behaviour is seen for the $x$-interaction, but during the $x$-stroke (white stripes in Fig. 3.5 (b)). In general, the magnitude of the work features depends on the specific disorder realisation within the system.

What seems clear is that when the system is coupled to the environment, the time crystal signature inevitably decays. The unstructured environment we consider in this paper leads to the loss of crucial coherences, causing the signature of the DTC to fade away. To demonstrate this behaviour we decreased the inverse temperature $\beta$ (Fig. 3.6), and we integrated the thermodynamic quantities defined above. For high enough temperatures or coupling strength the system tends to a quasi-periodic non-equilibrium steady state. This regime can be observed by examining the fidelity between the system state and the thermal states $\rho = \frac{e^{-\beta\hat{\mathcal{H}}}}{\mathrm{Tr}\left[e^{-\beta\hat{\mathcal{H}}}\right]}$ (where $\hat{\mathcal{H}}$ is $\hat{\mathcal{H}}_z$ or $\hat{\mathcal{H}}_x$), and additional insights can be gained from the entropy, as shown in Fig. 3.6.
Initially, the system's entropy increases during both strokes. However, in the $z$-interaction case (Fig. 3.6 (a)), the steady state is characterized by an increase in entropy during the $z$-stroke, followed by a corresponding decrease during the $x$-stroke. The reverse behaviour is observed in the $x$-interaction case (b). During the $\hat{\mathcal{H}}_z$ stroke, the process leads to pure dephasing, which can only increase the system's entropy. Conversely, the $\hat{\mathcal{H}}_x$ stroke is not

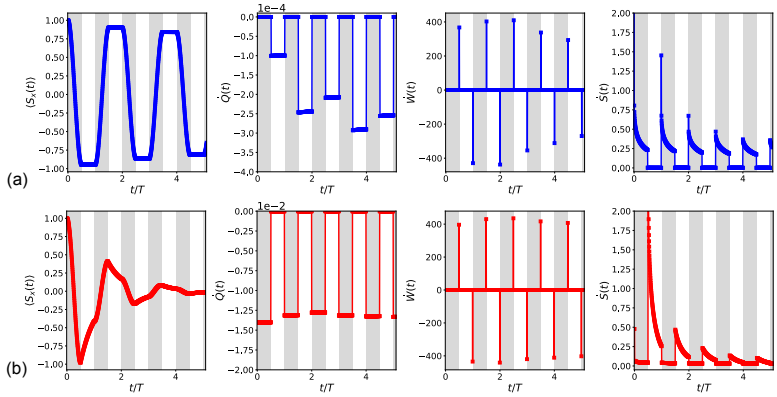


Figure 3.5: This figure shows the thermodynamic rates and the time crystal signature for two different choices of interaction between the time crystal and the bath. Grey and white stripes correspond to the z- and x-strokes, respectively. (a): z-interaction, (b): x-interaction. Other parameters: $N = 6$, $\beta = 0.5$, $\Gamma = 0.1$. As can be seen, heat dissipation occurs in two different strokes depending on the chosen interaction. Work is performed on the system when the Hamiltonians are switched, finally $\dot{S}(t)$ is always positive (with different rates depending on the stroke) in accordance with the second law.

thermalizing and can lead to a reduction in entropy, as depicted in Fig. 3.6.

Throughout this process, when the steady state is reached, the work done on the system $\Delta W$ is positive and it grows indefinitely with a periodic time modulation, while heat $\Delta Q$ is consistently decreasing again with a periodic time modulation. These features indicate that the system acts like a dissipator: it absorbs work and releases heat into the bath. Additionally, at least in the z-interaction case, we find that energy flows into the system during the $\hat{\mathcal{H}}_x$ stroke and out of the system during the $\hat{\mathcal{H}}_z$ stroke while the DTC is still active. Once the DTC phase decays, energy consistently flows out of the system. Entropy quickly reaches the value of a fully mixed state, and the system reaches a periodic non-equilibrium steady state, as evidenced by the fidelity fluctuations with the thermal states of the two Hamiltonians. Finally, we note that in the low $\beta$ limit, thermalization occurs much more

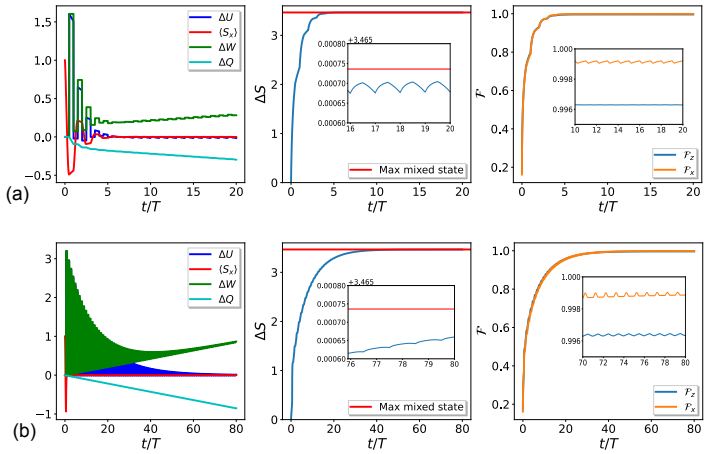


Figure 3.6: The death of the time crystal: Time crystal signature and thermodynamic quantities (first column), half chain Von Neumann entropy (second column) and fidelities with $\hat{\mathcal{H}}_x$ and $\hat{\mathcal{H}}_z$ thermal states (third column) as a function of time; for the DTC with: $N = 5$, low $\beta$: $\beta = 0.05$, $\Gamma = 0.1$. (a): $z$-interaction, (b): $x$-interaction.

slowly in the $x$-interaction case, even though the time crystal signature decays faster, as depicted in Fig. 3.6.

### 3.2.2.2 *Measurements*

In the previous sections, we explored the thermodynamic properties of a discrete time crystal. Our analysis demonstrated that, inevitably, the system decays when coupled to a thermal bath. This decay is a consequence of the environment-induced loss of coherence, which erases the signature of the DTC.

Given these findings, we now turn our attention to a critical question: can we somehow enhance the lifespan of the DTC? One promising approach involves the consideration of repeated measurement schemes. By strategically implementing these measurements, we aim to investigate whether it is possible to stabilize the DTC phase and extend its coherence time in the presence of environmental interactions. In this section, we will explore this approach, examining the potential benefits and mechanisms through which repeated measurements can influence the DTC's behaviour and longevity.

The idea, which we describe in the following, is particularly suited for the selected parameters, where the time crystal oscillates between $|+\rangle$ and $|-\rangle$. Every period $T$ the system approaches one of these states and, with this in mind, we measure the total magnetization $\hat{S}_x = \frac{1}{N}\sum_i \hat{\sigma}_x^i$ at each period to "reset" and purify the system. By performing these measurements, the aim is to counteract the decoherence induced by the environment and potentially stabilize the oscillatory behaviour of the time crystal, thereby extending its coherence and lifespan. A similar scheme has been considered in [95], where the authors implemented a continuously monitored Floquet time crystal on a quantum computer. Their approach is based on the application of a periodical quantum-classical feedback protocol. They show that single-qubit corrections based on measurement outcomes of randomly chosen qubits are able to enhance spatiotemporal order of the DTC signal. The difference is that in our case an experimentally simpler protocol without feedback after measurement is considered, to let the system evolve on its own, without any external "help".

Starting from a generic initial state $\rho(0)$ at time $t = 0$, the state after one period of the evolution is then:

$$\rho(T) = \Lambda(T)\rho(0) = \Lambda_x(T_x)\Lambda_z(T_z)\rho(0). \tag{3.22}$$

Now, if we measure the total magnetization $\hat{S}_x$, the state after the measurement is given by:

$$\rho_i'(T) = \frac{\hat{\Pi}_i \rho(T) \hat{\Pi}_i}{p_i}, \tag{3.23}$$

where $p_i$ is the probability of measuring the eigenvalue $m_i$ of $\hat{S}_x$, and $\hat{\Pi}_i$ is the corresponding projector. The procedure is then repeated with $\rho_i'(T)$ as the initial state for the next period. Note how the period of the measurement is the same as that of the driving and cannot hence induce a sub-harmonic response.

Furthermore, since we are interested in the time crystal signature, we need to average the observable over all possible mea-

surement outcomes. By definition, assuming that $T < t \leqslant 2T$, this is given by:

$$\begin{aligned}\overline{\langle S_x(t)\rangle} &= \sum_i p_i \langle S_x(t)\rangle_i = \sum_i p_i \mathrm{Tr}\left[\hat{\mathcal{S}}_x \Lambda(t)\rho_i'(T)\right] \\ &\equiv \mathrm{Tr}\left[\hat{\mathcal{S}}_x \Lambda(t)\rho''\right], \end{aligned} \tag{3.24}$$

where we have defined $\rho'' \equiv \sum_i \hat{\Pi}_i \rho(T)\hat{\Pi}_i$. In this way, the average is conveniently calculated by determining the statistical mean value of the state $\Lambda(t)\rho''$, which is nothing more than the time evolution of the incoherent mixture of all possible eigenstates of the observable $\hat{\mathcal{S}}_x$. It is straightforward to see that the procedure can be iterated for $2T < t \leqslant 3T$ by replacing $\rho''$ with $\rho''' \equiv \sum_i \hat{\Pi}_i \Lambda(T)\rho''\hat{\Pi}_i$, and so on for larger times.

With this formula, we can compute the DTC signature as a function of time and inverse temperature. First, we notice that for the $z$-interaction, measurements do not improve the DTC lifespan; however, there is a stabilization of periodicity in the presence of an external field. More interestingly, in the case of the $x$-interaction, the results are notably different. In Fig. 3.7, we have plotted the absolute relative difference between the time crystal signature without measurements and with measurements performed every $T$:

$$E_r = \frac{|\langle S_x\rangle_0| - |\overline{\langle S_x\rangle}|}{|\langle S_x\rangle_0|} \tag{3.25}$$

as a function of time and inverse temperature. As can be seen, there is a moderate advantage (roughly an order of magnitude) for high temperatures and long times (darker region of the plot) whereby the mean DTC's signature in the presence of measurements (red curve in the right panel) has a larger amplitude than the signature without measurements (blue curve in the right panel).

This improvement can be interpreted as a sort of sub-Zeno effect caused by measurements. The quantum Zeno effect is a phenomenon in quantum mechanics in which frequent measurements can inhibit the evolution of a quantum system [96]. This effect is particularly significant and better understood in closed

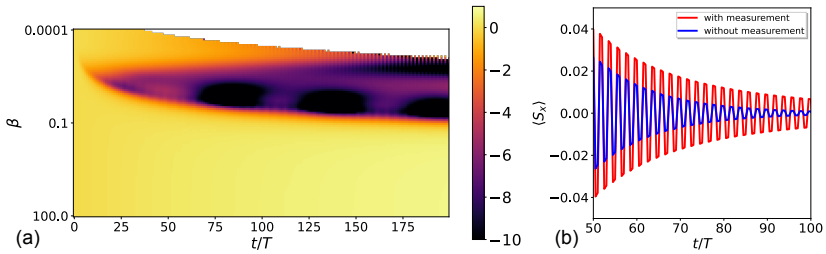


Figure 3.7: (a): The relative difference $E_r$ as a function of time and inverse temperature. (b): $E_r$ as a function of time for $\beta = 0.05$. Other parameters: $N = 5$, $\Gamma = 0.01$.

quantum systems, where continuous observation can effectively freeze the dynamics by repeatedly collapsing the wave function due to the short time quadratic behaviour of the fidelity. In open quantum systems, the situation is quite different. In general, it is not possible to determine a-priori whether a system can be frozen or not, and indeed, measurements typically have the opposite effect [97, 98]. However, Zeno dynamics can manifest itself as a slowed down decoherence or even stabilization of certain states due to frequent measurements. In our case, the frequency of the measurements is determined by the driving period, which is more or less of the same order as the decay time of the time crystal. This prevents a true Zeno effect from occurring, and for this reason, we refer to it as a sub-Zeno effect.

Moreover, the reason why this improvement here occurs only at high temperatures and not at low temperatures can be intuitively understood through the disordered nature of the DTC's Hamiltonians. At low temperatures, the time crystal does not evolve into the states $|+\rangle$ and $|-\rangle$ precisely. Therefore, the probability of measuring one of these magnetizations is never one, which inevitably leads to "errors" due to the measurement process. This randomness prevents a proper Zeno effect from occurring at low temperatures.

As we have seen before, on average, the advantage of the measurement scheme is limited to high temperature regions. However, we can obtain interesting insights into the DTC by examining individual trajectories and in particular the outcomes of measurements. Using the outcomes, we define a vector $\mathbf{m}$, where each component represents an outcome, and its length

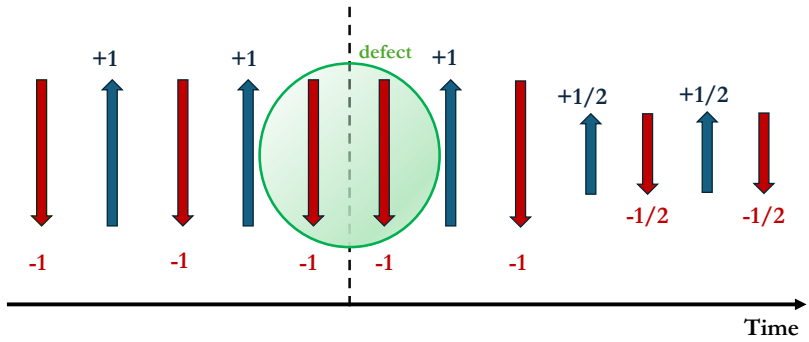


Figure 3.8: Pictorial example of measurement string for $N = 4$. Each measurement is performed every time $T$. Negative measurement results are shown in red and positive results in blue. When there are two consecutive measurements of the same sign we have a defect (represented in green), the dotted line divides two different domains. The possible outcomes for $N = 4$ are $1, 1/2, 0, -1/2, 1$; note that we do not consider the consecutive measurements $-1$ and $1/2$ as defects.

corresponds to $\mathcal{T}$, the total number of periods driven (total time is $\mathcal{T}T$). For all intents and purposes, this vector can be considered a kind of classical spin system in the time domain, allowing us to calculate various quantities that could provide information about the time crystal. In principle, in the zero-temperature limit for the chosen parameters, as we measure $\hat{S}_x$ each period, we expect to observe an alternation of 1 and -1, except for possible errors due to the imperfect spin flip pulses. This approach enables us to gain a deeper understanding of the DTC's behaviour under different conditions. We can define a *time-staggered magnetization*:

$$M \equiv \frac{1}{\mathcal{T}} \sum_{i=1}^{\mathcal{T}} m_i (-1)^i, \tag{3.26}$$

which would take the maximum values $\pm 1$ in the case of perfect alternation of signs. In general, it assumes values between -1 and 1: due to the coupling with the bath, errors may occur, manifesting as intermediate measurements (e.g., in the case of four spins, we may measure $1/2$ instead of 1) or, in the most extreme cases, as changes in sign. We refer to these changes in sign as *defects*: a defect occurs whenever the magnetization at

two consecutive times $(m_i, m_{i+1})$ does not change sign. Thus, we can define the defect density as:

$$dw = \frac{1}{\mathcal{T}} \sum_{i=1}^{\mathcal{T}} \frac{1 + \text{sgn}(m_i)\text{sgn}(m_{i+1})}{2}. \tag{3.27}$$

This quantity can take values between 0 and 1. In the case of perfect alternation of signs, it is 0, while in the case of completely aligned signs, it reaches 1. Furthermore, we can define *domains* as sets of consecutive defect-free measurements. We therefore define the mean size of these domains as

$$A = \frac{1}{\text{No. of domains}} \sum_{\text{domains}} l(\text{domain}), \tag{3.28}$$

where $l$ indicates the length of a domain. This quantity is related to the width of the measurement string auto-correlation function, since the latter measures the characteristic time scale over which the signal remains correlated with itself, indicating how quickly the correlations in the signal decay.

In Fig. 3.9, the quantities defined earlier are shown as functions of the measurement string length $\mathcal{T}$, averaged over 100 different realizations and for various system sizes. As can be observed, for the chosen temperature, the staggered magnetization $\overline{M}$ (where the bar indicates the average over the different realizations) decays for each system size following what appears to be a power law. More interestingly, both $\overline{dw}$ and $\overline{A}$ seem to settle on distinct plateaus. In the case of $dw$, the height of the plateau decreases with increasing system size, while for $A$, it appears to increase. The measurement string thus seems to form distinct domains that indicate the underlying time crystal phase, suggesting an increasing robustness of the time crystal with system size.

A natural question that arises at this point is what happens when the temperature of the system is varied. To address this question, we varied the inverse temperature $\beta$ while keeping $\mathcal{T} = 500$ fixed. As shown in Fig. 3.10, the system exhibits interesting behaviour. Two distinct regimes can be observed: a disordered one, which occurs for small $\beta$ values and characterized by a non-zero defect density and almost unit-sized domains dimension, and an ordered regime, where the defect density

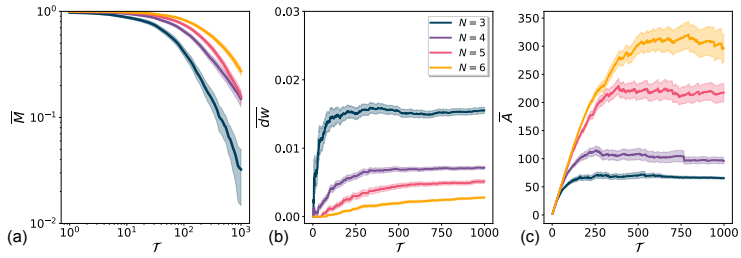


Figure 3.9: Time-staggered magnetization of the time crystal (a), defect density (b) and average domain size (c) as function of $\mathcal{T}$ for different time crystal sizes for $\beta = 10$ and $\Gamma = 0.01$.

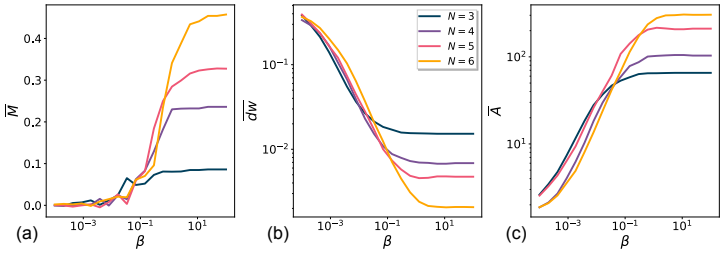


Figure 3.10: Staggered magnetization (a), defect density (b) and average domain size (c) as a function of $\beta$ for different time crystal sizes for $\mathcal{T} = 500$ and $\Gamma = 0.01$.

tends to zero and the domains dimension becomes macroscopic. Interestingly, information about the time crystal phase can be extracted directly from the results of repeated measurements, without the need for reconstructing averages, as even a few trajectories already provide the relevant information. This feature could be particularly advantageous in experimental applications.

### 3.2.3 *Conclusions*

In this work, we examined the properties of a DTC coupled to a global bosonic thermal bath, in the weak-coupling and Markovian limit. In particular, we have derived the proper form of the jump operators from the microscopic model and we have calculated some relevant thermodynamic quantities, such as heat, work and entropy.

Our analysis demonstrates that, for any temperature of the thermal bath, the coupling to the latter suppresses the subharmonic response characteristic of DTC. Therefore, we have focused on trying to stabilize these systems, specifically using a simple protocol involving repeated projective measurements. As expected, on average, these measurements have a moderate or even a negative effect, since they essentially mimic decoherence. However, when considering individual trajectories, we observed a stabilization of the DTC dynamics, characterized by time intervals of stability defined by certain parameters associated with the measurement outcomes. We thus observe that the signature of the DTC remains stable over long times. Notably, the size of these stability intervals appears to increase as the system size grows, suggesting that the protocol may offer some robustness in the thermodynamic limit. Nevertheless, further analysis with larger sizes would be needed to determine whether there is a phase transition or simply a crossover between a stable and a suppressed DTC. These findings may be valuable for future experimental implementations, where decoherence due to the environment plays a key role in the dynamics and stability of these systems.

## 3.3 OUTLOOKS

In this chapter, we introduced the fascinating concept of time crystals. Our contribution shows that when a DTC is coupled to a thermal environment, it loses the characteristic subharmonic response. Interestingly, however, if the system is continuously monitored at discrete times with respect to a given observable, the subharmonic response is stabilized, counteracting the effects of decoherence.

What remains to be done? It would be interesting to apply this methodology to different DTCs implementations, using different measurement operators or monitoring the environment rather than the system itself.

Another promising direction is to investigate whether such measurements can induce entanglement-driven phase transitions, or explore metrological applications by studying how Fisher information is affected by this continuous monitoring.

In conclusion, this work opens new perspectives on using measurements not only to preserve quantum coherence, but also to control collective dynamics and harness time crystals for advanced applications.

# 4

# QUANTUM BATTERIES

Quantum batteries represent a promising platform for the controlled storage and extraction of energy at the quantum scale. Their study is relevant for both technological and fundamental reasons: from a technological perspective, a quantum advantage has already been demonstrated in the collective charging of quantum batteries; from a fundamental point of view, their open-system version lies at the intersection of quantum thermodynamics, quantum information theory, and the dynamics of open quantum systems, offering new insights into how correlations and measurements can influence energetic processes.

This chapter introduces the concept of quantum batteries, discussing their theoretical foundations and surveying recent experimental implementations. Building on this background, we present our results on the enhancement of extractable work in continuously monitored batteries, focusing on the role of correlations between the battery and the charger subsystems.

The material presented in the second part of this chapter is largely inspired by our forthcoming work [46].

## 4.1 INTRODUCTION TO QUANTUM BATTERIES

Almost two centuries after Alessandro Volta's invention of the pile, the idea of storing energy in a controllable and reusable way remains one of the driving forces of modern technology. Classical batteries, operating through electrochemical reactions, have become essential for powering everything from small portable devices to large-scale energy grids. Yet, as technological progress continues to push the boundaries of miniaturization, the question naturally arises: can the notion of a battery be extended to the quantum limit?

The emergence of quantum technologies, ranging from quantum computers [3, 99] and simulators [48] to sensors [100] and communication networks [101], has inspired a profound rethinking of how energy is processed, stored, and transferred at the microscopic scale. In this context, Quantum Batteries (QBs) have been proposed as elementary devices capable of storing and releasing energy through purely quantum mechanical processes. The concept, first formalized in 2013 by Alicki and Fannes [102], opened a new field of investigation that connects quantum thermodynamics, information theory, and open quantum systems.

Collective charging protocols, exploiting global entangling operations, have been shown to outperform independent, local strategies, leading to what has been termed a quantum advantage in charging power [103]. Although the realization of such collective effects in real devices remains experimentally challenging, several recent implementations in platforms such as optical microcavities, superconducting qubits, trapped ions, and solid-state spin ensembles have demonstrated the feasibility of storing and manipulating energy at the quantum level [104].

In this section, we will introduce the theoretical framework of QBs, review their main operational principles and figures of merit, and summarize the current experimental progress in this rapidly growing field.

### 4.1.1 *Foundational concepts and figure of merits*

At the most basic level, a QB is a quantum system capable of being driven from its lowest-energy configuration, typically the

ground state, to an excited state, which corresponds to a charged condition, through the interaction with an external charger. The charger can be either a quantum system or a classical external drive. Formally, in the case of a quantum charger, the total Hamiltonian of the composite system can be expressed as:

$$\hat{\mathcal{H}}(t) = \hat{\mathcal{H}}_B + \hat{\mathcal{H}}_C + \hat{\mathcal{H}}_{int}(t), \tag{4.1}$$

where $\hat{\mathcal{H}}_B$ describes the battery, $\hat{\mathcal{H}}_C$ the charger, and $\hat{\mathcal{H}}_{int}(t)$ accounts for the time-dependent coupling between B and C, which, in the simplest charging protocol, is activated only during the charging stage of duration $\tau$.

The battery can be made of a single quantum system, such as a TLS or an harmonic oscillator, or of several subsystems forming a multipartite device. Once the interaction is turned off, the charger is effectively disconnected, and the battery is left in a reduced state described by $\rho_B(\tau) = \mathrm{Tr}_C\left[\rho(\tau)\right]$, obtained by tracing out the charger degrees of freedom from the composite density matrix $\rho(\tau)$. This reduced state represents the *charged battery*, with *stored energy* given by

$$E(\tau) = \mathrm{Tr}_B[\hat{\mathcal{H}}_B \rho_B(\tau)] - \mathrm{Tr}_B[\hat{\mathcal{H}}_B \rho_B(0)]. \tag{4.2}$$

In general we assume that the initial state is the empty state of the battery, which usually coincides with the ground-state of $\hat{\mathcal{H}}_B$. A second fundamental quantity, in addition to the stored energy, is the *average charging power*,

$$P(\tau) = \frac{E(\tau)}{\tau}, \tag{4.3}$$

which measures the amount of energy transferred to the battery per unit time. From a practical perspective, higher charging power is generally desirable, as it allows for faster energy storage.

When considering *multipartite batteries* composed of N quantum cells, both the total stored energy (often called the *capacity*) and the charging power depend on the system size. The capacity typically scales extensively, $E(\tau) \propto N$, while the power may, in certain conditions, display a super-extensive scaling, $P(\tau) \propto N^k$ with $k > 1$. Such scaling indicates that, although the total stored energy naturally increases with the number of subsystems, the remarkable feature is that the charging speed grows faster than

linearly with the number of cells. In general, two distinct physical mechanisms can lead to super-extensive scaling: the first raises from collective effects that may also occur in classical systems, and in this case we talk about *collective advantage*. The second, the *quantum advantage*, relies on genuinely quantum resources such as coherence and entanglement. These two regimes can be discriminated by considering the upper bound on the charging power [105]:

$$P(\tau) \leqslant \sqrt{\Delta E^2(\tau)\mathcal{F}(\tau)}, \tag{4.4}$$

where $\Delta E^2(\tau) = \langle \hat{\mathcal{H}}_B^2 \rangle - \langle \hat{\mathcal{H}}_B \rangle^2$ denotes the energy variance of the battery [106], and $\mathcal{F}(\tau) = 2\sum_{i,j} \frac{(r_i - r_j)^2}{(r_i + r_j)} |\langle i| \hat{\mathcal{H}}_B |j\rangle|^2$ is the Quantum Fisher information with the respect of the Hamiltonian of the battery $\hat{\mathcal{H}}_B$ and the state $\rho_B(\tau) = \sum_i r_i |i\rangle\langle i|$ [107, 108]. The Fisher information, originating from information theory, quantifies how sensitively the energy distribution of the state changes over time, thereby connecting informational and dynamical aspects of charging. Super-extensive scaling of $\mathcal{F}(\tau)$ yields the collective advantage, i.e., an accelerated evolution through the state space that does not necessarily rely on quantum effects [109]. A genuine quantum advantage, instead, requires the emergence of multipartite entanglement, whose nonlocal structure enables the system to follow more efficient trajectories in the energy landscape, leading to super-extensive energy fluctuations and consequently faster charging dynamics [103, 110, 111].

After the charging phase, a central question arises: how much of the stored energy can be extracted as useful work? To ensure reversibility and prevent dissipative losses, the extraction must be carried out through unitary operations [112]. As introduced in the previous chapter, the maximum extractable energy, referred to as the *ergotropy*, $\mathcal{E}$, quantifies the portion of the energy that can be converted into work via coherent, reversible dynamics:

$$\mathcal{E}(\tau) = \mathrm{Tr}_B\left[\hat{\mathcal{H}}_B \rho_B(\tau)\right] - \mathrm{Tr}_B\left[\hat{\mathcal{H}}_B \rho_{B,p}(\tau)\right], \tag{4.5}$$

where $\rho_{B,p}(\tau)$ is the passive state related to $\rho_B(\tau)$ and from which no additional work can be obtained. For a more detailed discussion about ergotropy and its properties, the reader is referred

back to Chapter 2. Furthermore, another figure of merit one can consider is the *ergotropic power*:

$$\mathcal{W}(\tau) = \frac{\mathcal{E}(\tau)}{\tau}, \tag{4.6}$$

which quantifies the amount of work that can be unitarily extracted per unit time.

For a multipartite battery, the optimal extraction of ergotropy generally requires global unitary operations acting on the full system [102]. These operations can generate entanglement among different subsystems, which can speed up work extraction [110]. On the other hand, if only local operations are available, entanglement may become detrimental, reducing the amount of extractable energy [113, 36, 114].

In general, it is useful to define the efficiency of a QB as the ratio $\mathcal{R} = \mathcal{E}/\mathsf{E}$, which compares the ergotropy to the total energy stored in the battery state. This quantity provides a direct measure of how much of the stored energy can be converted into useful work through coherent, unitary operations. In the context of continuously monitored quantum systems, we introduce a new notion of efficiency defined as

$$\eta = \frac{\overline{\mathcal{E}} - \mathcal{E}}{\mathsf{E} - \mathcal{E}}, \tag{4.7}$$

where $\overline{\mathcal{E}}$ denotes the daemonic ergotropy of the conditional state under consideration, while $\mathcal{E}$ represents the ergotropy of the corresponding unconditional state. The efficiency $\eta \in [0, 1]$ quantifies the relative enhancement of extractable work due to measurement: it reaches unity when all the available energy is converted into extractable energy in the conditional case, and vanishes when no measurement-induced advantage is present.

### 4.1.2 *A paradigmatic example: Dicke quantum batteries*

Dicke quantum batteries represent one of the most extensively studied models of QBs [115]. Dicke model [116] was originally introduced to describe matter-radiation interactions across systems ranging from molecular ensembles to solid-state platforms [117], paving the way to both cavity and circuit quantum electrodynamics [118, 119]. They consist of an optical cavity (the charger) with,

in general, a single mode of the electromagnetic field coupled in the dipole approximation to an ensemble of N non-interacting TLSs (the battery). When more than one TLS is present in the cavity, collective effects emerge, leading to a super-extensive scaling in the number of TLSs of the battery charging power, $P_{max} \propto N^k$, with $1.5 \leqslant k \leqslant 2$, depending on the specific charging protocol. Various extensions of this model have been explored in the literature, including three-level charging processes [120], two-photon charging schemes [121], anisotropic variants where the rotating and counter-rotating terms have distinct coupling strengths [122], off-resonant regimes [123], and finally leveraging machine learning for optimizing the extraction process [124].

Interestingly, a similar super-extensive scaling also appears in the classical analogue of the Dicke model, reflecting that such behaviour rises from the model intrinsic collective dynamics rather than being an genuine quantum effect [113].

The model has been investigated in the presence of both cavity photon losses [125] and local incoherent processes affecting the individual TLS, such as dephasing and decay [126], which are the most commonly considered in the literature. In all these cases, the asymptotic super-extensive scaling is preserved, confirming the existence of an asymptotic freedom [113] that remains robust under such noises. This behaviour can be intuitively understood by noting that, while entanglement entropy in integrable many-body systems typically scales *sub-extensively* (following a so-called *area law*), energy is an extensive quantity that grows linearly with system size. As a result, in the thermodynamic limit, the symmetries of the Dicke model ensure that the fraction of stored energy inaccessible to work extraction becomes negligible.

In the following, to set the stage for the next section, we will briefly report some results obtained for closed Dicke quantum batteries, as well as for their open counterparts considering cavity photon losses.

#### 4.1.2.1 *Closed system*

Let us briefly review the closed-system case and reproduce some of the results presented in [115]. We consider a collection of N identical non-interacting TLSs coupled to a single mode of the

electromagnetic field in an optical cavity. Let $\hat{a}$ and $\hat{a}^\dagger$ be the annihilation and creation operators of the cavity mode with frequency $\omega_c$, the Hamiltonian of the system in the dipole approximation (namely, the Dicke Hamiltonian) reads:

$$\hat{\mathcal{H}}_\lambda^{(N)}(t) = \hbar\omega_c \hat{a}^\dagger \hat{a} + \omega_a \hat{S}_z + 2\omega_c \lambda(t) \hat{S}_x (\hat{a}^\dagger + \hat{a}), \tag{4.8}$$

where, $\hat{S}_\alpha = (\hbar/2) \sum_i^N \hat{\sigma}_\alpha^i$ with $\alpha = x, y, z$ are the component of the collective spin operator expressed in terms of the Pauli matrices $\hat{\sigma}_\alpha^i$ of the $i$-th TLS. Being $|g\rangle$ and $|e\rangle$ the ground and the excited state of a single TLS, the quantity $\hbar\omega_a$ is the energy splitting between $|g\rangle$ and $|e\rangle$. From now on, we will assume $\hbar = 1$. The interaction strength is governed by the dimensionless time-dependent parameter $\lambda(t)$, whose explicit time dependence is determined by the specific charging (or discharging) protocol. From now on we focus on the resonant regime $\omega_a = \omega_c = 1$.

As initial state of the system we assume

$$|\Psi^{(N)}(0)\rangle = |N\rangle \otimes |g\rangle^{\otimes N}, \tag{4.9}$$

where the single cavity mode is initialized in the N photons Fock state $|N\rangle$ while the battery state is the tensor product of the single TLS ground states. In the present study, we consider the simplest charging protocol, which consists of switching on the interaction at time $t = 0$ and keeping it active until charging time $\tau_c$. The interaction strength is fixed at a constant value $\bar{\lambda}$ throughout the entire protocol. We numerically simulate the system using QuTiP [127]. Since the number of photons in the cavity is neither conserved nor inherently bounded, we introduce a cutoff in the Fock Hilbert space by limiting the maximum photon number. In the following, we set $N_{ph} = 20$ for $N < 5$, and $N_{ph} = 4N$ for $N \geqslant 5$. With this choice, numerical convergence is ensured. The results are presented for $N = 1, \ldots, 20$.

The energy stored in the battery at time $\tau_c$ is given by

$$E_{\bar{\lambda}}(\tau_c) = \omega_c \left[ \langle \Psi_{\bar{\lambda}}^{(N)}(\tau_c)| \hat{S}_z |\Psi_{\bar{\lambda}}^{(N)}(\tau_c)\rangle - \langle \Psi^{(N)}(0)| \hat{S}_z |\Psi^{(N)}(0)\rangle \right], \tag{4.10}$$

where $|\Psi_{\bar{\lambda}}^{(N)}(\tau_c)\rangle = e^{-i\hat{\mathcal{H}}_{\bar{\lambda}}^{(N)}\tau_c} |\Psi^{(N)}(0)\rangle$. As introduced earlier, throughout this section and the following, we also consider the

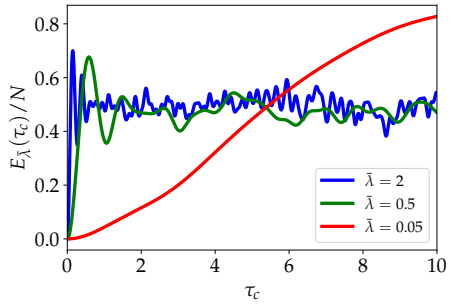


Figure 4.1: Stored energy as a function of the charging time. Here $N = 10$

ergotropy as a key figure of merit. Here, we recall its definition for the specific Hamiltonian and state under consideration:

$$\mathcal{E}_{\bar{\lambda}}(\tau_c) = \mathrm{Tr}_B\left[\hat{\mathcal{H}}_B \rho_B(\tau_c)\right] - \min_{\hat{U}}\left\{\mathrm{Tr}_B\left[\hat{\mathcal{H}}_B(\hat{U}\rho_B(\tau_c)\hat{U}^\dagger)\right]\right\}, \quad (4.11)$$

where the trace operation is performed on the battery degrees of freedom, $\hat{\mathcal{H}}_B = \omega_a S_z$ is the local Hamiltonian of the battery, and $\rho_B(\tau_c) = \mathrm{Tr}_C\left[|\Psi^{(N)}_{\bar{\lambda}}(\tau_c)\rangle\langle\Psi^{(N)}_{\bar{\lambda}}(\tau_c)|\right]$ is the reduced density matrix of the battery (the trace operation is performed on the charger degrees of freedom).

This quantity represents the maximum amount of work that can be extracted from the state $\rho_B(\tau_c)$ using unitary operations. In Figure 4.1, we show the energy charging process of the Dicke quantum battery for different coupling strengths. Some basic observations can be made: the larger the coupling, the faster the charging. For small coupling values the dynamics is smooth and a greater amount of energy per TLS can be stored, whereas for stronger coupling a more complex pattern emerges characterized by oscillations and beatings. In Figure 4.2, and throughout the analysis, we consider the maximum value of each figure of merit defined above (stored energy $E_{\bar{\lambda}} \equiv \max_{\tau_c}\left[E_{\bar{\lambda}}(\tau_c)\right]$ and charging power $P_{\bar{\lambda}} \equiv \max_{\tau_c}\left[E_{\bar{\lambda}}(\tau_c)/\tau_c\right]$) over the charging time interval. In the case of ergotropy, however, we evaluate it at the time of maximum energy ($\mathcal{E}_{\bar{\lambda}} \equiv \mathcal{E}_{\bar{\lambda}}(\mathrm{argmax}_{\tau_c}\left[E_{\bar{\lambda}}(\tau_c)\right])$), since ergotropy is upper bounded by the energy and this choice simplifies the analysis (as it avoids to carry out diagonalization of the density matrix for every time step). The data confirm previously

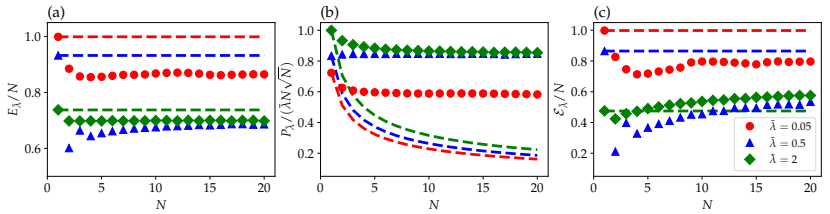


Figure 4.2: Charging energy (a), power (b), and ergotropy (c) as a function of the number of two-level systems in the cavity (N) for different coupling strengths. Markers refer to the case of collective charging, while the dashed lines correspond to the parallel charging scenario, where each TLS is independently charged by its own cavity. As expected, the collective enhancement is visible only in the case of superextensive scaling, and thus appears clearly in the power.

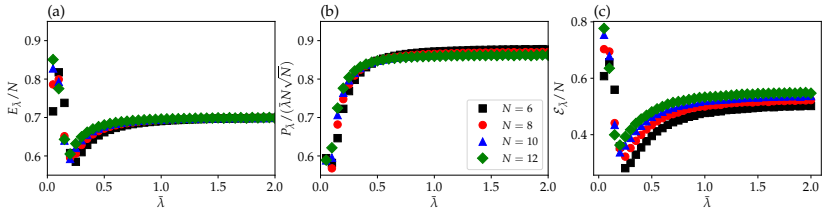


Figure 4.3: Charging energy (a), power (b), and ergotropy (c) as a function of the coupling strength $\bar{\lambda}$ for different system sizes.

known results: both energy and ergotropy exhibit extensive scaling, while the charging power scales superextensively, with an exponent of approximately $3/2$.

Figure 4.3 shows the dependence of the results on the coupling strength. The ergotropy reaches its maximum in the weak coupling regime, whereas all figures of merit exhibit saturation and converge to a plateau as $\bar{\lambda}$ increases.

#### 4.1.2.2 *Open system*

We consider a regime where, during the charging time, the dissipation rate of the battery is negligible compared to that of the cavity. Taking into account environmental losses, we describe

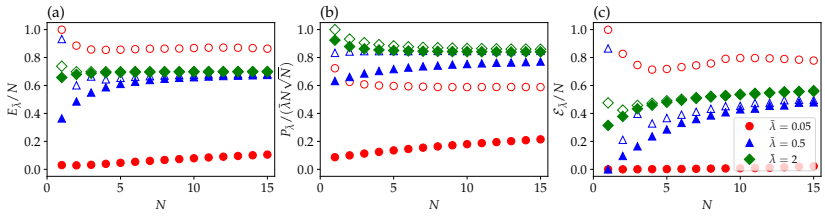


Figure 4.4: Charging energy (a), power (b), and ergotropy (c) as a function of the number of two-level systems in the cavity (N) for different coupling strengths. Solid markers refer to dissipative case ($\kappa = 0.5$) while empty markers refer to the closed system ($\kappa = 0$).

the system dynamics using the Lindblad master equation for the density matrix $\rho_{\bar{\lambda}}$:

$$\frac{d\rho_{\bar{\lambda}}}{dt} = -i\left[\hat{\mathcal{H}}_{\bar{\lambda}}^{(N)}, \rho_{\bar{\lambda}}\right] + \hat{c}\rho_{\bar{\lambda}}\hat{c}^\dagger - \frac{1}{2}\left\{\hat{c}^\dagger\hat{c}, \rho_{\bar{\lambda}}\right\}, \tag{4.12}$$

where the jump operator $\hat{c} = \sqrt{2\kappa}\hat{a}$, and $\kappa$ is the dissipation rate of the cavity. More generally, this expression corresponds to the zero-temperature limit of a thermal photon environment, adopted here to suppress re-population effects associated with finite temperatures, and to consider only non-perfect mirrors[1].

The scaling behaviour analogous to that shown in Figure 4.2 is presented in Figure 4.4. This figure clearly illustrates that the collective effects of the Dicke model preserve the scaling of both energy and power, especially for large system sizes. However, it also highlights how ergotropy is significantly affected in the weak-coupling regime, with this trend even more evident in Figure 4.5. This reduction can be understood as a consequence of the competition between the charging timescale and the cavity dissipation rate: at small coupling strengths, the charging process proceeds more slowly than the cavity coherence time, allowing dissipation to significantly impact the dynamics. As the number of TLSs increas, however, the collective speed-up shortens the

1 At non-zero temperature, the environment is characterized by the following jump operators:

$$\hat{\mathcal{L}}_1 = \sqrt{2\kappa(n_{th}+1)}\hat{a}, \qquad \hat{\mathcal{L}}_2 = \sqrt{2\kappa n_{th}}\hat{a}^\dagger,$$

where $n_{th} = 1/(e^{\omega_c/k_B T} - 1)$ is the mean thermal photon occupation number.

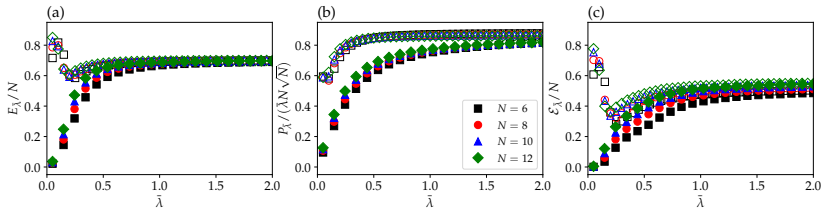


Figure 4.5: Charging energy (a), power (b), and ergotropy (c) as a function of the coupling strength $\bar{\lambda}$ for different system sizes. Solid markers refer to dissipative case ($\kappa = 1$) while empty markers refer to the closed system ($\kappa = 0$).

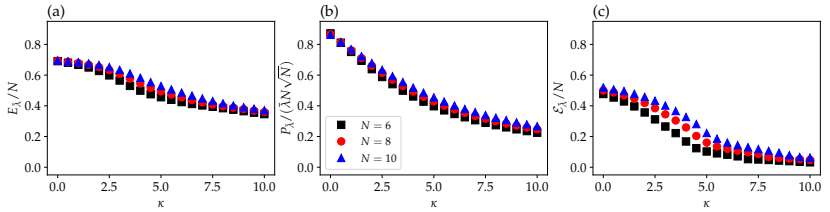


Figure 4.6: Charging energy (a), power (b), and ergotropy (c) as a function of the dissipation strength $\kappa$ for different system sizes. Here ($\bar{\lambda} = 1$).

charging time, thereby mitigating the effects of cavity losses and stabilizing the process. Figure 4.6 further supports this interpretation, showing that for finite-size systems, the ergotropy rapidly decreases at large values of $\kappa$, while the total stored energy is less affected. This behaviour confirms that dissipation predominantly limits the extractable work, leaving the passive component of the stored energy essentially intact.

### 4.1.3 *Other architectures and experimental realizations*

Beyond cavity based implementations, several alternative physical platforms have been explored as candidates for quantum batteries.

A notable example is provided by spin-chain systems, where TLSs interact through various coupling schemes, and can be charged either by the action of a classical external field [128] or by quenching one or more of their internal parameters [129], leading

to remarkably long energy storage times exploiting many-body localization and disorder [130, 131, 132] or topological effects [133, 134]. While their charging power typically scales extensively, a genuine quantum advantage has been identified in the Sachdev-Ye-Kitaev (SYK) model [135, 136]. In this case, random non-local spin interactions generate multipartite entanglement that enables super-extensive scaling of the charging power, $P_{max} \propto N^{\alpha}$ with $\alpha \approx 1.5$. However, the high level of connectivity required by the SYK Hamiltonian makes its experimental realization extremely demanding, although recent proposals suggest that solid-state implementations may become feasible in the near future [137].

Another versatile architecture relies on quantum harmonic oscillators, one of the most universal and, at the same time, one of the few analytically tractable quantum system. Quantum batteries based on harmonic oscillators benefit from their infinite energy spectrum, allowing for large energy storage capacities, and can be charged and discharged via continuous variable operations such as displacement and squeezing [138]. Interestingly, even within this paradigm, a genuine quantum advantage can emerge when nonlinear interactions are engineered between two oscillators, one acting as the charger and the other as the battery, enabling more efficient energy transfer [139]. Further studies have shown that advantages may arise in strongly non-Markovian environments, where dynamical blockade effects can prevent energy leakage and promote highly efficient charging [140], as well as in micromaser-based implementations, where a cavity mode charged by coherent qubits operates as an effective steady-state quantum battery, even in the ultrastrong coupling regime [141, 142].

Recent years have seen the emergence of many concrete experimental implementations of quantum batteries. The first breakthrough was based on organic fluorescent molecules embedded within an optical cavity, with an external laser acting as the charger [143]. In this setup, the strength of the matter-radiation interaction is proportional to the molecular density in the cavity, increasing it drives a transition to the Dicke regime, where the charging power scales super-extensively, and stable storage lasting tens of nanoseconds is achieved [149, 150]. Despite operating at room temperature, these systems suffer from limited capac-

Table 4.1: Comparison of different quantum battery platforms and a classical Li-ion battery: (a) Dicke quantum batteries implemented via fluorescent molecules in optical microcavities [143]; (b) Nuclear spins quantum batteries in a NMR setup [144]; (c) Solid state platforms based on quantum dots [145] and superconducting circuits [146, 147, 148]; (d) Classical batteries.

| Platform | Energy density | Charging time | Storage time | Power density |
|---|---|---|---|---|
| (a) | $10^{-20}$ J/mol. | $10^{-14}$ s | $10^{-8}$ s | $10^{-6}$ W/mol. |
| (b) | $10^{-27}$ J/spin | $10^{-1}$ s | $10^{2}$ s | $10^{-26}$ W/spin |
| (c) | $10^{-24}$ J/qubit | $10^{-8}$ s | $10^{-4}$ s | $10^{-16}$ W/qubit |
| (d) | $10^{5}$ J/kg | $10^{3}$ s | $> 10^{5}$ s | $10^{2}$ W/kg |

ity due to molecular crowding effects that lead to detrimental interactions among molecules (see Table 4.1).

Nuclear-spin quantum batteries have also been demonstrated using Nuclear Magnetic Resonance (NMR) techniques [144, 151]. In these systems, the spin states are manipulated by time-dependent magnetic fields, they can operate at room temperature and they exhibit exceptional stability and long storage times, though the energy per molecule remains extremely small, as reported in Table 4.1.

At low temperatures, implementations based on semiconducting quantum dots, acting as artificial atoms, [145] and superconducting circuits [152, 153] have been developed. These systems offer precise control and fast response times, but currently operate with limited energy storage (per element) and are limited to individual or few-element configurations, far from the scalability required to compete with classical batteries. Nonetheless, superconducting circuits, being central to quantum computing architectures [154, 146, 147, 148, 155, 156, 157], provide a promising route for scalable, controllable QB experiments.

While the comparison with classical batteries may appear discouraging (Table 4.1), given their vastly superior energy capacity and practicality, this perspective misses the true purpose of QBs. They are not designed or even thinked to power macroscopic devices like smartphones or electric cars, but rather to operate at the quantum scale, serving as functional components of quantum

technologies, from computation to sensing. In particular, quantum batteries could play a key role in enabling energy efficient and reversible quantum computation, where dedicated qubits act as energy reservoirs supplying coherent energy to computational qubits during logical operations [158, 159].

## 4.2 DAEMONIC ERGOTROPY ENHANCEMENT IN CORRELATED SYSTEMS

Having established in the previous section the general framework of quantum batteries, together with their main figures of merit and current experimental implementations, we now turn to the analysis of continuously monitored systems.

After briefly recalling some theoretical tools introduced earlier, we present three representative examples illustrating how continuous measurements can enhance the ergotropy of a QB. This enhancement, as we shall see, typically emerges in regimes where quantum correlations between the battery and the charger are significant, correlations that, in the absence of monitoring, are usually detrimental to performance.

We begin with a simple spin-spin model, then move to a configuration where the energy transfer is mediated by a cavity mode, and finally discuss Dicke quantum batteries, for which we adopt the same notation introduced in the previous section.

### 4.2.1 *Introduction*

Realistic quantum batteries do not evolve in isolation. Their inevitable interaction with the surrounding environment leads to decoherence and dissipation processes typically associated with energy and ergotropy losses [160, 161], even worst in the strong coupling regime [162, 163]. This observation has motivated the study of *open quantum batteries* [103], in which the device exchanges both energy and information with its environment. Surprisingly, such interactions are not necessarily detrimental. Under suitable conditions, they can instead be harnessed as valuable resources: examples include controlled dissipation [164, 165], engineered reservoirs [166, 167, 168, 169, 170] and continuous measurements. A promising strategy to mitigate the deleteri-

ous effects of the environment consists indeed in continuously monitoring not the quantum battery itself [171], but rather the environment which it interacts with [4]. Exploiting the information extracted from measurements, it becomes possible to design feedback-based protocols [172, 173] that either enhance work extraction or stabilize stored energy, thereby bridging the fields of quantum thermodynamics and quantum control theory.

In this section, we focus on analyzing the role of continuous measurements and system correlations in enhancing the extractable work from an open quantum battery. Entanglement between the battery and the charger tends to reduce the ergotropy that can be extracted from the battery alone. Introducing a moderate level of dissipation, either on the battery or on the charger, could weaken such correlations, thereby improving the energy extraction performances. This enhancement can be further amplified when continuous measurements are performed on the environment, as the additional information gained through the measurement process can be exploited to increase the extractable work.

This mechanism will be illustrated through three representative models. We begin with two coupled spins acting respectively as charger and battery, initially prepared in an entangled state. We then consider a less fine-tuned configuration, in which correlations arise dynamically between two spins coupled via a (lossy) cavity mode. In this latter case, dissipation is induced by photon leakage from the cavity, and the continuous measurement of the environment has a clear experimental interpretation. Finally, we turn to *Dicke quantum batteries*, that, as we have seen, are one of the most studied and experimentally relevant QB architectures. Here, we focus on the finite-size regime and a dissipative cavity: to recover the ergotropy lost due to dissipation, we couple the system to a detector (either a photo-detector or a homodyne detector) that continuously monitors the stream of lossy photons. Remarkably, the resulting *daemonic ergotropy*, that is, the extractable work when accounting for the information gathered through measurement, not only compensates for dissipative losses, but in certain parameter regimes even surpasses the ideal, lossless value.

### 4.2.2 *Recap on daemonic ergotropy and SMEs*

When the environment of an open quantum system is continuously monitored over time, the induced dynamics is conditioned by the inherently stochastic nature of quantum measurements, leading to a stochastic evolution of the system wavefunction, commonly referred to as *quantum trajectory*.

The information gained from continuous measurements can be exploited in two ways: either during the charging process, through real-time feedback aimed to steer the quantum state toward one with higher ergotropy, or during the extraction phase, where the unitary extracting work is adapted to each conditional state based on the measurement outcomes [27, 28, 147]. In the latter case, we talk about *daemonic ergotropy* in analogy with the classical Maxwell demon. Suppose that $\rho_{B|k}$ is the conditional battery state given the measurement $k$ with probability $p_k$, we assume that a demon can perform a $k$-dependent unitary operator $\hat{U}_k$ optimized for each conditional state in order to extract the amount of work $\mathcal{W}_k(\rho_{B|k})$, then the average extractable work is

$$\mathbb{E}[\mathcal{W}] \equiv \overline{\mathcal{W}} = \sum_k p_k \mathcal{W}_k(\rho_{B|k}) \leqslant \sum_k p_k \mathcal{E}(\rho_{B|k}) = \overline{\mathcal{E}} \equiv \mathbb{E}[\mathcal{E}], \tag{4.13}$$

where the upper bound is given by the ensemble average of the ergotropy of the conditional states, known as the daemonic ergotropy. In general, it has been shown that daemonic ergotropy can exceed the unconditional one, allowing for the extraction of energy even from the passive component of the state, and it is bounded above by the total energy of the state,

$$E(\rho_B) \geqslant \overline{\mathcal{E}} \geqslant \mathcal{E}(\rho_B) \tag{4.14}$$

where $E(\rho_B)$ is the internal energy of the battery. Since energy is a linear function of the state, it is the same whether evaluated on the conditional or unconditional state.

In general, different types of measurements lead to different forms of stochastic master equations, depending on the specific measurement operators involved. In the case of on/off PD, the POVM associated with the quantum measurement is given by the

Fock basis $\{|n\rangle\langle n|\}$. This framework leads to the following SSE, since the initial state is pure, the conditional evolution remains confined to the manifold of pure states:

$$\begin{aligned} d|\Psi^{(c)}_{B,C}(t)\rangle &= \left[-i\hat{\mathcal{H}}(t)dt + \frac{1}{2}\left(\langle\hat{c}^\dagger\hat{c}\rangle - \hat{c}^\dagger\hat{c}\right)dt + \right. \\ &+ \left.\left(\frac{\hat{c}}{\sqrt{\langle\hat{c}^\dagger\hat{c}\rangle}} - 1\right)dN_t\right]|\Psi^{(c)}_{B,C}(t)\rangle\,, \end{aligned} \tag{4.15}$$

where $\hat{\mathcal{H}}(t)$ is the Hamiltonian of the system, $|\Psi_{B,C}(t)\rangle$ is the battery-charger state at time $t$ and the jump operator $\hat{c}$ depends on the specific system under consideration. $dN_t$ denotes a Poisson increment, which takes values $0$ (no detection) or $1$ (detection). The corresponding Poisson process $N_t$ is characterized by a time-dependent rate $\nu(t)$, such that the probability of more than one detection event occurring within an infinitesimal interval $dt$ is negligible. The detection rate is determined by the expected number operator associated to $\hat{c}$ in the conditional state, and is given by $\nu(t) = \langle\Psi^{(c)}_{B,C}(t)|\,\hat{c}^\dagger\hat{c}\,|\Psi^{(c)}_{B,C}(t)\rangle$. The unconditional state can be recovered by averaging over the ensemble of conditional pure state trajectories, that is, by performing the unraveling of the stochastic evolution:

$$\mathbb{E}\left[|\Psi^{(c)}_{B,C}(t)\rangle\langle\Psi^{(c)}_{B,C}(t)|\right] = \rho_{B,C}(t), \tag{4.16}$$

where the expectation is taken over all possible realizations of the measurement outcomes. The conditional state of the battery is then $\rho^{(c)}_B(t) = \mathrm{Tr}_C\left[|\Psi^{(c)}_{B,C}(t)\rangle\langle\Psi^{(c)}_{B,C}(t)|\right]$, where the trace is performed on the charger degrees of freedom.

In the case of HD, the measurement process corresponds to a continuous monitoring of the environment field quadrature. Formally, it can be described by a POVM $|x_\theta\rangle\langle x_\theta|$ associated with the quadrature operator $\hat{x}_\theta$, where $\theta$ sets the local oscillator phase. A detailed microscopic derivation, based on collision models, can be found in chapter 1. From now on, we will consider the $\theta = 0$ quadrature, unless otherwise specified, leading to the corresponding SSE for HD:

$$\begin{aligned} d|\Psi^{(c)}_{B,C}(t)\rangle &= \left[-i\hat{\mathcal{H}}(t)dt - \frac{1}{2}\left(\hat{c}^\dagger\hat{c} - \hat{c}\langle\hat{c}+\hat{c}^\dagger\rangle + \frac{\langle\hat{c}+\hat{c}^\dagger\rangle^2}{4}\right)dt + \right. \\ &+ \left.\left(\hat{c} - \frac{\langle\hat{c}+\hat{c}^\dagger\rangle}{2}\right)dw_t\right]|\Psi^{(c)}_{B,C}(t)\rangle\,, \end{aligned} \tag{4.17}$$

where $dw_t$ is a Wiener increment, a Gaussian stochastic variable with zero mean and variance $dt$ representing the intrinsic noise contribution to the measured photocurrent arising from the continuous quantum measurement.

### 4.2.3 *Results*

#### 4.2.3.1 *A simple example*

In this first pedagogical example, we consider two spins: one (labeled C) acting as the charger, and the other (labeled B) acting as the battery. The Hamiltonian of the system reads

$$\hat{\mathcal{H}} = \frac{1}{2}\omega_B \hat{\sigma}_B^z + \frac{1}{2}\omega_C \hat{\sigma}_C^z + g\hat{\sigma}_B^x \otimes \hat{\sigma}_C^x, \tag{4.18}$$

where $\hat{\mathcal{H}}_B = \frac{1}{2}\omega_B \hat{\sigma}_B^z$ is the Hamiltonian of the battery, and the XX interaction term is assumed to be active only during the charging. From now on, we consider the resonant case $\omega_B = \omega_C = 1$ and we set the coupling strength to $g = 1$. As the initial state of the system, we choose the following, generally entangled, state:

$$|\psi(0)\rangle_p = \sqrt{p}\,|\downarrow\rangle_B \otimes |\uparrow\rangle_C + \sqrt{1-p}\,|\uparrow\rangle_B \otimes |\downarrow\rangle_C\,, \tag{4.19}$$

where the parameter $p \in [0.5, 1]$ quantifies the amount of bipartite quantum entanglement between the battery and the charger, and $\{|\downarrow\rangle_{B(C)}, |\uparrow\rangle_{B(C)}\}$ are the eigenstates of $\hat{\sigma}_{B(C)}^z$. When $p = 1$, the system starts in a separable state and undergoes a perfect transfer of energy from C to B, leading to the maximum extractable ergotropy, which in this case equals one. Conversely, for $p = 0.5$, the system is initially in a maximally entangled Bell state, and no ergotropy can be extracted. In general, given the battery reduced state $\rho_B(0) = \mathrm{Tr}_C\left[|\psi(0)\rangle_p \langle\psi(0)|_p\right]$, its purity $\mathrm{Tr}\left[\rho_B^2(0)\right] = 2p^2 - 2p + 1$ is related to the second order Rényi entropy, which is a measure of entanglement between the battery and the charger.[2]

2 Given a bipartite system $\mathbb{H}_A \otimes \mathbb{H}_B$, the second order Rényi entropy $S_2$ is a measure of quantum entanglement that can be calculated from the trace of the squared reduced density operator $\rho_A = \mathrm{Tr}_B\left[\rho_{AB}\right]$ of one subsystem, $S_2 = -\ln \mathrm{Tr}_A\left[\rho_A^2\right]$. The greater the entropy, the greater the bipartite entanglement between the two subsystems.

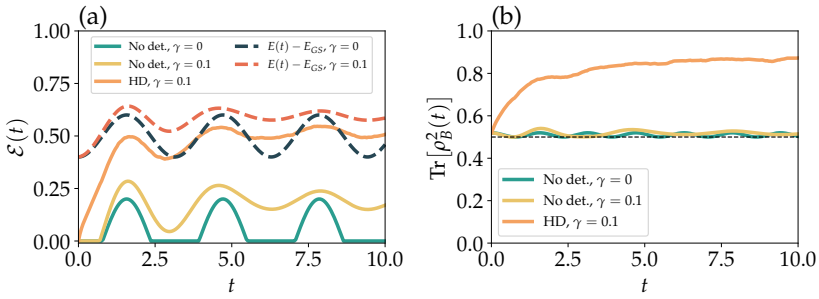


Figure 4.7: Ergotropy (a) and purity (b) of the battery as functions of the charging time in the spin-spin QB. In (a), the blue and red dashed lines indicate the upper energy bounds for the non-dissipative and dissipative ergotropies, respectively. In (b), the black dashed line represents the minimum possible purity corresponding to a maximally entangled state. Here, $p = 0.6$, and the HD unraveling is averaged over $n = 1000$ trajectories.

The purity increases monotonically with $p$, meaning that the larger the value of $p$, the lower is the initial entanglement between B and C.

Although the choice of starting from a state with non-zero quantum correlations between B and C is of course not optimal for work extracion, it serves the purpose already mentioned in the introduction of this section: when dissipation is included, the extractable ergotropy may be enhanced. In order to prove that, we consider dissipation in the form of population-relaxation jump operators $\hat{c}_B = \sqrt{\gamma}\,\hat{\sigma}_B^x$ and $\hat{c}_C = \sqrt{\gamma}\,\hat{\sigma}_C^x$, with $\gamma$ denoting the dissipation rate. The corresponding dynamics is described by a Lindblad master equation. We further consider an unraveling of this unconditional evolution through the HD SSE. At first glance, the use of HD in this context may seem odd, since the physical meaning of such measurement is not straightforward for spin jump operators (or, more precisely, for the input-output mode they couples to). However, this should not be a concern: from a mathematical standapoint, the description remains fully consistent and it is employed here purely as a pedagogical example, without any claim of direct physical applicability.

In Figure 4.7 (a), we show the ergotropy for different values of the dissipation rate, together with the corresponding daemonic

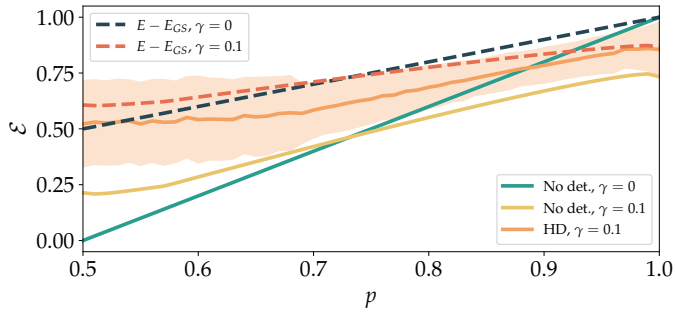


Figure 4.8: Maximum ergotropy as a function of p in the spin-spin QB. The larger the value of p, the lower the entanglement of the initial state. The blue and red dashed lines indicate the upper energy bounds for the non-dissipative and dissipative ergotropies, respectively. The HD unraveling is averaged over $n = 1000$ trajectories, and the shaded area represents one standard deviation of the daemonic ergotropy.

ergotropy, as a function of the charging time. As can be seen, when the dissipation rate is non-zero, both the unconditional and the conditional ergotropy outperform the noiseless case. The underlying mechanism is clearly illustrated in Figure 4.7 (b), where we observe that the purity of the battery state without detection remains close to the maximally mixed value of 0.5, while in the presence of measurement the purity increases over time, going towards a low-entanglement configuration. The maximum ergotropy $\mathcal{E} = \max_t \mathcal{E}(t)$ for different values of p is shown in Figure 4.8. The noiseless unconditional ergotropy grows linearly with p, while the daemonic ergotropy clearly outperforms the unconditional one for a wide range of initially entangled states. This result becomes even more evident in Figure 4.9, where the corresponding efficiency $\mathcal{R} = \mathcal{E}/E$ approaches its upper bound, $\mathcal{R} = 1$, for almost all values of p.

#### 4.2.3.2 *Cavity mediated energy transfer*

In the previous example, entanglement was embedded in the initial state, a situation that is neither ideal nor common in the context of quantum batteries, since the battery is typically prepared in its ground state. Nonetheless, correlations between

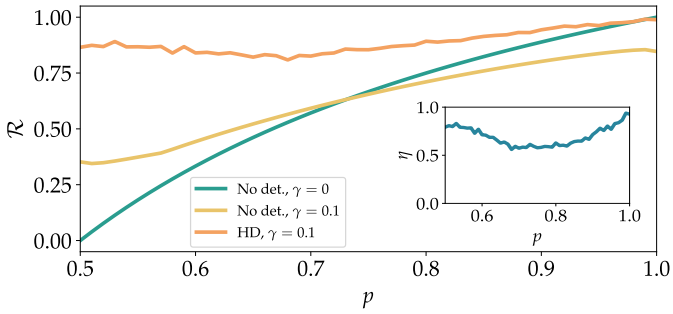


Figure 4.9: Maximum ergotropy efficiency ratio $\mathcal{R}$ as a function of $p$ in the spin-spin QB, the inset shows the daemonic conversion efficiency $\eta$. The HD unraveling is averaged over $n = 1000$ trajectories.

the battery and the charger can arise dynamically during the charging process, as we show in the example presented here.

We consider again a two-spins system, but in this case the spins are not directly coupled; rather, their interaction is mediated by a cavity mode $\hat{a}$. The Hamiltonian of the system [174, 175] is given by

$$\begin{aligned}\hat{\mathcal{H}} &= \frac{1}{2}\omega_B \hat{\sigma}_B^z + \frac{1}{2}\omega_C \hat{\sigma}_C^z + \omega_A \hat{a}^\dagger \hat{a} + \\ &+ g_B(\hat{\sigma}_B^+ \hat{a} + \hat{\sigma}_B^- \hat{a}^\dagger) + g_C(\hat{\sigma}_C^+ \hat{a} + \hat{\sigma}_C^- \hat{a}^\dagger),\end{aligned} \tag{4.20}$$

where $\hat{\sigma}^{\pm}_{B(C)} = \frac{1}{2}(\hat{\sigma}^x_{B(C)} \pm i\hat{\sigma}^y_{B(C)})$, and the interaction terms are considered to be active only during the charging process. The cavity is initially prepared in the zero-photon Fock state $|0\rangle_A$, while the charger is excited and the battery is in the ground state:

$$|\psi(0)\rangle = |\downarrow\rangle_B \otimes |\uparrow\rangle_C \otimes |0\rangle_A . \tag{4.21}$$

From now on, we consider the resonant case $\omega_C = \omega_B = \omega_A = 1$ and we set $g_B = 1$, allowing the coupling strength of the charger, $g_C$, to vary. When $g_C = 1$ the system is in perfect resonace and there is a complete energy transfer from C towards B, while if $g_C \neq 1$ the energy transfer is not optimal.

Here, the dissipation is modeled as a lossy cavity, as in the Dicke quantum battery case. The corresponding jump operator is $\hat{c} = \sqrt{\gamma}\hat{a}$, and again we consider an unraveling of this unconditional evolution through the HD SSE.

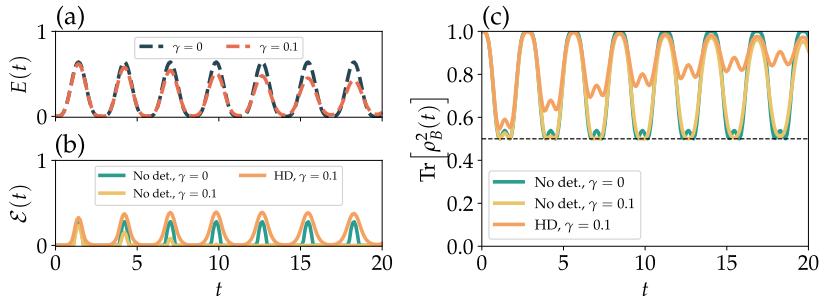


Figure 4.10: Energy upper bounds (a) for the non-dissipative and dissipative ergotropies, ergotropy (b) and purity (c) of the battery qubit as functions of the charging time in the cavity mediated spin-spin QB. In (c), the black dashed line represents the minimum possible purity corresponding to a maximally entangled state. Here, $g_C = 2$, and the HD unraveling is averaged over $n = 1000$ trajectories.

As before, the ergotropy for different values of the dissipation rate, together with the corresponding daemonic ergotropy, is shown in Figure 4.10 (b) as a function of the charging time. The ergotropy exhibits Rabi oscillations that are damped for non-zero dissipation. In the conditional case, the oscillatory behaviour is recovered, and the peak heights even surpass the noiseless case. In Figure 4.10 (c), we observe that the purity of the battery state reaches periodically values close to complete mixture, oscillating with the same period as the ergotropy maxima. Once again, in the presence of continuous measurements, the depth of the valleys increases over time, and the state evolves toward a low-entanglement configuration, confirming the phenomena observed before.

Figure 4.11 shows the maximum ergotropy, $\mathcal{E} = \max_t \mathcal{E}(t)$, as a function of $g_C \in [0.5, 2.5]$. While the noiseless unconditional ergotropy peaks at $g_C = 1$, the daemonic ergotropy surpasses the unconditional case for $g_C \gtrsim 1.75$. This behaviour is further highlighted in Figure 4.12, where the corresponding efficiency $\mathcal{R}$ matches or even exceeds that of the noiseless unconditional scenario.

In this case, the interpretation is straightforward. When the coupling between the charger qubit and the cavity is strong, the

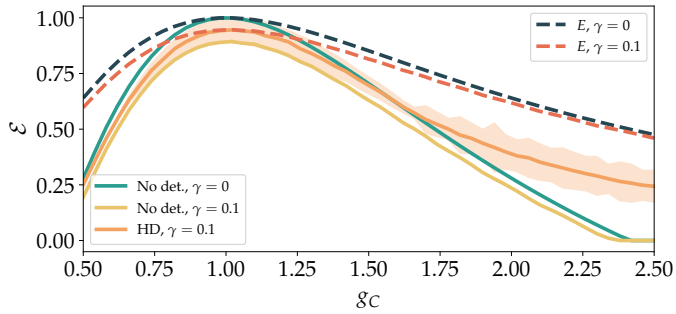


Figure 4.11: Maximum ergotropy as a function of $g_C$ in the cavity mediated spin-spin QB. The blue and red dashed lines indicate the upper energy bounds for the non-dissipative and dissipative ergotropies, respectively. The HD unraveling is averaged over $n = 1000$ trajectories, and the shaded area represents one standard deviation of the daemonic ergotropy.

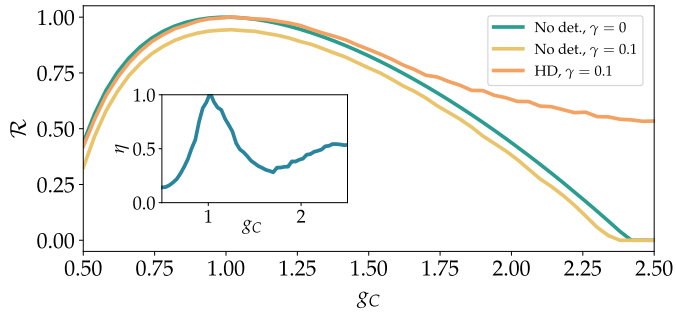


Figure 4.12: Maximum ergotropy efficiency ratio $\mathcal{R}$ as a function of $g_C$ in the cavity mediated spin-spin QB, the inset shows the daemonic conversion efficiency $\eta$. The HD unraveling is averaged over $n = 1000$ trajectories.

coherent energy remains trapped within these two systems, and the battery gets charged only by passive energy. The effect of the measurements, together with the entanglement between the battery and the rest of the system, renders the previously blocked energy accessible for extraction. As the coupling $g_C$ increases further ($g_C \sim 10$, well beyond the range shown in Fig. 4.11), the battery is effectively excluded from the dynamics, and no energy transfer occurs.

#### 4.2.3.3 *Dicke quantum batteries*

We turn now our attention on a more realistic model. As discussed in the previous section, in a finite-size setting where asymptotic freedom does not play a role, the ergotropy of the Dicke quantum battery, initialized in a Fock state, rapidly decreases once the cavity is coupled to an external environment. This suggests that collective finite-size quantum effects alone are not sufficient to protect the extractable work against the detrimental influence of decoherence, at least for fixed $\bar{\lambda}$. Continuously monitoring is particularly well-suited in this scenario, since monitoring the environment basically consists of detecting the stream of photons leaking from the cavity.

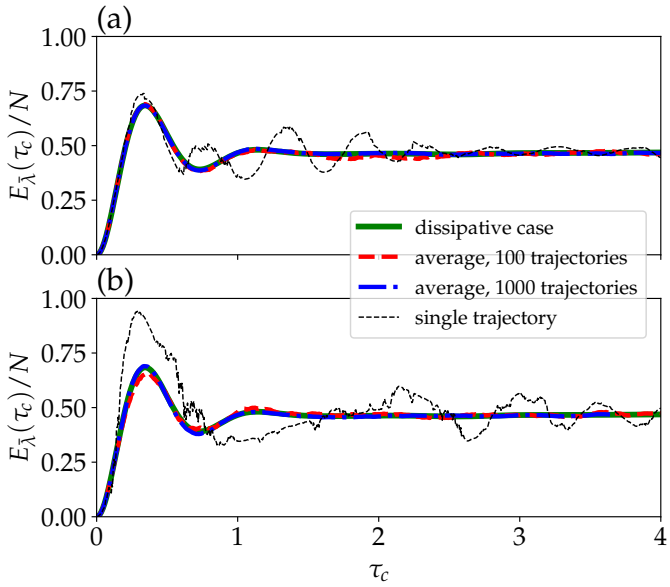


Figure 4.13: Energy of the battery as a function of the charging time for the unconditional dissipative state (green solid line) and the average over conditional trajectories (dashed lines) for (a) PD and (b) HD. Parameters: $\kappa = 1$, $\bar{\lambda} = 1$, $N = 10$.

From Figure 4.13, we can see that for the battery energy, the quantum trajectories, when averaged, unravel into the unconditional value, as expected. We can also observe energy fluctuations at the single-trajectory level, which could potentially be exploited to enhance the charging process. This possibility will be explored

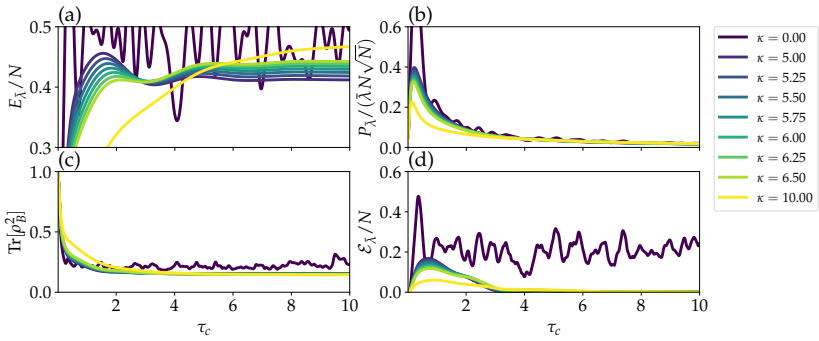


Figure 4.14: Energy (a), power (b), purity (c) and ergotropy (d) of the battery reduced state as a function of charging time for the unconditional case. Parameters: $\bar{\lambda} = 1$, $N = 6$.

in the following for both the cases of photo-detection and homodyne detection.

First, we computed the battery energy, ergotropy, power, and purity as functions of the charging time for different values of $\kappa$ (Figure 4.14). The results reveal a clear transition: for small dissipation rates, the first energy peak is the dominant one, whereas above a certain threshold in $\kappa$ ($\kappa \sim 6$) the maximum energy is reached only asymptotically. In all cases, the maximum ergotropy is reached at an intermediate time, later than the peak of the power but earlier than the maximum of the energy. The purity of the battery state in unconditional dynamics remains generally low, especially in the low dissipation regime, which suggests the presence of strong correlations between the battery and the charger; for larger $\kappa$, the loss of purity can instead be attributed to decoherence at the global level. When considering conditional dynamics (Figure 4.15), we find that the averaged energy and power correctly unravel to their unconditional counterparts, confirming the consistency of the stochastic description. Interestingly, however, conditional purity and ergotropy are systematically enhanced with respect to the unconditional case, and in particular, conditional ergotropy can increase even asymptotically, a behaviour that is absent in unconditional evolution, where it decays to zero. The scaling behaviour in the conditional case is illustrated in Figure 4.16. Once again, energy and power closely follow the trends observed in the unconditional dynamics. How-

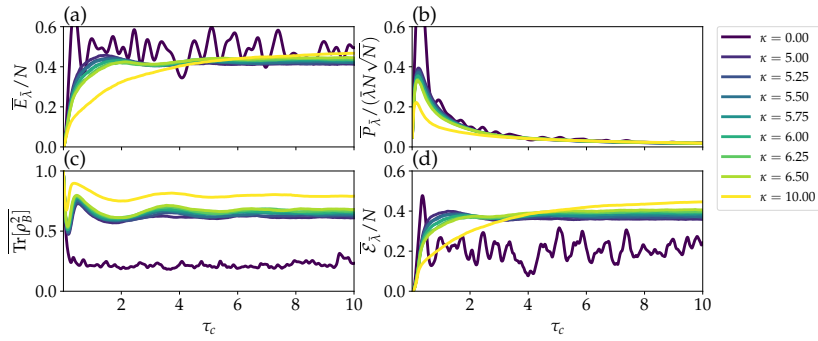


Figure 4.15: Same as Figure 4.14 but averages over the conditional states for PD scheme. Here we considered $n = 1000$ trajectories.

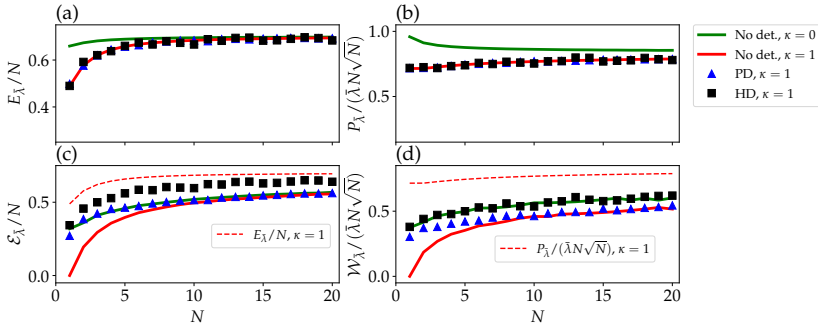


Figure 4.16: Maximum charging energy (a), power (b), ergotropy (c), and ergotropic power (d) of the battery reduced state as functions of the system size N. Solid lines represent the unconditional values, while markers correspond to the conditional values averaged over $n = 1000$ trajectories. The parameters are set to $\kappa = 1$ and $\bar{\lambda} = 1$. The ergotropic power is evaluated at the same time at which the ergotropy is computed.

ever, regarding the ergotropy, a striking difference emerges: for PD, the conditional ergotropy recovers the scaling observed in the dissipation-free scenario, while in the HD case, it even surpasses the closed-system value in the same fashion as the examples given previously. This raises an important question regarding the generality of this behaviour, is it a robust feature across different parameter regimes, or does it only hold for this specific choice of parameters?

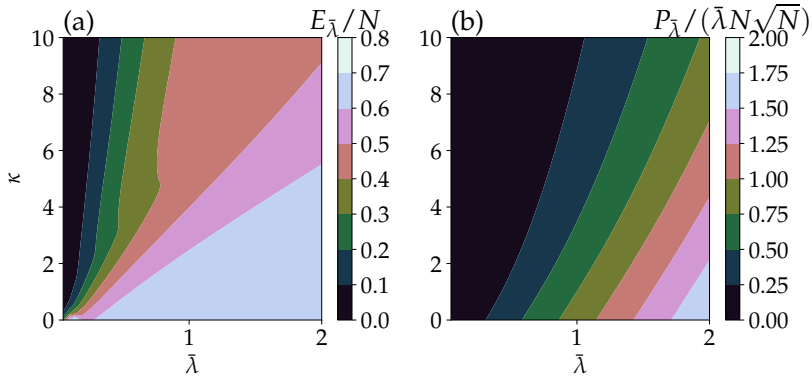


Figure 4.17: Contour plots of energy (a) and power (b) as a function of the coupling strength $\bar{\lambda}$ and the dissipation rate $\kappa$, here $N = 6$.

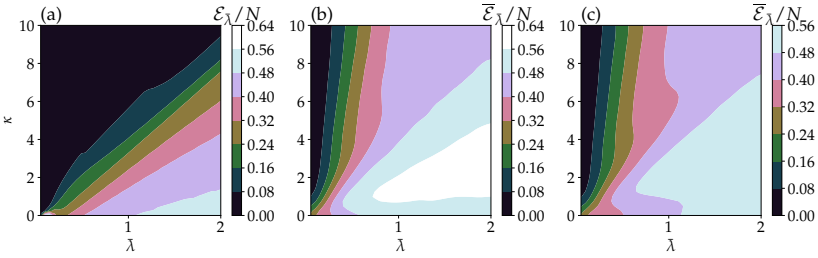


Figure 4.18: Contour plots of ergotropy (a), HD daemonic ergotropy (b) PD daemonic ergotropy (c) as a function of the coupling strength $\bar{\lambda}$ and the dissipation rate $\kappa$, here $N = 6$ and the number of trajectories considered is $n = 1000$.

The parameter landscapes are shown in Figures 4.17 and 4.18, which display, respectively, the energy and power, and the ergotropy for the different cases. As shown in Figure 4.17 (a), the stored energy exhibits two distinct regimes characterized by different slopes, while the power does not seem to follow the same behaviour. In the following, however, we will focus only on the energy and ergotropy. From Figure 4.18, we observe a clear enhancement of the daemonic ergotropy compared to the unconditional one. As expected, the daemonic ergotropy closely follows the energy landscape.

In order to better quantify this enhancement and assess its efficiency, we compute two parameters. The first is the ratio between

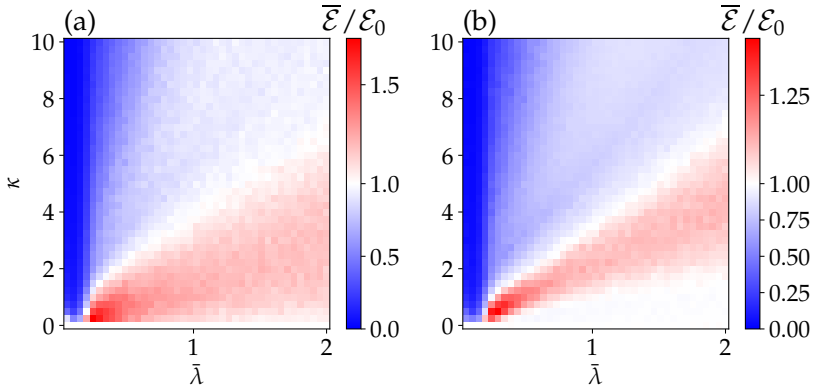


Figure 4.19: Daemonic ergotropy enhancement ratio as a function of the coupling strength $\bar{\lambda}$ and the dissipation rate $\kappa$ for HD (a) and PD (b). In the red regions of the plots, the presence of dissipation combined with continuous measurement leads to an increase in daemonic ergotropy compared to the ideal dissipation-free case. Here, $N = 6$ and the number of trajectories considered is $n = 1000$.

the daemonic ergotropy $\overline{\mathcal{E}}$ and the ergotropy of the unconditional state without dissipation $\mathcal{E}_0$ (see Figure 4.19). This comparison reveals that, over a wide region of the parameter space, the presence of dissipation combined with continuous measurement leads to an increase in ergotropy compared to the ideal dissipation-free case, for both homodyne and photo-detection schemes. Notably, the enhancement regions are approximately separated from the other regimes by linear boundaries with distinct slopes, which may be connected to the superradiant phase transition of the Dicke model. Indeed, the functional form of these boundaries appears to follow the same dependence as the critical parameter of the superradiant phase transition, $\lambda_c = \frac{1}{4}\sqrt{\frac{1+\kappa^2}{N}}$ [176], although with similar but distinct asymptotic slopes that, moreover, seem to depend on the specific detection scheme considered. The second parameter is the efficiency $\eta = \frac{\overline{\mathcal{E}}-\mathcal{E}}{E-\mathcal{E}}$ for which we recall that $\eta \in [0, 1]$ and that it takes the value one when all the available energy is converted into extractable energy in the conditional case, and zero when no advantage is present.

In Figure 4.20, we see that the daemonic ergotropy saturates the maximum possible extractable energy over a large region of

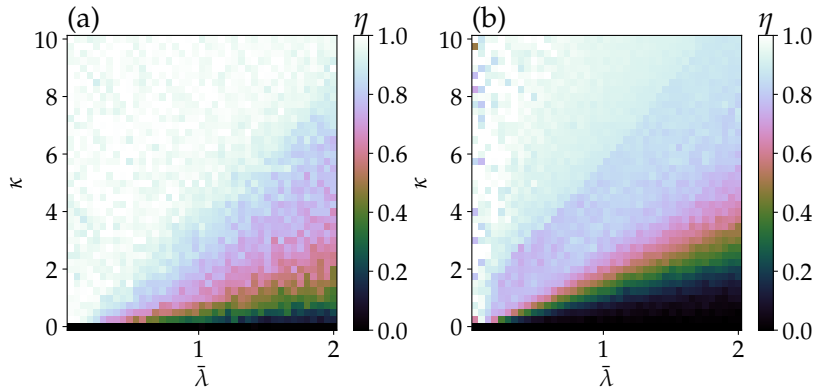


Figure 4.20: Daemonic ergotropy efficiency as a function of the coupling strength $\bar{\lambda}$ and the dissipation rate $\kappa$ for HD (a) and PD (b). In the white regions of the plots, almost all the available energy is converted into extractable daemonic ergotropy. Here, $N = 6$ and the number of trajectories considered is $n = 1000$.

the parameter space (roughly corresponding to the blue regions of Figure 4.19), corresponding to the high dissipation regime for both HD and PD. This, of course, does not by itself guarantee a high absolute value of ergotropy, but rather indicates that all the available energy (if there is any) in that regime is, in principle, fully convertible into useful work.

Finally, only minor differences are observed when measuring different quadratures in homodyne detection, and the overall behaviour remains unchanged. In particular, in Figure 4.21 we compare the two orthogonal quadratures corresponding to $\theta = 0$ and $\theta = \pi/2$. Their ratio clearly reveals regions where measuring one quadrature is preferable over the other, offering the opportunity for further optimization in this direction.

### 4.2.4 *Conclusions*

In this section, we have investigated how continuous measurements can enhance the performance of open quantum batteries by mitigating the detrimental effects of correlations and dissipation. Through three representative models of increasing complexity, we demonstrated that the information extracted from the envi-

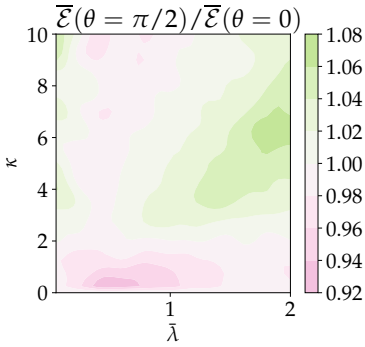


Figure 4.21: Ratio between the daemonic ergotropy obtained from measuring the $\theta = \pi/2$ and $\theta = 0$ quadratures in homodyne detection. Values above unity indicate regions where $\theta = \pi/2$ yields higher ergotropy, while values below unity favor $\theta = 0$. Here $N = 6$, $\bar{\lambda}$ and $\kappa$ vary as shown, and results are averaged over $n = 1000$ trajectories.

ronment can be effectively exploited to recover the ergotropy lost in dissipative settings and, in certain regimes, even surpass the noiseless value.

Starting from the spin-spin model, we showed that both dissipation and measurement backaction can reduce quantum correlations between the battery and the charger, thereby increasing the extractable work. This behaviour was confirmed in the cavity-mediated setup, where entanglement naturally arises during the charging process: in this case, dissipation combined with continuous measurements makes otherwise inaccessible, passive energy available for extraction.

Finally, for the Dicke quantum battery, we showed that continuous monitoring of the emitted photons, through either homodyne or photo-detection schemes, restores the ergotropy scaling observed in the closed-system case, and in some regimes even enhances it beyond that limit. In this system, as pointed out in Ref. [113], the ergotropy is strongly limited when the charger is initialized in a Fock state, due to the entanglement that builds up between the two subsystems. The presence of dissipation, when combined with continuous measurements, effectively suppresses these correlations, thereby increasing the fraction of stored energy that can be converted into useful work. However, the same

limitation can be mitigated by preparing the cavity in a coherent state, which naturally reduces charger-battery entanglement, providing further insight into the semiclassical nature of the Dicke QBs collective behaviour.

More generally, our findings suggest that appropriately designed measurement protocols, tailored to the specific dissipation mechanisms of a given experimental platform, can be used as an active resource to enhance the ergotropy of quantum batteries in situations where correlations limit the extractable work. Continuous monitoring the environment thus emerges not only as a tool to counteract decoherence, but also as a means to suppress unwanted correlations that naturally build up during the charging dynamics.

## 4.3 OUTLOOKS

In this chapter, we have introduced the fascinating and rapidly developing field of quantum batteries. Our contribution demonstrates how continuous measurements can be harnessed to condition work extraction and mitigate the detrimental effects of decoherence, a challenge that all quantum technologies must inevitably face.

What remains to be done? Quite a lot, of course. Regarding the models discussed here, it would be interesting to investigate the impact of imperfect detection. We do not expect major qualitative changes: the daemonic ergotropy should gradually approach the unconditional value as the detector efficiency decreases. Another natural direction is to consider QBs models where the advantage is genuinely quantum (e.g., SYK QBs), and to study their behaviour under suitably engineered continuous measurements. Furthermore, one could explore the fluctuations of the conditional ergotropy and perform post-selection on trajectories yielding maximal work extraction.

Finally, an important step ahead would be to experimentally validate these theoretical predictions. This, however, requires developing an efficient method to measure ergotropy in practice, a task that, to the best of our knowledge, has not yet been achieved beyond full state tomography.

In summary, while much remains to be explored, our results highlight how the interplay between measurements and information opens a promising route towards controllable and resilient quantum energy storage devices.

# CONCLUSIONS

This thesis has explored how measurements, traditionally viewed as disruptive or passive processes, can instead be harnessed as constructive elements in the dynamics of open quantum systems, starting from theoretical foundations towards two distinct applications.

The first part established the formal setting required to describe systems interacting with their environment and subjected to continuous measurements. It reviewed the postulates of quantum mechanics, the theory of Markovian dissipative dynamics subjected to continuous measurements, and the thermodynamic interpretation of quantum processes, thus providing the conceptual foundation for the following investigations.

In the second part, two specific examples were analyzed. In the study of Discrete Time Crystals (DTCs), both measurement and dissipation were shown to affect the emergence and persistence of temporal ordered oscillations. While dissipation tends to suppress time crystalline behaviour, projective measurements of the system can partially mitigate this destructive effect and even assist in revealing and characterizing the time crystal phase. In addition, the thermodynamic properties of the phase were examined, and a correction to previous literature on open DTCs was provided.

In the context of Quantum Batteries (QBs), continuous measurements of the environment were found to enhance energy extraction in correlated battery-charger systems. Remarkably, performance improvements were demonstrated even beyond the idealized dissipation-free scenario, a result that appears counterintuitive at first sight. Three models of increasing complexity were presented to support the generality of this phenomenon, showing that dissipation together with measurement back-action can be exploited as a resource rather than a limitation.

Future research directions include, in the case of DTCs, the exploration of feedback-assisted stabilization protocols and the investigation of how measurements affect sensing capabilities.

For QBs, promising developments involve the integration of post-selected feedback strategies, the extension to more complex architectures such as Sachdev-Ye-Kitaev (SYK) QBs, and the development of experimental implementations of our continuous measurements scheme, particularly in platforms such as Dicke quantum batteries in optical microcavities.

The centenary of quantum mechanics, celebrated in the same year in which this thesis was completed, marks not only a moment of reflection on the conceptual foundations laid by the pioneers of the field, but also a renewed commitment to exploiting quantum systems as technological resources. In this perspective, measurements emerge not as the endpoint of quantum processes, but as a means of actively steering such technologies toward more robust, controllable, and functionally meaningful regimes.

# BIBLIOGRAPHY


[1] Matteo GA Paris. "The modern tools of quantum mechanics: A tutorial on quantum states, measurements, and operations." In: *The European Physical Journal Special Topics* 203.1 (2012), pp. 61–86.

[2] Heinz-Peter Breuer and Francesco Petruccione. *The theory of open quantum systems*. Oxford University Press, USA, 2002.

[3] Giuliano Benenti, Giulio Casati, Davide Rossini, and Giuliano Strini. *Principles of quantum computation and information: a comprehensive textbook*. World Scientific, 2019.

[4] Francesco Albarelli and Marco G Genoni. "A pedagogical introduction to continuously monitored quantum systems and measurement-based feedback." In: *Physics Letters A* 494 (2024), p. 129260.

[5] Bassano Vacchini. *Open Quantum Systems*. Springer, 2024.

[6] Vittorio Gorini, Andrzej Kossakowski, and Ennackal Chandy George Sudarshan. "Completely positive dynamical semigroups of N-level systems." In: *Journal of Mathematical Physics* 17.5 (1976), pp. 821–825.

[7] Goran Lindblad. "On the generators of quantum dynamical semigroups." In: *Communications in mathematical physics* 48.2 (1976), pp. 119–130.

[8] Francesco Ciccarello, Salvatore Lorenzo, Vittorio Giovannetti, and G Massimo Palma. "Quantum collision models: Open system dynamics from repeated interactions." In: *Physics Reports* 954 (2022), pp. 1–70.

[9] Angel Rivas and Susana F Huelga. *Open quantum systems*. Vol. 10. Springer, 2012.

[10] Tameem Albash, Sergio Boixo, Daniel A Lidar, and Paolo Zanardi. "Quantum adiabatic Markovian master equations." In: *New Journal of Physics* 14.12 (2012), p. 123016.

[11] Kater W Murch, SJ Weber, Christopher Macklin, and Irfan Siddiqi. "Observing single quantum trajectories of a superconducting quantum bit." In: *Nature* 502.7470 (2013), pp. 211–214.

[12] Philippe Campagne-Ibarcq, Pierre Six, Landry Bretheau, Alain Sarlette, Mazyar Mirrahimi, Pierre Rouchon, and Benjamin Huard. "Observing quantum state diffusion by heterodyne detection of fluorescence." In: *Physical Review X* 6.1 (2016), p. 011002.

[13] Quentin Ficheux, Sebastien Jezouin, Zaki Leghtas, and Benjamin Huard. "Dynamics of a qubit while simultaneously monitoring its relaxation and dephasing." In: *Nature communications* 9.1 (2018), p. 1926.

[14] Massimiliano Rossi, David Mason, Junxin Chen, Yeghishe Tsaturyan, and Albert Schliesser. "Measurement-based quantum control of mechanical motion." In: *Nature* 563.7729 (2018), pp. 53–58.

[15] Witlef Wieczorek, Sebastian G Hofer, Jason Hoelscher-Obermaier, Ralf Riedinger, Klemens Hammerer, and Markus Aspelmeyer. "Optimal state estimation for cavity optomechanical systems." In: *Physical Review Letters* 114.22 (2015), p. 223601.

[16] Rodrigo A Thomas, Michał Parniak, Christoffer Østfeldt, Christoffer B Møller, Christian Bærentsen, Yeghishe Tsaturyan, Albert Schliesser, Jürgen Appel, Emil Zeuthen, and Eugene S Polzik. "Entanglement between distant macroscopic mechanical and spin systems." In: *Nature Physics* 17.2 (2021), pp. 228–233.

[17] Yoshitaka Tanimura. "Stochastic Liouville, Langevin, Fokker–Planck, and master equation approaches to quantum dissipative systems." In: *Journal of the Physical Society of Japan* 75.8 (2006), p. 082001.

[18] Howard M Wiseman and Gerard J Milburn. *Quantum measurement and control*. Cambridge university press, 2009.

[19] Kurt Jacobs. *Quantum measurement theory and its applications*. Cambridge University Press, 2014.

[20] Roberto Livi and Paolo Politi. *Nonequilibrium statistical physics: a modern perspective*. Cambridge University Press, 2017.

[21] Sebastian Deffner and Steve Campbell. *Quantum Thermodynamics: An introduction to the thermodynamics of quantum information*. Morgan & Claypool Publishers, 2019.

[22] Robert Alicki. "The quantum open system as a model of the heat engine." In: *Journal of Physics A: Mathematical and General* 12 (1979), p. L103.

[23] Herbert Spohn. "Entropy production for quantum dynamical semigroups." In: *Journal of Mathematical Physics* 19.5 (1978), pp. 1227–1230.

[24] Armen E Allahverdyan, Roger Balian, and Th M Nieuwenhuizen. "Maximal work extraction from finite quantum systems." In: *Europhysics Letters* 67.4 (2004), p. 565.

[25] Gianluca Francica, Felix C Binder, Giacomo Guarnieri, Mark T Mitchison, John Goold, and Francesco Plastina. "Quantum coherence and ergotropy." In: *Physical Review Letters* 125.18 (2020), p. 180603.

[26] Leo Szilard. "On the decrease of entropy in a thermodynamic system by the intervention of intelligent beings." In: *Behavioral Science* 9.4 (1964), pp. 301–310.

[27] Gianluca Francica, John Goold, Francesco Plastina, and Mauro Paternostro. "Daemonic ergotropy: Enhanced work extraction from quantum correlations." In: *npj Quantum Information* 3.1 (2017), p. 12.

[28] Daniele Morrone, Matteo AC Rossi, and Marco G Genoni. "Daemonic ergotropy in continuously monitored open quantum batteries." In: *Physical Review Applied* 20.4 (2023), p. 044073.

[29] William Thomson. "Kinetic Theory of the Dissipation of Energy." In: *Nature* 9 (1874), pp. 441–444.

[30] John Goold, Mauro Paternostro, and Kavan Modi. "Nonequilibrium quantum Landauer principle." In: *Physical review letters* 114.6 (2015), p. 060602.

[31] Tan Van Vu and Keiji Saito. "Finite-time quantum Landauer principle and quantum coherence." In: *Physical Review Letters* 128.1 (2022), p. 010602.

[32] Paolo Malgaretti and Holger Stark. "Szilard engines and information-based work extraction for active systems." In: *Physical Review Letters* 129.22 (2022), p. 228005.

[33] Sang Wook Kim, Takahiro Sagawa, Simone De Liberato, and Masahito Ueda. "Quantum szilard engine." In: *Physical Review Letters* 106.7 (2011), p. 070401.

[34] Rolf Landauer. "Irreversibility and heat generation in the computing process." In: *IBM journal of research and development* 5.3 (1961), pp. 183–191.

[35] Harold Ollivier and Wojciech H Zurek. "Quantum discord: a measure of the quantumness of correlations." In: *Physical Review Letters* 88.1 (2001), p. 017901.

[36] Raffaele Salvia and Vittorio Giovannetti. "Extracting work from correlated many-body quantum systems." In: *Physical Review A* 105.1 (2022), p. 012414.

[37] Martí Perarnau-Llobet, Karen V Hovhannisyan, Marcus Huber, Paul Skrzypczyk, Nicolas Brunner, and Antonio Acín. "Extractable work from correlations." In: *Physical Review X* 5.4 (2015), p. 041011.

[38] Jonathan Oppenheim, Michał Horodecki, Paweł Horodecki, and Ryszard Horodecki. "Thermodynamical approach to quantifying quantum correlations." In: *Physical Review Letters* 89.18 (2002), p. 180402.

[39] Wojciech Hubert Zurek. "Quantum discord and Maxwell's demons." In: *Physical Review A* 67.1 (2003), p. 012320.

[40] Koji Maruyama, Fumiaki Morikoshi, and Vlatko Vedral. "Thermodynamical detection of entanglement by Maxwell's demons." In: *Physical Review A* 71.1 (2005), p. 012108.

[41] Eric G Brown, Nicolai Friis, and Marcus Huber. "Passivity and practical work extraction using Gaussian operations." In: *New Journal of Physics* 18.11 (2016), p. 113028.

[42] Mario A Ciampini, Luca Mancino, Adeline Orieux, Caterina Vigliar, Paolo Mataloni, Mauro Paternostro, and Marco Barbieri. "Experimental extractable work-based multipartite separability criteria." In: *npj Quantum Information* 3.1 (2017), p. 10.

[43] Matteo Brunelli, Marco G Genoni, Marco Barbieri, and Mauro Paternostro. "Detecting Gaussian entanglement via extractable work." In: *Physical Review A* 96.6 (2017), p. 062311.

[44] Dominik Šafránek, Dario Rosa, and Felix C Binder. "Work extraction from unknown quantum sources." In: *Physical Review Letters* 130.21 (2023), p. 210401.

[45] Gabriele Cenedese, Samuel T Mister, Mauro Antezza, Giuliano Benenti, and Gabriele De Chiara. "Thermodynamics and protection of discrete time crystals." In: *Physical Review B* 112.5 (2025), p. 054303.

[46] Gabriele Cenedese, Marco G Genoni, Dario Ferraro, and Giuliano Benenti. "Daemonic ergotropy enhancement in correlated quantum battery-charger systems." In: *Preparation* (2025).

[47] Andrew J Daley. "Quantum trajectories and open many-body quantum systems." In: *Advances in Physics* 63.2 (2014), pp. 77–149.

[48] Iulia M Georgescu, Sahel Ashhab, and Franco Nori. "Quantum simulation." In: *Reviews of Modern Physics* 86.1 (2014), pp. 153–185.

[49] Andrew J Daley, Immanuel Bloch, Christian Kokail, Stuart Flannigan, Natalie Pearson, Matthias Troyer, and Peter Zoller. "Practical quantum advantage in quantum simulation." In: *Nature* 607.7920 (2022), pp. 667–676.

[50] Jens Eisert, Mathis Friesdorf, and Christian Gogolin. "Quantum many-body systems out of equilibrium." In: *Nature Physics* 11.2 (2015), pp. 124–130.

[51] Frank Wilczek. "Quantum time crystals." In: *Physical Review Letters* 109.16 (2012), p. 160401.

[52] Fernando Iemini, Rosario Fazio, and Anna Sanpera. "Floquet time crystals as quantum sensors of ac fields." In: *Phys. Rev. A* 109 (5 2024), p. L050203.

[53] Albert Cabot, Federico Carollo, and Igor Lesanovsky. "Continuous Sensing and Parameter Estimation with the Boundary Time Crystal." In: *Phys. Rev. Lett.* 132 (5 2024), p. 050801.

[54] Victor Montenegro, Marco G Genoni, Abolfazl Bayat, and Matteo GA Paris. "Quantum metrology with boundary time crystals." In: *Communications Physics* 6.1 (2023), p. 304.

[55] Nikolay I Zheludev. "Time crystals for photonics and timetronics." In: *Nature Photonics* 18.11 (2024), pp. 1123–1125.

[56] Krzysztof Sacha and Jakub Zakrzewski. "Time crystals: a review." In: *Reports on Progress in Physics* 81.1 (2017), p. 016401.

[57] Dominic V Else, Christopher Monroe, Chetan Nayak, and Norman Y Yao. "Discrete time crystals." In: *Annual Review of Condensed Matter Physics* 11.1 (2020), pp. 467–499.

[58] Michael P Zaletel, Mikhail Lukin, Christopher Monroe, Chetan Nayak, Frank Wilczek, and Norman Y Yao. "Colloquium: Quantum and classical discrete time crystals." In: *Reviews of Modern Physics* 95.3 (2023), p. 031001.

[59] Dominic V Else, Bela Bauer, and Chetan Nayak. "Floquet time crystals." In: *Physical Review Letters* 117.9 (2016), p. 090402.

[60] Roberto Gargiulo, Gianluca Passarelli, Procolo Lucignano, and Angelo Russomanno. "Swapping Floquet time crystal." In: *Physical Review B* 109.17 (2024), p. 174310.

[61] Soonwon Choi, Joonhee Choi, Renate Landig, Georg Kucsko, Hengyun Zhou, Junichi Isoya, Fedor Jelezko, Shinobu Onoda, Hitoshi Sumiya, Vedika Khemani, et al. "Observation of discrete time-crystalline order in a disordered dipolar many-body system." In: *Nature* 543.7644 (2017), pp. 221–225.

[62] William Beatrez, Christoph Fleckenstein, Arjun Pillai, Erica de Leon Sanchez, Amala Akkiraju, Jesus Diaz Alcala, Sophie Conti, Paul Reshetikhin, Emanuel Druga, Marin Bukov, et al. "Critical prethermal discrete time crystal created by two-frequency driving." In: *Nature Physics* 19.3 (2023), pp. 407–413.

[63] Jiehang Zhang, Paul W Hess, A Kyprianidis, Petra Becker, A Lee, J Smith, Gaetano Pagano, I-D Potirniche, Andrew C Potter, Ashvin Vishwanath, et al. "Observation of a discrete time crystal." In: *Nature* 543.7644 (2017), pp. 217–220.

[64] Hossein Taheri, Andrey B Matsko, Lute Maleki, and Krzysztof Sacha. "All-optical dissipative discrete time crystals." In: *Nature communications* 13.1 (2022), p. 848.

[65] Matteo Ippoliti, Kostyantyn Kechedzhi, Roderich Moessner, SL Sondhi, and Vedika Khemani. "Many-body physics in the nisq era: Quantum programming a discrete time crystal." In: *PRX Quantum* 2.3 (2021), p. 030346.

[66] Phatthamon Kongkhambut, Jim Skulte, Ludwig Mathey, Jayson G Cosme, Andreas Hemmerich, and Hans Keßler. "Observation of a continuous time crystal." In: *Science* 377.6606 (2022), pp. 670–673.

[67] Samuli Autti, VB Eltsov, and GE Volovik. "Observation of a time quasicrystal and its transition to a superfluid time crystal." In: *Physical Review Letters* 120.21 (2018), p. 215301.

[68] Giovanni Ferioli, Antoine Glicenstein, Igor Ferrier-Barbut, and Antoine Browaeys. "A non-equilibrium superradiant phase transition in free space." In: *Nature Physics* 19.9 (2023), pp. 1345–1349.

[69] Alfred Shapere and Frank Wilczek. "Classical time crystals." In: *Physical Review Letters* 109.16 (2012), p. 160402.

[70] Yakir Aharonov and David Bohm. "Significance of electromagnetic potentials in the quantum theory." In: *Physical review* 115.3 (1959), p. 485.

[71] Yakir Aharonov and David Bohm. "Further considerations on electromagnetic potentials in the quantum theory." In: *Physical Review* 123.4 (1961), p. 1511.

[72] Patrick Bruno. "Impossibility of spontaneously rotating time crystals: a no-go theorem." In: *Physical Review Letters* 111.7 (2013), p. 070402.

[73] Haruki Watanabe and Masaki Oshikawa. "Absence of quantum time crystals." In: *Physical Review Letters* 114.25 (2015), p. 251603.

[74] Fernando Iemini, Angelo Russomanno, Jonathan Keeling, Marco Schirò, Marcello Dalmonte, and Rosario Fazio. "Boundary time crystals." In: *Physical Review Letters* 121.3 (2018), p. 035301.

[75] Federico Carollo, Igor Lesanovsky, Mauro Antezza, and Gabriele De Chiara. "Quantum thermodynamics of boundary time-crystals." In: *Quantum Science and Technology* 9.3 (2024), p. 035024.

[76] Eric M Kessler, Geza Giedke, Atac Imamoglu, Susanne F Yelin, Mikhail D Lukin, and J Ignacio Cirac. "Dissipative phase transition in a central spin system." In: *Physical Review A* 86.1 (2012), p. 012116.

[77] Luca D'Alessio and Marcos Rigol. "Long-time behavior of isolated periodically driven interacting lattice systems." In: *Physical Review X* 4.4 (2014), p. 041048.

[78] Pedro Ponte, Anushya Chandran, Z Papić, and Dmitry A Abanin. "Periodically driven ergodic and many-body localized quantum systems." In: *Annals of Physics* 353 (2015), pp. 196–204.

[79] Achilleas Lazarides, Arnab Das, and Roderich Moessner. "Equilibrium states of generic quantum systems subject to periodic driving." In: *Physical Review E* 90.1 (2014), p. 012110.

[80] Dmitry A Abanin and Zlatko Papić. "Recent progress in many-body localization." In: *Annalen der Physik* 529.7 (2017), p. 1700169.

[81] Dmitry A Abanin, Ehud Altman, Immanuel Bloch, and Maksym Serbyn. "Colloquium: Many-body localization, thermalization, and entanglement." In: *Reviews of Modern Physics* 91.2 (2019), p. 021001.

[82] Fabien Alet and Nicolas Laflorencie. "Many-body localization: An introduction and selected topics." In: *Comptes Rendus Physique* 19.6 (2018), pp. 498–525.

[83] Phil Richerme. "How to create a time crystal." In: *Physics* 10 (2017), p. 5.

[84] Marin Bukov, Sarang Gopalakrishnan, Michael Knap, and Eugene Demler. "Prethermal floquet steady states and instabilities in the periodically driven, weakly interacting bose-hubbard model." In: *Physical Review Letters* 115.20 (2015), p. 205301.

[85] Dmitry A Abanin, Wojciech De Roeck, and François Huveneers. "Exponentially slow heating in periodically driven many-body systems." In: *Physical Review Letters* 115.25 (2015), p. 256803.

[86] Dmitry Abanin, Wojciech De Roeck, Wen Wei Ho, and François Huveneers. "A rigorous theory of many-body prethermalization for periodically driven and closed quantum systems." In: *Communications in Mathematical Physics* 354.3 (2017), pp. 809–827.

[87] Francisco Machado, Dominic V Else, Gregory D Kahanamoku-Meyer, Chetan Nayak, and Norman Y Yao. "Long-range prethermal phases of nonequilibrium matter." In: *Physical Review X* 10.1 (2020), p. 011043.

[88] Antonis Kyprianidis, Francisco Machado, William Morong, Patrick Becker, Kate S Collins, Dominic V Else, Lei Feng, Paul W Hess, Chetan Nayak, Guido Pagano, et al. "Observation of a prethermal discrete time crystal." In: *Science* 372.6547 (2021), pp. 1192–1196.

[89] Norman Y Yao, Andrew C Potter, I-D Potirniche, and Ashvin Vishwanath. "Discrete time crystals: Rigidity, criticality, and realizations." In: *Physical Review Letters* 118.3 (2017), p. 030401.

[90] Paulo J Paulino, Albert Cabot, Gabriele De Chiara, Mauro Antezza, Igor Lesanovsky, and Federico Carollo. "Thermodynamics of coupled time crystals with an application to energy storage." In: *arXiv preprint arXiv:2411.04836* (2024).

[91] Vedika Khemani, Achilleas Lazarides, Roderich Moessner, and Shivaji L Sondhi. "Phase structure of driven quantum systems." In: *Physical Review Letters* 116.25 (2016), p. 250401.

[92] Achilleas Lazarides and Roderich Moessner. "Fate of a discrete time crystal in an open system." In: *Physical Review B* 95.19 (2017), p. 195135.

[93] Mariya V Medvedyeva, Tomaž Prosen, and Marko Žnidarič. "Influence of dephasing on many-body localization." In: *Physical Review B* 93.9 (2016), p. 094205.

[94] Maria Popovic, Mark T Mitchison, and John Goold. "Thermodynamics of decoherence." In: *Proceedings of the Royal Society A* 479.2272 (2023), p. 20230040.

[95] Gonzalo Camacho and Benedikt Fauseweh. "Prolonging a discrete time crystal by quantum-classical feedback." In: *Physical Review Research* 6.3 (2024), p. 033092.

[96] Paolo Facchi and Saverino Pascazio. "Quantum Zeno dynamics: mathematical and physical aspects." In: *Journal of Physics A: Mathematical and Theoretical* 41.49 (2008), p. 493001.

[97] John Gough. "Zeno dynamics for open quantum systems." In: *Russian Journal of Mathematical Physics* 21.3 (2014), pp. 337–347.

[98] Wei Wu and Hai-Qing Lin. "Quantum Zeno and anti-Zeno effects in quantum dissipative systems." In: *Physical Review A* 95.4 (2017), p. 042132.

[99] Michael A Nielsen and Isaac L Chuang. *Quantum computation and quantum information*. Cambridge university press, 2010.

[100] Christian L Degen, Friedemann Reinhard, and Paola Cappellaro. "Quantum sensing." In: *Reviews of Modern Physics* 89.3 (2017), p. 035002.

[101] Christopher Portmann and Renato Renner. "Security in quantum cryptography." In: *Reviews of Modern Physics* 94.2 (2022), p. 025008.

[102] Robert Alicki and Mark Fannes. "Entanglement boost for extractable work from ensembles of quantum batteries." In: *Physical Review E* 87.4 (2013), p. 042123.

[103] Francesco Campaioli, Stefano Gherardini, James Q Quach, Marco Polini, and Gian Marcello Andolina. "Colloquium: quantum batteries." In: *Reviews of Modern Physics* 96.3 (2024), p. 031001.

[104] James Q Quach, Giulio Cerullo, and Tersilla Virgili. "Quantum batteries: The future of energy storage?" In: *Joule* 7.10 (2023), pp. 2195–2200.

[105] Sergi Julià-Farré, Tymoteusz Salamon, Arnau Riera, Manabendra N Bera, and Maciej Lewenstein. "Bounds on the capacity and power of quantum batteries." In: *Physical Review Research* 2.2 (2020), p. 023113.

[106] Nicolai Friis and Marcus Huber. "Precision and work fluctuations in gaussian battery charging." In: *Quantum* 2 (2018), p. 61.

[107] Ronald A Fisher. "On the mathematical foundations of theoretical statistics." In: *Philosophical transactions of the Royal Society of London. Series A, containing papers of a mathematical or physical character* 222.594-604 (1922), pp. 309–368.

[108] Ole E Barndorff-Nielsen and Richard D Gill. "Fisher information in quantum statistics." In: *Journal of Physics A: Mathematical and General* 33.24 (2000), p. 4481.

[109] Gian Marcello Andolina, Maximilian Keck, Andrea Mari, Vittorio Giovannetti, and Marco Polini. "Quantum versus classical many-body batteries." In: *Physical Review B* 99.20 (2019), p. 205437.

[110] Francesco Campaioli, Felix A Pollock, Felix C Binder, Lucas Céleri, John Goold, Sai Vinjanampathy, and Kavan Modi. "Enhancing the charging power of quantum batteries." In: *Physical Review Letters* 118.15 (2017), p. 150601.

[111] Ju-Yeon Gyhm, Dominik Šafránek, and Dario Rosa. "Quantum charging advantage cannot be extensive without global operations." In: *Physical Review Letters* 128.14 (2022), p. 140501.

[112] Sourav Bhattacharjee and Amit Dutta. "Quantum thermal machines and batteries." In: *The European Physical Journal B* 94.12 (2021), p. 239.

[113] Gian Marcello Andolina, Maximilian Keck, Andrea Mari, Michele Campisi, Vittorio Giovannetti, and Marco Polini. "Extractable work, the role of correlations, and asymptotic freedom in quantum batteries." In: *Physical Review Letters* 122.4 (2019), p. 047702.

[114] Riccardo Castellano, Donato Farina, Vittorio Giovannetti, and Antonio Acin. "Extended local ergotropy." In: *Physical Review Letters* 133.15 (2024), p. 150402.

[115] Dario Ferraro, Michele Campisi, Gian Marcello Andolina, Vittorio Pellegrini, and Marco Polini. "High-power collective charging of a solid-state quantum battery." In: *Physical Review Letters* 120.11 (2018), p. 117702.

[116] Robert H Dicke. "Coherence in spontaneous radiation processes." In: *Physical review* 93.1 (1954), p. 99.

[117] Peter Kirton, Mor M Roses, Jonathan Keeling, and Emanuele G Dalla Torre. "Introduction to the Dicke model: From equilibrium to nonequilibrium, and vice versa." In: *Advanced Quantum Technologies* 2.1-2 (2019), p. 1800043.

[118] Serge Haroche and J-M Raimond. *Exploring the quantum: atoms, cavities, and photons*. Oxford university press, 2006.

[119] Alexandre Blais, Arne L Grimsmo, Steven M Girvin, and Andreas Wallraff. "Circuit quantum electrodynamics." In: *Reviews of Modern Physics* 93.2 (2021), p. 025005.

[120] Dong-Lin Yang, Fang-Mei Yang, and Fu-Quan Dou. "Three-level Dicke quantum battery." In: *Physical Review B* 109.23 (2024), p. 235432.

[121] Alba Crescente, Matteo Carrega, Maura Sassetti, and Dario Ferraro. "Ultrafast charging in a two-photon Dicke quantum battery." In: *Physical Review B* 102.24 (2020), p. 245407.

[122] Lu Wang, Shu-Qian Liu, Feng-lin Wu, Hao Fan, and Si-Yuan Liu. "Deep strong charging in a multiphoton anisotropic Dicke quantum battery." In: *Physical Review A* 110.4 (2024), p. 042419.

[123] Giulia Gemme, Gian Marcello Andolina, Francesco Maria Dimitri Pellegrino, Maura Sassetti, and Dario Ferraro. "Off-resonant Dicke quantum battery: Charging by virtual photons." In: *Batteries* 9.4 (2023), p. 197.

[124] Paolo Andrea Erdman, Gian Marcello Andolina, Vittorio Giovannetti, and Frank Noé. "Reinforcement learning optimization of the charging of a Dicke quantum battery." In: *Physical Review Letters* 133.24 (2024), p. 243602.

[125] Javier Carrasco, Jerónimo R Maze, Carla Hermann-Avigliano, and Felipe Barra. "Collective enhancement in dissipative quantum batteries." In: *Physical Review E* 105.6 (2022), p. 064119.

[126] Andrea Canzio, Vasco Cavina, Marco Polini, and Vittorio Giovannetti. "Single-atom dissipation and dephasing in Dicke and Tavis-Cummings quantum batteries." In: *Physical Review A* 111.2 (2025), p. 022222.

[127] J Robert Johansson, Paul D Nation, and Franco Nori. "QuTiP: An open-source Python framework for the dynamics of open quantum systems." In: *Computer Physics Communications* 183.8 (2012), pp. 1760–1772.

[128] Thao P Le, Jesper Levinsen, Kavan Modi, Meera M Parish, and Felix A Pollock. "Spin-chain model of a many-body quantum battery." In: *Physical Review A* 97.2 (2018), p. 022106.

[129] Riccardo Grazi, Daniel Sacco Shaikh, Maura Sassetti, Niccoló Traverso Ziani, and Dario Ferraro. "Controlling energy storage crossing quantum phase transitions in an integrable spin quantum battery." In: *Physical Review Letters* 133.19 (2024), p. 197001.

[130] Davide Rossini, Gian Marcello Andolina, and Marco Polini. "Many-body localized quantum batteries." In: *Physical Review B* 100.11 (2019), p. 115142.

[131] Srijon Ghosh, Titas Chanda, and Aditi Sen. "Enhancement in the performance of a quantum battery by ordered and disordered interactions." In: *Physical Review A* 101.3 (2020), p. 032115.

[132] Mohammad B Arjmandi, Hamidreza Mohammadi, Andreia Saguia, Marcelo S Sarandy, and Alan C Santos. "Localization effects in disordered quantum batteries." In: *Physical Review E* 108.6 (2023), p. 064106.

[133] Alberto Giuseppe Catalano, Salvatore Marco Giampaolo, Oliver Morsch, Vittorio Giovannetti, and Fabio Franchini. "Frustrating quantum batteries." In: *PRX Quantum* 5.3 (2024), p. 030319.

[134] Zhi-Guang Lu, Guoqing Tian, Xin-You Lü, and Cheng Shang. "Topological quantum batteries." In: *Physical Review Letters* 134.18 (2025), p. 180401.

[135] Davide Rossini, Gian Marcello Andolina, Dario Rosa, Matteo Carrega, and Marco Polini. "Quantum advantage in the charging process of Sachdev-Ye-Kitaev batteries." In: *Physical Review Letters* 125.23 (2020), p. 236402.

[136] Dario Rosa, Davide Rossini, Gian Marcello Andolina, Marco Polini, and Matteo Carrega. "Ultra-stable charging of fast-scrambling SYK quantum batteries." In: *Journal of High Energy Physics* 2020.11 (2020), pp. 1–29.

[137] Andrea Camposeo, Tersilla Virgili, Floriana Lombardi, Giulio Cerullo, Dario Pisignano, and Marco Polini. "Quantum Batteries: A Materials Science Perspective." In: *Advanced Materials* 37.17 (2025), p. 2415073.

[138] Tanoy Kanti Konar, Ayan Patra, Rivu Gupta, Srijon Ghosh, and Aditi Sen. "Multimode advantage in continuous-variable quantum batteries." In: *Physical Review A* 110.2 (2024), p. 022226.

[139] Gian Marcello Andolina, Vittoria Stanzione, Vittorio Giovannetti, and Marco Polini. "Genuine Quantum Advantage in Anharmonic Bosonic Quantum Batteries." In: *Physical Review Letters* 134.24 (2025), p. 240403.

[140] Fabio Cavaliere, Giulia Gemme, Giuliano Benenti, Dario Ferraro, and Maura Sassetti. "Dynamical blockade of a reservoir for optimal performances of a quantum battery." In: *Communications Physics* 8.1 (2025), p. 76.

[141] Vahid Shaghaghi, Varinder Singh, Giuliano Benenti, and Dario Rosa. "Micromasers as quantum batteries." In: *Quantum Science and Technology* 7.4 (2022), 04LT01.

[142] Vahid Shaghaghi, Varinder Singh, Matteo Carrega, Dario Rosa, and Giuliano Benenti. "Lossy micromaser battery: Almost pure states in the Jaynes–Cummings regime." In: *Entropy* 25.3 (2023), p. 430.

[143] James Q Quach, Kirsty E McGhee, Lucia Ganzer, Dominic M Rouse, Brendon W Lovett, Erik M Gauger, Jonathan Keeling, Giulio Cerullo, David G Lidzey, and Tersilla Virgili. "Superabsorption in an organic microcavity: Toward a quantum battery." In: *Science advances* 8.2 (2022), eabk3160.

[144] Jitendra Joshi and TS Mahesh. "Experimental investigation of a quantum battery using star-topology NMR spin systems." In: *Physical Review A* 106.4 (2022), p. 042601.

[145] I Maillette de Buy Wenniger, SE Thomas, M Maffei, SC Wein, M Pont, N Belabas, S Prasad, A Harouri, A Lemaître, I Sagnes, et al. "Experimental analysis of energy transfers between a quantum emitter and light fields." In: *Physical Review Letters* 131.26 (2023), p. 260401.

[146] Giulia Gemme, Michele Grossi, Dario Ferraro, Sofia Vallecorsa, and Maura Sassetti. "IBM quantum platforms: A quantum battery perspective." In: *Batteries* 8.5 (2022), p. 43.

[147] Daniele Morrone, Matteo AC Rossi, Andrea Smirne, and Marco G Genoni. "Charging a quantum battery in a non-Markovian environment: A collisional model approach." In: *Quantum Science and Technology* 8.3 (2023), p. 035007.

[148] Giulia Gemme, Michele Grossi, Sofia Vallecorsa, Maura Sassetti, and Dario Ferraro. "Qutrit quantum battery: Comparing different charging protocols." In: *Physical Review Research* 6.2 (2024), p. 023091.

[149] Kieran Hymas, Jack B Muir, Daniel Tibben, Joel van Embden, Tadahiko Hirai, Christopher J Dunn, Daniel E Gómez, James A Hutchison, Trevor A Smith, and James Q Quach. "Experimental demonstration of a scalable

room-temperature quantum battery." In: *arXiv preprint arXiv:2501.16541* (2025).

[150] Daniel J Tibben, Enrico Della Gaspera, Joel van Embden, Philipp Reineck, James Q Quach, Francesco Campaioli, and Daniel E Gómez. "Extending the self-discharge time of Dicke quantum batteries using molecular triplets." In: *PRX Energy* 4.2 (2025), p. 023012.

[151] Clebson Cruz, Maron F Anka, Mario S Reis, Romain Bachelard, and Alan C Santos. "Quantum battery based on quantum discord at room temperature." In: *Quantum Science and Technology* 7.2 (2022), p. 025020.

[152] Chang-Kang Hu, Jiawei Qiu, Paulo JP Souza, Jiahao Yuan, Yuxuan Zhou, Libo Zhang, Ji Chu, Xianchuang Pan, Ling Hu, Jian Li, et al. "Optimal charging of a superconducting quantum battery." In: *Quantum Science and Technology* 7.4 (2022), p. 045018.

[153] Li Li, Si-Lu Zhao, Yun-Hao Shi, Bing-Jie Chen, Xinhui Ruan, Gui-Han Liang, Wei-Ping Yuan, Jia-Cheng Song, Cheng-Lin Deng, Yu Liu, et al. "Stable and Efficient Charging of Superconducting C-shunt Flux Quantum Batteries." In: *arXiv preprint arXiv:2504.07464* (2025).

[154] Philip Krantz, Morten Kjaergaard, Fei Yan, Terry P Orlando, Simon Gustavsson, and William D Oliver. "A quantum engineer's guide to superconducting qubits." In: *Applied physics reviews* 6.2 (2019).

[155] Luca Razzoli, Giulia Gemme, Ilia Khomchenko, Maura Sassetti, Henni Ouerdane, Dario Ferraro, and Giuliano Benenti. "Cyclic solid-state quantum battery: thermodynamic characterization and quantum hardware simulation." In: *Quantum Science and Technology* 10.1 (2025), p. 015064.

[156] Beatrice Donelli, Stefano Gherardini, Raffaele Marino, Francesco Campaioli, and Lorenzo Buffoni. "Charging a quantum spin network with superextensive precision." In: *Physical Review E* 111.6 (2025), p. L062102.

[157] Thomas Alexander, Naoki Kanazawa, Daniel J Egger, Lauren Capelluto, Christopher J Wood, Ali Javadi-Abhari, and David C McKay. "Qiskit pulse: programming quantum computers through the cloud with pulses." In: *Quantum Science and Technology* 5.4 (2020), p. 044006.

[158] Giulio Chiribella, Yuxiang Yang, and Renato Renner. "Fundamental energy requirement of reversible quantum operations." In: *Physical Review X* 11.2 (2021), p. 021014.

[159] Yaniv Kurman, Kieran Hymas, Arkady Fedorov, William J Munro, and James Quach. "Quantum Computation with Quantum Batteries." In: *arXiv preprint arXiv:2503.23610* (2025).

[160] Francesco Caravelli, Bin Yan, Luis Pedro García-Pintos, and Alioscia Hamma. "Energy storage and coherence in closed and open quantum batteries." In: *Quantum* 5 (2021), p. 505.

[161] Shadab Zakavati, Fatemeh T Tabesh, and Shahriar Salimi. "Bounds on charging power of open quantum batteries." In: *Physical Review E* 104.5 (2021), p. 054117.

[162] Matteo Carrega, Alba Crescente, Dario Ferraro, and Maura Sassetti. "Dissipative dynamics of an open quantum battery." In: *New Journal of Physics* 22.8 (2020), p. 083085.

[163] Mahima Yadav, Devvrat Tiwari, and Subhashish Banerjee. "(Thermo-) dynamics of the spin-boson model in the weak coupling regime: Application as a quantum battery." In: *arXiv preprint arXiv:2504.15712* (2025).

[164] FT Tabesh, FH Kamin, and S Salimi. "Environment-mediated charging process of quantum batteries." In: *Physical Review A* 102.5 (2020), p. 052223.

[165] Srijon Ghosh, Titas Chanda, Shiladitya Mal, and Aditi Sen. "Fast charging of a quantum battery assisted by noise." In: *Physical Review A* 104.3 (2021), p. 032207.

[166] Borhan Ahmadi, Paweł Mazurek, Shabir Barzanjeh, and Paweł Horodecki. "Superoptimal charging of quantum batteries via reservoir engineering: Arbitrary energy transfer unlocked." In: *Physical Review Applied* 23.2 (2025), p. 024010.

[167] Kai Xu, Han-Jie Zhu, Guo-Feng Zhang, and Wu-Ming Liu. "Enhancing the performance of an open quantum battery via environment engineering." In: *Physical Review E* 104.6 (2021), p. 064143.

[168] Meng-Long Song, Li-Juan Li, Xue-Ke Song, Liu Ye, and Dong Wang. "Environment-mediated entropic uncertainty in charging quantum batteries." In: *Physical Review E* 106.5 (2022), p. 054107.

[169] Wen-Li Yu, Yun Zhang, Hai Li, Guang-Fen Wei, Li-Ping Han, Feng Tian, and Jian Zou. "Enhancement of charging performance of quantum battery via quantum coherence of bath." In: *Chinese Physics B* 32.1 (2023), p. 010302.

[170] Federico Centrone, Luca Mancino, and Mauro Paternostro. "Charging batteries with quantum squeezing." In: *Physical Review A* 108.5 (2023), p. 052213.

[171] Stefano Gherardini, Francesco Campaioli, Filippo Caruso, and Felix C Binder. "Stabilizing open quantum batteries by sequential measurements." In: *Physical Review Research* 2.1 (2020), p. 013095.

[172] Mark T Mitchison, John Goold, and Javier Prior. "Charging a quantum battery with linear feedback control." In: *Quantum* 5 (2021), p. 500.

[173] Y Yao and XQ Shao. "Optimal charging of open spin-chain quantum batteries via homodyne-based feedback control." In: *Physical Review E* 106.1 (2022), p. 014138.

[174] Alba Crescente, Dario Ferraro, Matteo Carrega, and Maura Sassetti. "Enhancing coherent energy transfer between quantum devices via a mediator." In: *Physical Review Research* 4.3 (2022), p. 033216.

[175] Alba Crescente, Dario Ferraro, and Maura Sassetti. "Boosting energy transfer between quantum devices through spectrum engineering in the dissipative ultrastrong coupling regime." In: *Physical Review Research* 6.2 (2024), p. 023092.

[176] David Villaseñor and Pablo Barberis-Blostein. "Analysis of chaos and regularity in the open Dicke model." In: *Physical Review E* 109.1 (2024), p. 014206.